INVESTIGATION INTO NONLINEARITY OF FREQUENCY AGILE ANTENNAS

by

Hugh Charles Hancock

A thesis submitted to the University of Birmingham for the degree of DOCTOR OF PHILOSOPHY

Department of Electronic, Electrical and Systems Engineering
College of Engineering and Physical Sciences
University of Birmingham
June 2019

Abstract

A series of investigations were undertaken to assess the tuning range, gain and linearity of frequency reconfigurable varactor loaded patch antennas with design frequencies ranging from 1.4 – 1.8GHz. These parameters were assessed using simulation and measurements, including two-tone testing of the fabricated antennas in an anechoic chamber.

To understand the effects of the antenna's design on tunability, gain and linearity, six separate investigations were undertaken. These were (i) effects of design frequency and antenna substrate properties (ii) location of varactors on the antenna (iii) number of varactors loading antenna (iv) use of abrupt and hyperabrupt varactor (v) use of common cathode configurations (vi) use of common cathode configuration with parasitic patches with U-slots cut outs.

It was found that the greater the area reduction in a patch, compared to a patch with no varactor, the greater tunability achieved. The reduction of a patch size from varactor loading decreases the gain of the antenna. Increasing the number of varactors on the patch improves linearity and tunability. Using a common cathode configuration of varactors on the radiating edge of an antenna maintains tunability while improving the linearity.

These findings led to a novel type of antenna that uses the common cathode configuration of varactors with parasitic patches with U-slot cut outs to maintain gain across the frequency band whilst maintaining linearity and tunability.

I would like to dedicate this work to my mother

Kathleen Hancock (1951-2017)

Acknowledgements

I would like to extend my sincerest gratitude to my supervisor Dr Timothy Jackson, it is with his unwavering support and patience that I have been able to complete this work.

I am also thankful for the support I have received from my co-supervisor Dr Alexandros Feresidis and Mr Alan Yates for the practical help he has given me which continues to be beneficial in my professional career.

I am very grateful to the Electronic, Electrical and Systems Engineering department for the opportunity to undertake this work by providing the funding. I am also appreciative of the support that was given to me both pastoral and with my career development.

Finally, I would like to thank my partner Leane Watkin for being so understanding and supporting during my time undertaking this work.

Contents

List of Figures

List of Tables

List of Abbreviations

AC	Alternating Current
ADS	Advanced Design System
AUT	Antenna Under Test
CST	Computer Simulation Technology
DC	Direct Current
GSM	Global System for Mobile Communications
HFSS	High Frequency Structure Simulator
IIP3	Input Intercept Point
IMD	Intermodulation Distortion
LTE	Long-Term Evolution
MEMS	Microelectromechanical System
MIM	Metal-Insulator-Metal
MIMO	Multiple Input Multiple Output
OFDM	Orthogonal Frequency Division Multiplexing
OIP3	Output Intercept Point
PSK	Phase Shift Keying
Q-Factor	Quality Factor
RF	Radiofrequency
SOLT	Short Open Load Thru
SMA	SubMiniature Version A
TOI	Third Order Intercept
VCO	Voltage Controlled Oscillator
VNA	Vector Network Analyzer
Wi-Fi	Wireless Fidelity
WLAN	Wireless Lan

1 Introduction

Reconfigurable antennas are a type of antenna that can change one or more of its fundamental properties. These are frequency, polarization type or radiation pattern. This functionality enables a single antenna to be used in a system instead of multiple antennas, or the ability to adapt the system for optimal performance with a changing environment [1].

Reconfigurability is generally achieved by adding in a tunable component such as a varactor, PIN diode, transistor or mechanical switch such as a MEMS device. An ideal tunable component would tune instantaneously, consume zero power, contribute zero loss and behave completely linearly.

Whenever a tunable component or material is added to a system it will have an impact on the linearity of the transmitter or receiver, unless it behaves completely linearly, which will degrade the performance and have the potential to effect other users in adjacent channels [2].

A simple transmitter model shown in Figure 1.1 illustrates how adding a nonlinear component to the transmit chain will affect the adjacent power leakage levels.

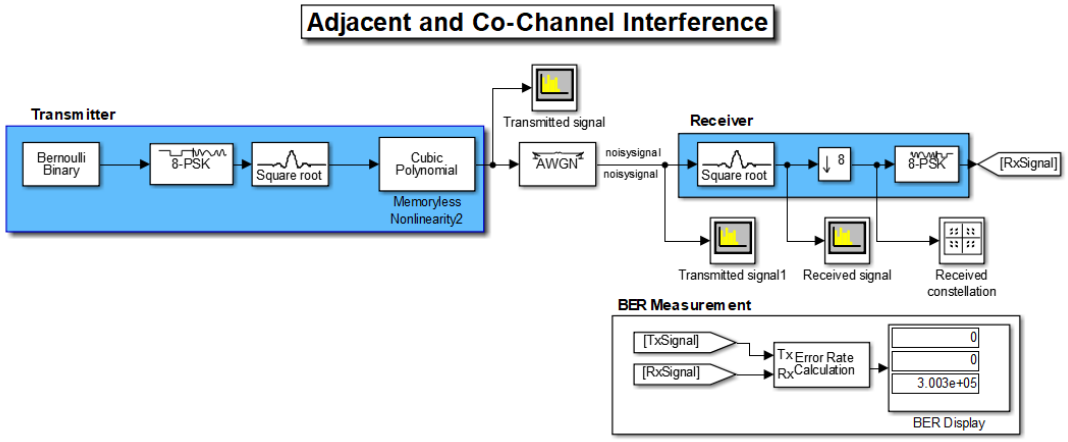

Figure 1.1 Transmitter model using 8-PSK

The simple model consists of a number generator that creates a stream of binary data, this is modulated using 8-bit phase-shift keying and then filtered using a square root filter. The generated signal is then passed through a nonlinear component. Here it is modelled by a box labelled Cubic Polynomial, where the third-order intercept point can be specified.

The output power spectral density for the transmitter is shown in Figure 1.2a and Figure 1.2b when the third order intercept point for the nonlinear block is set to +50dBM and +30dBm respectively.

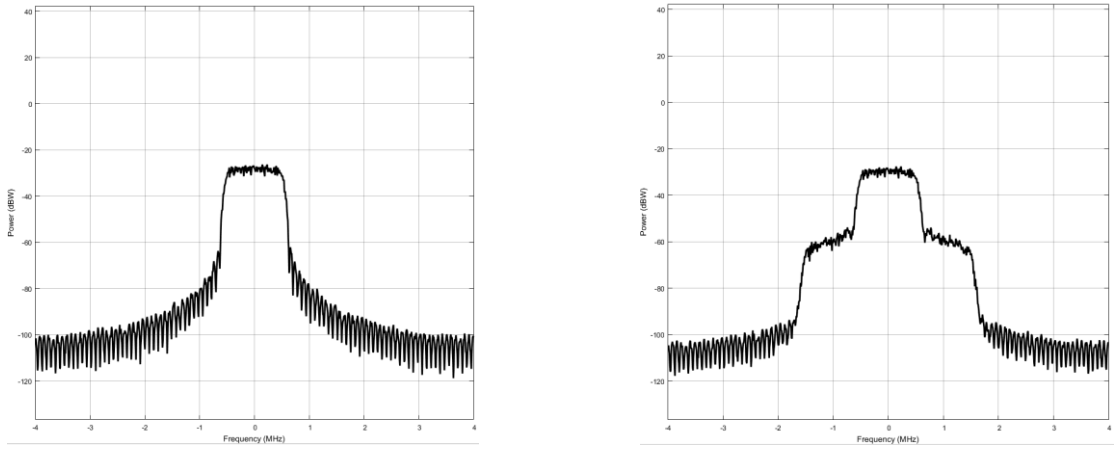

(a) (b)

Figure 1.2 Output power spectral density of transmitter model a) +50dBm IIP3 b) +30dBm IIP3

Comparing the two spectral densities, when the TOI point is +50dBm, the modulated signal extends up to the edge of its band. Reducing the TOI to +30dBm causes spectral regrowth that extends into the channel of other users.

The linearity requirements of the system will vary depending on the modulation scheme used, this model shows a system that uses Phase-shift keying. This will not be as sensitive to nonlinearities as amplitude modulation systems which are more effected by nonlinearities within the system [3]. Systems such as LTE use the OFDM to maximize spectral efficiency, these

multiplexing schemes are sensitive to the nonlinear behavior of components and require careful design work to ensure optimal performance [4,5]

Most research for improving linearity of a transmitter has focused primarily on the amplifier, as this has been the greatest source of nonlinearity in a transmitter chain, with techniques such as backing off the amplifier and digital pre-distortion [6]. There have been limited investigations into reconfigurable antennas and the effects of including nonlinear components.

This research was designed to address what parameters affect the tunability, gain and linearity of a simple reconfigurable patch antenna using varactor diodes and to investigate if there is any relationship between these three properties.

The novel contributions from this work first include the systematic study into the varactor loaded patch antennas investigating the effect on linearity, gain and tunability. This includes the following variations: different permittivity substrates, frequency of operation of patch, varactor placement on patch, number of varactors loading patch antennas and varactor type (Abrupt and Hyperabrupt). This work also includes the first investigation into the use of common cathode varactor topology on microstrip patch antenna for linearity improvement. Lastly, this work investigates the design of a novel frequency tunable antenna using common cathode varactor pairs with optimised parasitic patches for gain improvement across the frequency range.

1.1 References

[1] C. G. Christodoulou, Y. Tawk, S. A. Lane, and S. R. Erwin, “Reconfigurable Antennas for Wireless and Space Applications,” Proceedings of the IEEE, vol. 100, no. 7, pp. 2250–2261, 2012.

[2] A. Kiayani, V. Lehtinen, L. Anttila, T. Lahteensuo, and M. Valkama, “Linearity Challenges of LTE-Advanced Mobile Transmitters: Requirements and Potential Solutions,” IEEE Communications Magazine, vol. 55, no. 6, pp. 170–179, 2017.

[3] K. Entesari and G. M. Rebeiz, “RF MEMS, BST, and GaAs varactor system-level response in complex modulation systems,” International Journal of RF and Microwave Computer-Aided Engineering, vol. 18, no. 1, pp. 86–98, 2007.

[4] “The MobileBroadband Standard,” LTE. [Online]. Available: https://www.3gpp.org/technologies/keywords-acronyms/98-lte. [Accessed: 20-May-2019].

[5] M.Simon, “Interaction of Intermodulation Products between DUT and Spectrum Analyzer,” Rohde & Schwarz, Munchen, Germany, 1MA219_2e, 2012.

[6] O. Hammi, “Efficient Linear Amplification Using Digitally Predistorted Overdriven Power Amplifiers,” IEEE TRANSACTIONS ON BROADCASTING, vol. 63, no. 3, pp. 398–406, Sep. 2015.

2 Literature Review

This section reviews and assesses some of the most commonly seen types of reconfigurable antennas from the literature.

2.1 Reconfigurable Antennas

There are three main parameters that are tunable in antennas, these are frequency, polarization and pattern reconfigurability. The main ways to tune the properties of antennas are to alter its physical shape or change the electrical length of the antenna. This can be done with a variety of means; here the focus is on the use of tunable components. Mechanical tuning is also possible but is generally less amenable to closed loop control and less robust than electronic tuning and may have higher power consumption. The following examples look at the different types of reconfigurability and use examples from the literature to illustrate how this is performed.

2.1.1 Frequency Reconfigurability

One of the simplest methods of frequency tuning is shown in Figure 2.1. A tunable component is attached to a simple microstrip patch antenna, here it is a varactor diode [1]. The cathode of the varactor is soldered onto the patch antenna and the anode is grounded using a via connected to the ground plane. By attaching a varactor diode, the electrical length of the patch antenna can be tuned by altering the capacitance of the diode, which changes the resonant frequency of the patch.

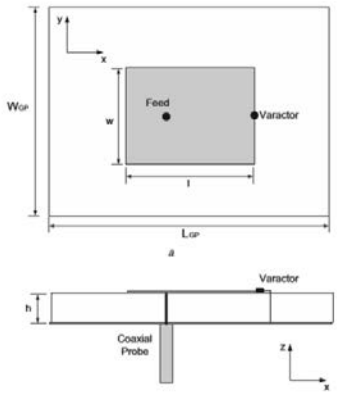

Figure 2.1 Frequency reconfigurable patch antenna using varactor diode [1]

The benefit of using a tunable component such as a varactor diode is that it enables continuous tuning of the resonant frequency of the patch against bias voltage.

This idea of applying varactors to a patch antenna can be extended to achieve multiband operation whilst only tuning one of the bands, an example of this is shown in Figure 2.2. Here the patch antenna is split into two sections that are connected by passive capacitors and a varactor diode, splitting the patch and connecting the two halves using passive capacitors allows a DC bias to be applied to the varactor [2].

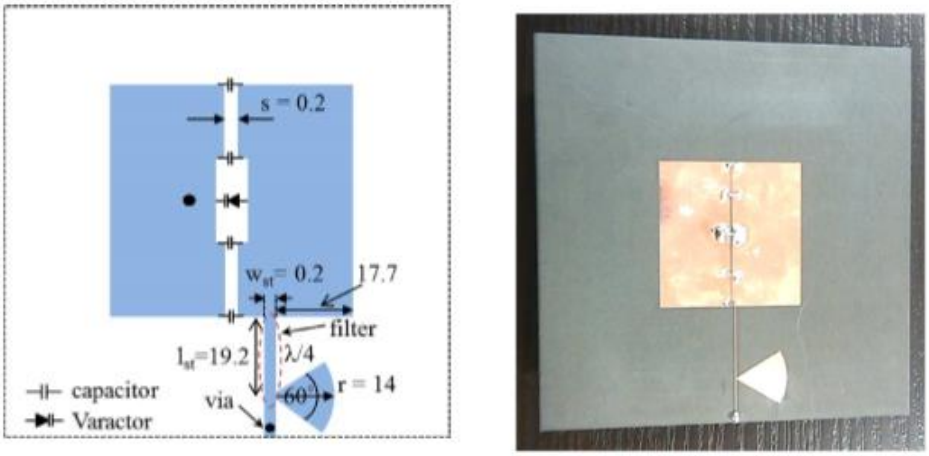

(a) (b)

Figure 2.2 Dual band frequency reconfigurable varactor antenna a) Layout b) Fabricated antenna [2]

While the patch is operating at the lower frequency it effectively does not see the varactor diode and is therefore only weakly affected when the capacitance of the varactor is tuned. At the higher band of operation, current flows through the varactor which makes it more influential and achieves the frequency tuning. It is the adaptability of microstrip patch antennas shown here that make them very popular for reconfigurable antennas.

A commonly seen method to achieve frequency reconfigurability in antennas is to use switches to short out sections of an antenna or to add in additional sections [3]. This is shown in Figure 2.3 where PIN diodes are used to short out sections of a patch-slot antenna. This shortening and lengthening of the slot-antenna increases or decreases the frequency of operation respectively.

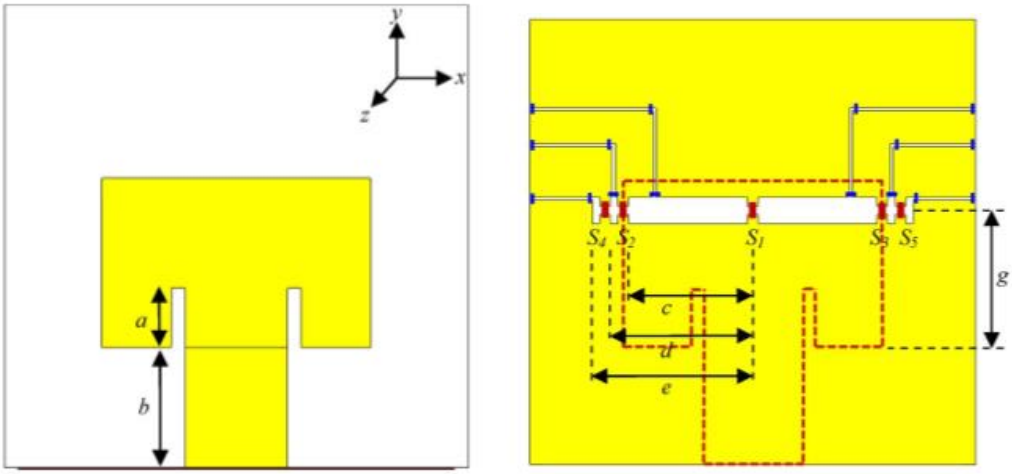

(a) (b)

Figure 2.3 Patch-Slot antenna using PIN diodes to lengthen or shorted resonant slot a) Top Patch b) Resonant slot [3]

A limitation of this type of antenna, that uses switches or PIN diodes to achieve frequency reconfigurability, is that it will only work at distinct frequency bands unlike the continuous frequency tuning offered by varactor in Figure 2.2.

2.1.2 Polarization Reconfigurability

Changing the polarization of an antenna between left- and right-hand circular as well as linear polarization is a technique that can be used by systems to mitigate against fading loss due to multipath effects [4].

Figure 2.4 shows a circular patch antenna that is connected to four sector shaped patches by varactor diodes that can reconfigure both its polarization and frequency characteristics.

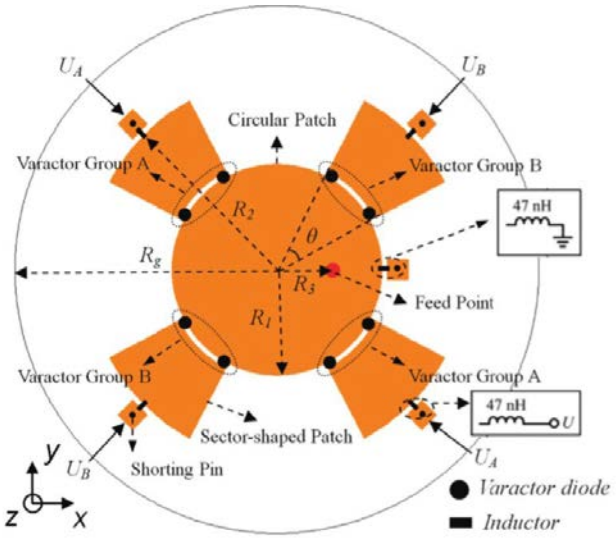

Figure 2.4 Frequency and polarization reconfigurable antenna using varactor diodes [4]

The feed point to the antenna is located within the circular patch to excite both the TM_{10} and TM_{01} modes. The varactors are grouped together diagonally across the circular patch into groups A and B. Each varactor group can be independently biased of the other. This independent bias of the varactor groups allows the patch to either be tuned in frequency, when both groups are biased simultaneously to same capacitance, or tuned in polarization by biasing the varactor groups separately to different capacitances.

The circular polarization orientation can be changed between right- and left-hand by reversing the capacitance values of the two groups of varactors; when the varactors have the same bias, the patch will have linear polarization.

PIN diodes are used to achieve polarization diversity in the antenna shown in Figure 2.5. Two L-shaped slots that can be shorted using the diodes are etched into the edge of a square patch [5].

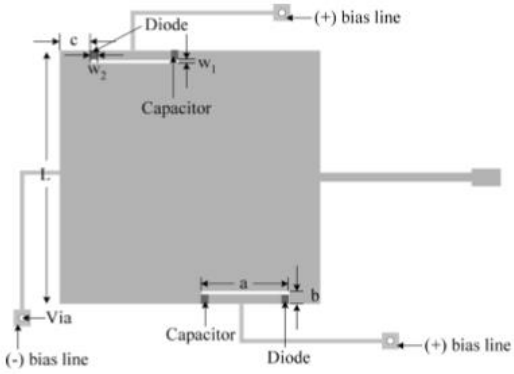

Figure 2.5 Polarization reconfigurable patch antenna using PIN diodes [5]

When the PIN diodes located in the L-slots are reverse biased they are turned off, and the patch exhibits circular polarization. Applying a forward bias to the PIN diodes turns them on allowing electric current to flow through them which transforms the shape of the slots from an L-shape to a rectangular slot. The slots are orientated parallel to the patch edge and thus have a minimal effect on the TM_{10} mode which produces linear polarization.

2.1.3 Pattern Reconfigurability

Changing the radiation pattern of an antenna is a technique that can be used to improve the main beam coverage of a desirable area whilst reducing sources of noise from other directions.

One technique used to manipulate a radiation pattern is to use parasitic reflectors and directors. Figure 2.6 shows a central driven circular patch antenna surrounded by parasitic patches connected to the ground plane via a PIN diode and shorting pin [6].

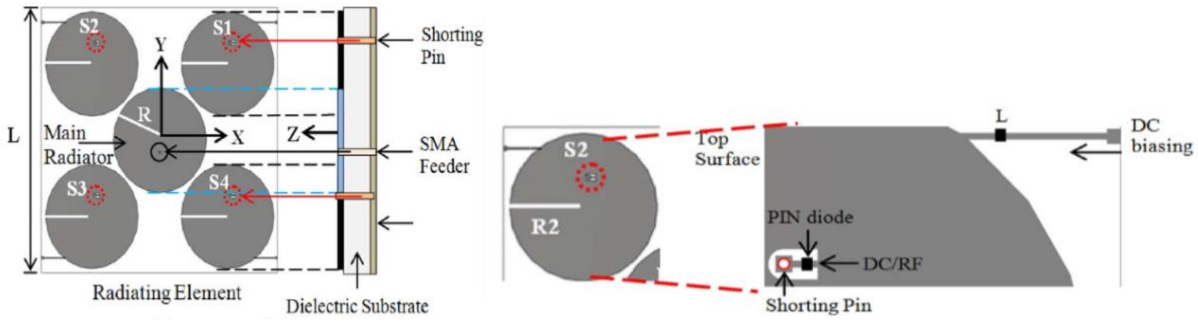

Figure 2.6 Pattern reconfigurable antenna a) Antenna layout b) Close up of PIN diode tuned reflector/director [6]

As the PIN diodes are turned on and off, the parasitic patches act either as a director (PIN diode off) or a reflector (PIN diode on). By biasing the PIN diodes correctly, the radiation pattern can be reconfigured into the desired direction. This type of antenna has discrete directions that the antenna can be reconfigured to, as there are limited configurations provided by the PIN diodes.

A pattern reconfigurable antenna that uses varactor diodes is shown in Figure 2.7. This antenna uses a microstrip patch antenna that has a line of grounded vias across the patch near the centre. Adding this metallic wall of vias creates two cavities that are closely related in resonant frequency. One of the radiating edges of the cavities is loaded with a varactor diode that allows for the electrical length to be tuned, similar to that seen in Figure 2.1.

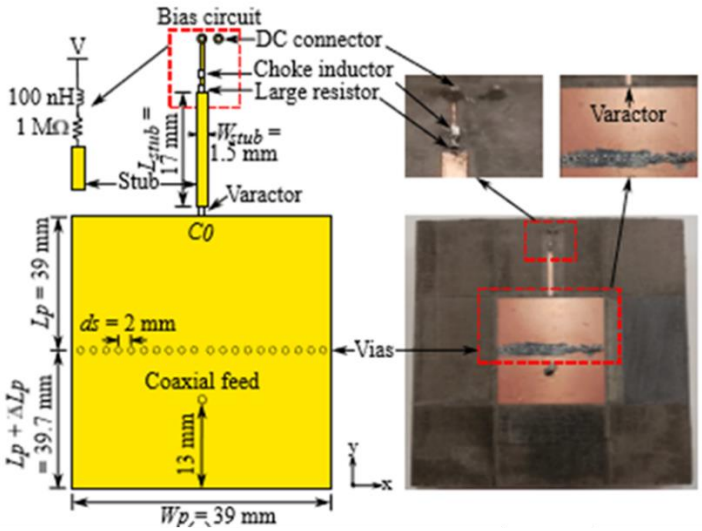

Figure 2.7 A pattern-reconfigurable single-element microstrip antenna [7]

When the electrical length of one of the cavities is altered it creates a phase difference between the two, this phase difference allows for tuning of the radiation pattern. A benefit of this configuration is that the beam is continuously tunable, although it is one direction only.

2.1.4 Antennas with Multiple Reconfigurable Properties

Some antennas are tunable in more than one characteristic which allows for increased adaptability.

Figure 2.8 shows an example of an antenna that can reconfigure both its radiation pattern and its resonant frequency. To achieve this dual reconfigurability both PIN diodes and varactors are utilized.

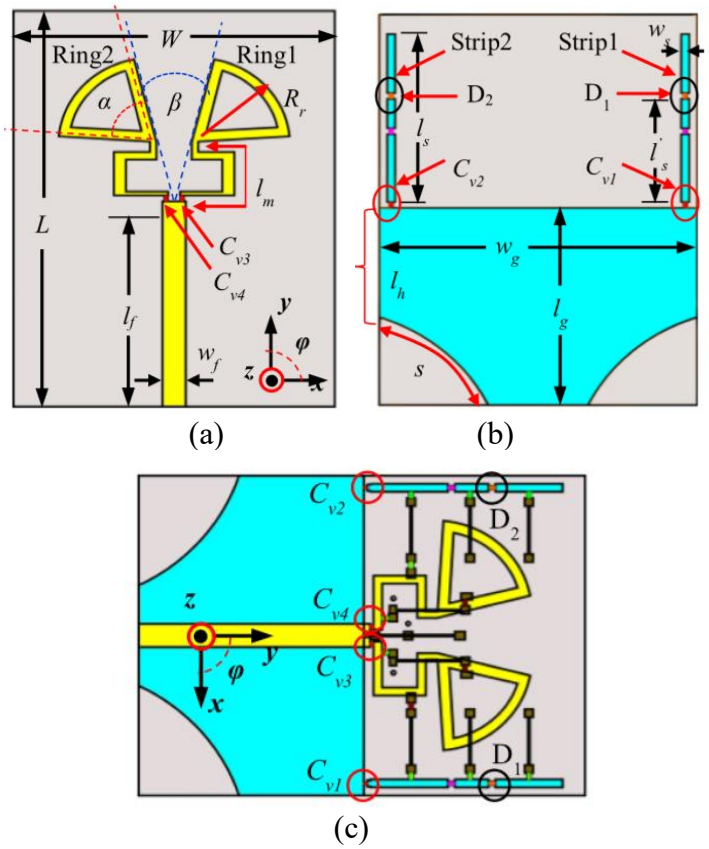

Figure 2.8 Frequency and pattern reconfigurable antenna a) Radiating antenna rings b) PIN and varactor tuned parasitic strips c) Top down view of antenna and ground plane [8]

Two radiating rings form the main antenna (shown in gold). These are connected to a feedline via a U-shaped section with two varactors, C_{v3} and C_{v4}. These two varactors are used to alter the impedance match to the antennas and therefore the operating frequency of the antennas.

The ground plane (shown in blue) is truncated to improve the impedance match to the antenna [8]. There are two parasitic strips that connect to the main body of the ground plane using two varactor diodes C_{v1} and C_{v2}. Two PIN diodes, D_1 and D_2, are included in the strips where they keep any self-resonances in the strips out of the frequency of operation of the antenna.

The varactors C_{v1} and C_{v2} are used for beam steering. When the capacitance of the varactors is high, they connect the strips to the ground plane, and the strip acts as a reflector. Whereas when the varactor capacitance is low, and the PIN diode is off, the strip acts as a director. Utilizing these two different modes of the parasitic strips allows for beam scanning, and when coupled with the frequency tuning facilitated by C_{v3} and C_{v4}, allows for a multifunctional antenna.

These examples highlight that there are a multitude of parameters and different types of antenna that are reconfigurable. The antennas discussed were all variations on a microstrip patch antenna, this type of antenna is very well adapted for tunability using components as they are easily integrated.

2.2 Linearity Investigations of Antennas

In the examples shown in Section 2.1 there was no discussion of the linearity performance of the antennas. This section will summarize the major investigations into the linearity of reconfigurable antennas to date.

2.2.1 PIN Diode Tuned Antennas

Figure 2.9 shows an antenna that works at the WLAN and GSM bands that uses a PIN diode to tune the frequency. The required power levels for GSM and WLAN are +39dBm and +30dBm respectively [9].

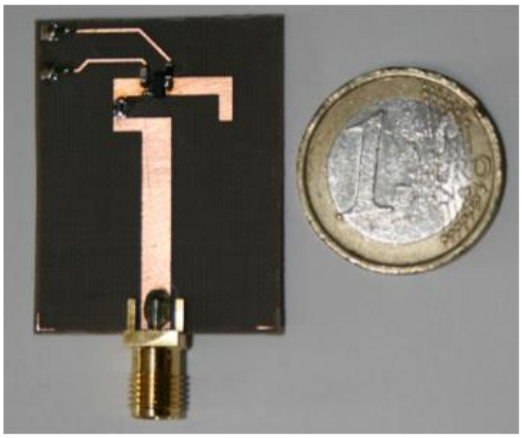

Figure 2.9 PIN diode tuned antenna [9]

A single-tone test was performed at 2.45GHz. It was found that the antenna went into gain compression at an applied power level of +14dBm. Two-tone testing of the antenna gave a TOI point of +26dBm showing that the antenna would be unable to operate up to the specified power levels without degraded performance. There was no investigation to see if the linearity performance could be improved.

Figure 2.10 shows a pair of frequency tunable slot antennas for MIMO that use two PIN diodes, D_1 and D_2. The PIN diodes act to change the electrical length of the slot. When the diode in the slot is turned on, the slot length decreases and the antenna operates at 1050MHz. Turning off the diode in the slot increases the slot length and the antenna works at 800MHz.

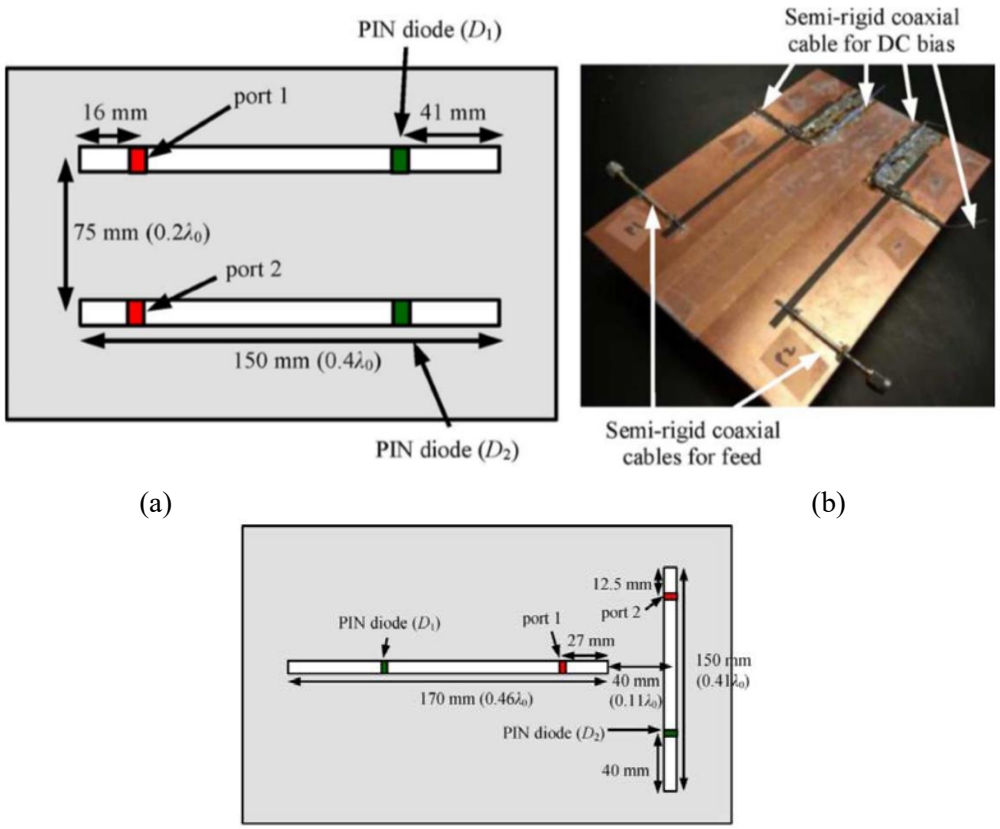

Figure 2.10 Frequency tunable MIMO antenna a) Parallel slot configuration b) Fabricated antenna c) Rotated slot configuration for reduced mutual coupling [10]

The two-tone test was undertaken by feeding one slot with an 840MHz tone with the PIN diode off whilst feeding the second slot antenna with a 1100MHz signal and the PIN diode on. Mutual coupling between the slots allowed the signals to interact and generated intermodulation products.

It was found that the linearity performance of the antenna was worse in transmit mode when compared to receive mode. This is attributed to the higher power levels that are incident on the antenna in transmit. To reduce nonlinear effects, it was shown that the PIN diodes should be completely turned off by applying a reverse bias.

By reducing the mutual coupling between the slots, the IMD products where reduced. This was achieved by rotating the second slot ninety degrees as shown in Figure 2.10c.

This investigation could be taken further by applying two closely spaced tones at both the 800MHz and 1050MHz bands and test them on a single slot one at a time. It would then be possible to compare the third order intercept points, measured at each frequency band, to see if the nonlinear performance of the antennas is frequency dependent.

2.2.2 Varactor Tuned Antennas

One of the most complete investigations of nonlinearities in frequency tunable antennas using varactors was undertaken in [11]. In this investigation two identical microstrip patches with a gap across the centre for the varactors were fabricated as shown in Figure 2.11.

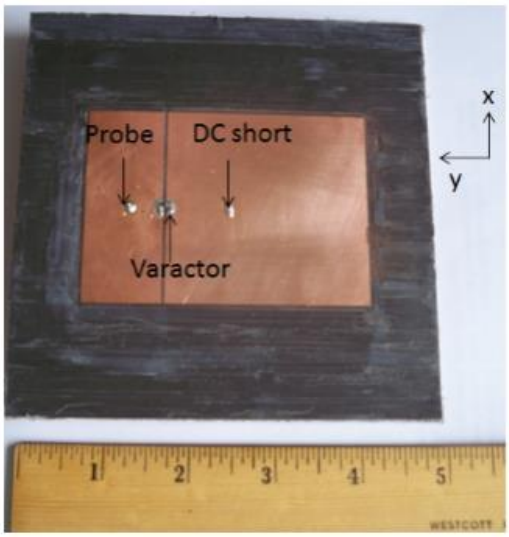

Figure 2.11 Frequency tunable patch antenna using varactor diodes [11]

The varactors placed in the gap allow for frequency tuning and two different varactors were investigated, the SMV1233 and SMV1235. These diodes were selected because of their difference in bias voltage ranges while having similar capacitance values. For comparable values of capacitance, the SMV1233 requires an applied bias of $0V \leq V_{bias} \leq 2V$ and the SMV1235 requires an applied bias of $4V \leq V_{bias} \leq 15V$.

The two antennas were tested using the two-tone test at 1.175GHz which corresponds to a bias voltage of 0V on the SMV1233 varactor and 3.95V on the SMV1235 varactor. It was found that

the SMV1235 diode with the larger bias voltage had better linearity performance compared to the SMV1233 diode.

Both antennas performed more linearly when in receive mode than in transmit mode. This is similar to the slot antennas loaded with PIN diodes [10].

The two-tone testing was repeated using higher bias voltages. The new bias voltages of 1.65V and 15V was applied to the SMV1233 and SMV1235 varactors respectively, this increases the antennas operating frequency to 1.35GHz. Increasing the bias voltage improves the linearity of the two antennas, as shown by an improvement of +7.1dBm in their respective third-order intercept points.

Additional tests were undertaken to measure the gain compression of the antennas using a single tone at 1.175GHz. The antenna with the SMV1233 diode starts to exhibit signs of gain compression at an applied power level of -2dBm while the SMV1235 diode showed no significant gain compression up to the maximum value applied of +5dBm.

This investigation shows that the linearity performance of a varactor-tuned antenna can be improved by using a varactor that is biased with a higher voltage for the same capacitance as that of an antenna using a varactor with a lower bias voltage. One consideration to be taken with this work is, that by having different applied bias voltages the varactors are not at the same points on their respective C-V curves. It is potentially this property that achieves the improved linearity performance as opposed to the magnitude of DC bias voltage. Typically, the gradient of a varactor's C-V curve becomes shallower as bias voltage is increased.

Having the SMV1233 diode biased with 0V will allow the diode to alternate between forward and reverse bias by an applied RF signal, the behavior in this mode of operation may be

contributing to the poor linearity performance. In contrast, the SMV1235 diode biased with 3.95V for the same RF signal will potentially maintain its operation in the reverse bias mode. A more application specific antenna is shown in Figure 2.12. This is a frequency tunable microstrip slot radiator antenna using varactors for use in mobile phones.

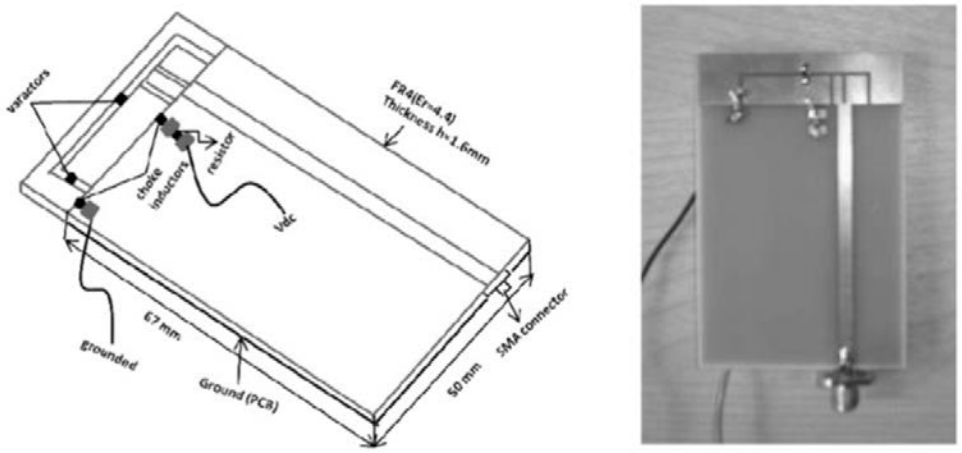

(a) (b)

Figure 2.12 Frequency tunable slot antenna for mobile handset a) Design b) Fabricated antenna [12]

The antenna operates at frequency points 1.7, 1.8, 1.9, 2.04GHz. A single tone was applied at each of the frequency points and the second and third harmonic tones generated were measured for five different power levels, -7, +3.5, +13.5, +18 and +21dBm.

To assess the harmonic performance a circuit model of the varactor was simulated in ADS using the harmonic balance simulation. The magnitude of the harmonic power levels generated by the simulation were entered into a HFSS model as a voltage source. The three-dimensional model of the antenna was then simulated to get the radiated power levels of the harmonics. The results of these simulations in ADS and HFSS were then combined and entered into the Friis equation [12] to calculate the power at the receiver. The simulated results of the antenna were compared to the measured harmonic power levels and a close agreement was found.

When comparing the measured second harmonic power levels for equivalent applied power levels, there was no significant difference as the frequency of operation of the antenna was changed. The third harmonics generated did show a reduction in measured power levels as the frequency of operation increased, which is expected as the varactors will be biased into a more linear region of their C-V curves.

In all of these investigations into tunable antennas there has not been any extensive research into what factors of the antenna design effect the tunability, the radiation characteristics or the nonlinear performance. When antennas using different tunable components have been compared for their linearity characteristics, there has not been a direct comparison at the same frequency with the diodes in comparable states of operation. Frequently, the antennas investigated have been complex; designed for a specific application such as Wi-Fi or GSM. This makes it difficult to ascertain what influences the different properties of tunability, gain and linearity.

2.3 Review of Tunable Components

There are two main types of tunable component used in reconfigurable antennas: components that have tunable reactance, most commonly this is from a tunable capacitance; and components that act as a switch. This section discusses the different types of components that are most commonly used to achieve these two tuning mechanisms and their strengths and weaknesses.

2.3.1 Reactive Tunable Components

These tunable components work by adding reactance to antennas which increase the electrical length in frequency tunable antennas.

2.3.1.1 Varactor Diodes

Discovery of these types of diodes occurred in the 1940s [13] and they have been consistently improved along with developments in manufacturing technology which means they are a mature technology. Varactor diodes are widely available and can be ordered online from major vendors in a variety of packages, wide range of capacitance tuning ratios, and bias voltages. This availability makes this tunable component very popular for reconfigurable devices including antennas.

Varactor diodes are formed by combining P- and N-type semiconductor materials, normally Silicon or Gallium Arsenide, to form a PN junction where they meet. The junction forms a depletion layer which creates a capacitance between the two semiconductor materials. Applying a reverse DC bias voltage increases the depletion layer width which reduces the capacitance [14]. A more in-depth analysis of varactor diodes is undertaken in Chapter 3.

The Q-factor of varactors is dependent on many factors such as the materials used in the construction and the doping profile to achieve the required tunability and breakdown voltage of the diode [15]. The Q-factor of varactors is very high at low frequencies, typically the Q-factor value is measured at 50MHz. As the frequency of operation increases the Q-factor reduces proportionally, this limits varactor diodes to frequencies below 10GHz [16]. One advantages varactor diodes have is that the tuning speed is very fast compared to other tunable components.

2.3.1.2 Dielectric Tunable Varactors

Dielectric tunable varactors are a type of varactor that will typically use a ferroelectric material for its tunable dielectric constant properties to achieve a variable capacitance [17]. Increasing an applied DC electric field to a ferroelectric material will reduce the dielectric constant which will in turn reduce the capacitance of the varactor.

The two main types of dielectric varactor are shown in Figure 2.13. A metal-insulator-metal varactor is shown in Figure 2.13a, this configuration has a layer of ferroelectric material sandwiched between two electrodes to form the varactor. The second configuration is the coplanar varactor as shown in Figure 2.13b and 2.13c. To form this type of varactor the two electrodes are closely spaced using interdigital fingers.

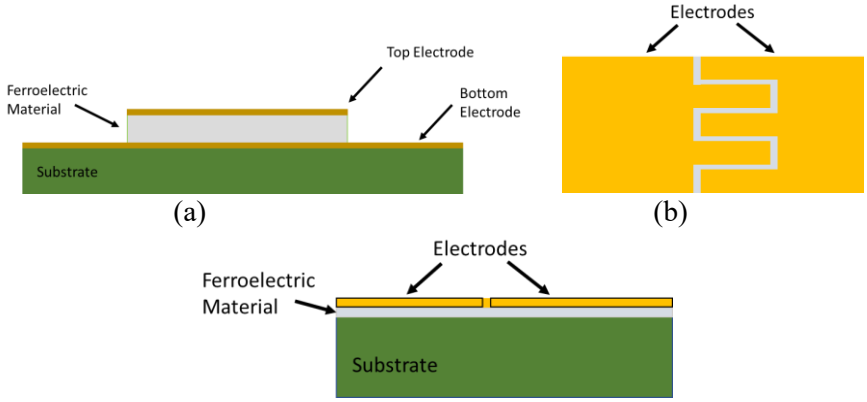

Figure 2.13 Main two configurations of dielectric tunable varactors a) Side profile of MIM varactor b) Top down view of coplanar interdigitated varactor c) Side profile of coplanar interdigitated varactor (Adapted from [17])

The benefit of the coplanar varactor is the simpler fabrication process, compared to the MIM varactor but comes at a cost of lower tuning range for the same applied E-field.

The benefit of ferroelectric varactors over the semiconductor varactor diodes are that they have higher Q-factors in the microwave and millimeter ranges, whilst having a lower power consumption [17].

A comparison of linearity performance between ferroelectric varactors and GaAs varactors was undertaken by Rebeiz et al and it was found that their performance was similar [18]. To improve the linearity performance the number of ferroelectric varactors used was increased to three, they were scaled in size to achieve the same capacitance value of the single varactor. Increasing the varactor number gave an increase in the TOI point by +10dBm [18]. This improvement comes from distributing the RF voltage across all the varactors rather than a single device [19].

One major drawback of ferroelectric varactors is their lack of availability commercially. This is reflected in the literature as the number of antennas that use this tuning component is lesser in number than the varactor diode.

2.3.2 Switching Components

Switching components are used to add, remove and short out sections of an antenna. The most important parameters for this are the insertion loss that will be added when they are used as a short circuit and the amount of isolation they provided when used as an open circuit.

2.3.2.1 RF MEMS

These are devices that use mechanical actuation of a metallic arm or bridge to create either a physical connection or a change in capacitance. Figure 2.14 shows a diagram of a lever arm in an inline configuration to create a switch. Other configurations such as broadside and capacitive shunt switches are also available [20]. When the arm is raised there is no physical connection as shown in Figure 2.14a, so the switch is an open circuit. Figure 2.14b shows the arm when it has been lowered, the switch is now a short circuit. There are different mechanisms to provide the actuation of the arm, such as electrostatic, magnetostatic, piezoelectric and thermal. The most reliable method and commonly used of these is electrostatic [20].

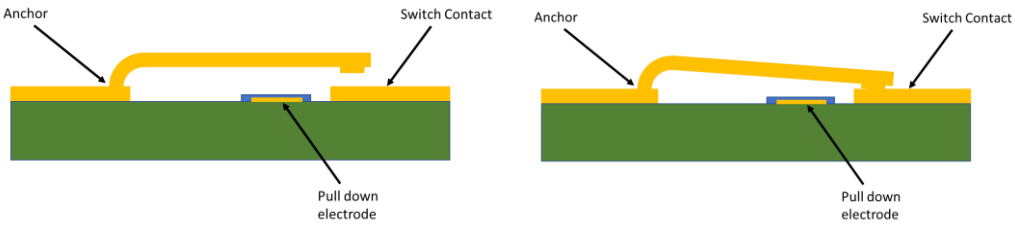

(a) (b)

Figure 2.14 Inline MEMS switch a) Open circuit b) Short circuit (Adapted from [20])

The benefits of RF MEMS switches are: that they can have low insertion loss at microwave and millimetre wave frequencies; consume a small amount of power; provide good isolation; and have good linearity performance [18, 20, 21].

The disadvantages of this technology are that the switching speeds are slow and the voltages required for actuation are high [20]. At present the devices are not widely available and the few products that are sold have a high cost compared to other switching components such as PIN diodes [22].

2.3.2.2 PIN Diodes

PIN diodes are a mature technology and are readily available, they are found in a variety of microwave devices such as attenuators and switches [23]. A diagram of a PIN diode construction and equivalent circuits of forward and reverse bias is shown in Figure 2.15. The diode consists of N^+ and P^+ material that is separated by an intrinsic layer. This intrinsic layer will ideally be formed of a Silicon crystal structure completely devoid of any impurities which is encapsulated in a protective glass layer as shown in Figure 2.15a [24].

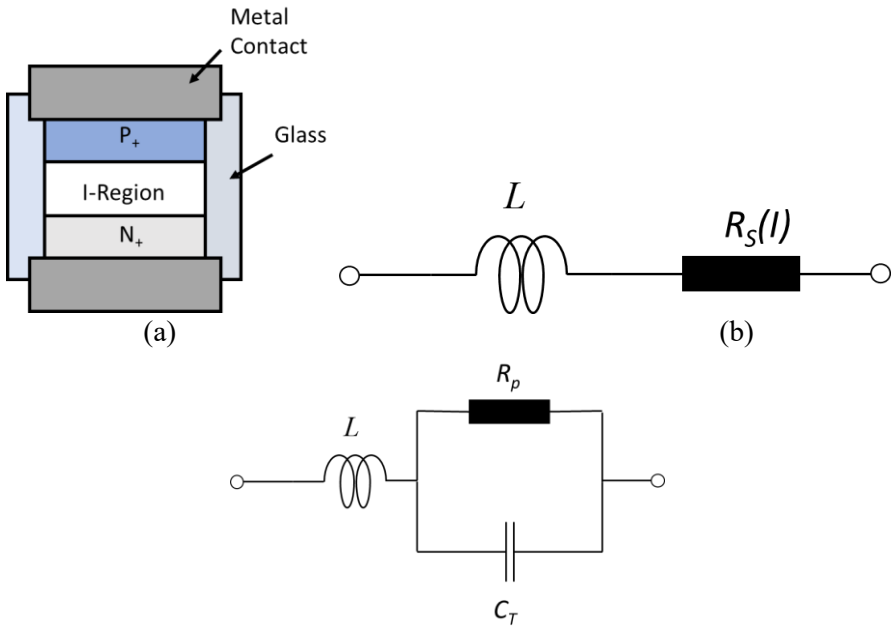

Figure 2.15 PIN diode a) Physical construction b) Forward bias equivalent circuit c) Reverse bias equivalent circuit (Adapted from [24])

When the PIN diode is forward biased it acts as a current controlled resistor. An equivalent circuit model of this mode is shown in Figure 2.15b. The value of $R_s(I)$ is dependent on the

amount of forward current; as the current increases the series resistance decreases. The inductance of the PIN diode, L, is dependent on the geometry of the device [24].

Applying a reverse bias to the diode results in no charge being stored within the I-region creating a capacitance, C_T, and a parallel resistance, R_p [24]. This stops the diode conducting and acts as an open circuit, an equivalent circuit model is shown in Figure 2.15c.

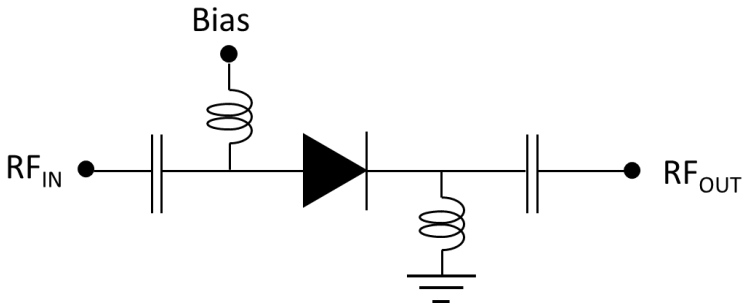

Figure 2.16 PIN diode in series switch configuration (Adapted from [24])

Figure 2.16 shows a PIN diode being used as a series switch. This is a common configuration for the PIN diode in reconfigurable antennas. The insertion loss for PIN diode given in Figure 2.16 is given by [24]:

$$IL = 20\log\left[1+\frac{R_s}{2Z_0}\right] \tag{1}$$

where:

IL : Insertion loss of PIN diode, dB

R_s : Series resistance of forward biased PIN diode, Ω

Z_0 : Characteristic impedance of system, Ω

The isolation provided by a PIN diode in a series configuration is given by [24]:

$$I = 10\log[1 + (4\pi fCZ_0)^{-2}] \tag{2}$$

where:

I : Isolation provided by PIN diode, dB

f : Frequency of operation, Hz

C : Reverse bias capacitance, F

Table 2.1 shows the theoretical difference in insertion loss and isolation using the extracted circuit parameters for two commercial diodes when used as a series switch at 2.4GHz in a 50Ω system.

Table 2.1 Calculated insertion loss and isolation PIN diodes

Diode	C_T (pF) V_R=10V	Rs (Ω) I_F=20mA	Insertion Loss (dB)	Isolation (dB) f=2.4GHz
GMP4201[25]	0.18	1.20	0.10	11.64
GMP4215 [25]	0.60	0.50	0.04	3.47

Decreasing the series resistance of the diode in forward bias reduces the insertion loss of the device. This is traded against the increase of the reverse bias capacitance, which will reduce the isolation as shown in Table 2.1.

Investigations into PIN diode linearity show that it is an important characteristic to be considered in both forward and reverse bias [26]. It is found that when PIN diodes are reverse biased there is a capacitance dependence on the reverse bias voltage, similarly to varactor diodes. The C-V dependence comes from a gradient in the doping of the P^+ and N^+ semiconductor [26]. An applied RF signal of sufficient power level will modulate the C-V curve causing harmonics and IMD products. This effect can be reduced by using a thicker diode [26]. The nonlinear behaviour

exhibited by reverse biased PIN diodes increases with the frequency of operation. To improve the linearity performance the reverse bias should be increased [10,26].

When the PIN diode is forward biased the nonlinear performance is also dependent on the construction of the diode. In a series configuration as shown in Figure 2.16, it is found that the nonlinear behaviour improves as the frequency of operation is increased, and the I-region thickness is decreased [27].

The turn-on time of a PIN diode is in the region of <1μS, which is quicker than the RF MEMS switches as there is no mechanical actuation involved but is slower than the varactors discussed previously [17].

2.4 Summary

Reviewing the current literature available on the linearities and performance of tunable antennas, it was shown that further investigation is required to understand how antenna design effects the different antenna properties of tunability, gain and linearity when combined with a nonlinear tunable component.

The area to be investigated in this thesis is frequency reconfigurability, as it is one of the simpler and most popular types of reconfigurable antenna. It was decided that a patch antenna loaded with a varactor diode is to be used, as they were identified as some of the most common type of reconfigurable antenna.

The research questions to be investigated with relation to the frequency tuning range, gain of the antenna and linearity performance were:

- How do the frequency and substrate affect the tunability, gain and linearity of a varactor tuned patch antenna?
- How does the location of the varactors on the radiating and non-radiating edge affect tunability, gain and linearity?
- How does the number of varactors affect the tunability, gain and linearity of a varactor tuned patch antenna?
- How do different varactor types affect the tunability, gain and linearity?
- Is there a configuration of varactors that improves all three of these parameters?

2.5 References

[1] C. Kalialakis and P. S. Hall, “Analysis and experiment on harmonic radiation and frequency tuning of varactor-loaded microstrip antennas," IET Microw. Ant. and Prop., vol. 1, no. 2, pp. 527-535, 2007.

[2] A. Khidre, F. Yang, and A. Z. Elsherbeni, “A patch antenna with a varactor-loaded slot for reconfigurable dual-band operation,” IEEE Transactions on Antennas and Propagation, vol. 63, pp. 755–760, Feb 2015.

[3] H. A. Majid, M. K. A. Rahim, M. R. Hamid, N. A. Murad, and M. F. Ismail, “Frequency reconfigurable microstrip patch-slot antenna,” IEEE Antennas Wireless Propag. Lett., vol. 12, pp. 218–220, 2013.

[4] H. Gu, J. Wang, L. Ge, and L. Xu, “A reconfigurable patch antenna with independent frequency and polarization agility,” Journal of Electromagnetic Waves and Applications, vol. 33, no. 1, pp. 31–40, 2018.

[5] Y. J. Sung, “Reconfigurable Patch Antenna for Polarization Diversity,” IEEE Transactions on Antennas and Propagation, vol. 56, no. 9, pp. 3053–3054, 2008.

[6] M. Jusoh, T. Aboufoul, T. Sabapathy, A. Alomainy, and M. R. Kamarudin, “Pattern-Reconfigurable Microstrip Patch Antenna With Multidirectional Beam for WiMAX Application,” IEEE Antennas and Wireless Propagation Letters, vol. 13, pp. 860–863, 2014.

[7] S. N. M. Zainarry, S. J. Chen, and C. Fumeaux, “A Pattern-Reconfigurable Single-Element Microstrip Antenna,” 2018 IEEE Radio and Antenna Days of the Indian Ocean (RADIO), 2018.

[8] M. S. Alam and A. Abbosh, “A Compact Reconfigurable Antenna With Wide Tunable Frequency and 360° Beam Scanning,” IEEE Antennas and Wireless Propagation Letters, vol. 18, no. 1, pp. 4–8, 2019.

[9] R. Goncalves, N. B. Carvalho, and P. Pinho, “Intermodulation in active reconfigurable antennas,” 2014 International Workshop on Integrated Nonlinear Microwave and Millimetre-wave Circuits (INMMiC), 2014.

[10] J.-B. Yan, S. Yong, and J. T. Bernhard, “Intermodulation and Harmonic Distortion in Frequency Reconfigurable Slot Antenna Pairs,” IEEE Transactions on Antennas and Propagation, vol. 62, no. 3, pp. 1138–1146, 2014.

[11] S. Yong, “Design and Analysis of Pattern Null Reconfigurable Antennas,” Ph.D dissertation, Dept. Electr. Comput. Eng., Univ. Illinois at Urbana-Champaign, Urbana, IL, 2012.

[12] I. Elfergani, T. Sadeghpour, R. Abd-Alhameed, A. Hussaini, J. Noras, S. Jones, and J. Rodriguez, “Reconfigurable antenna design for mobile handsets including harmonic radiation measurements,” IET Microwaves, Antennas & Propagation, vol. 6, no. 9, p. 990, 2012.

[13] M. Norwood and E. Shatz, “Voltage variable capacitor tuning: A review,” Proceedings of the IEEE, vol. 56, no. 5, pp. 788–798, 1968.

[14] K. E. Mortensen, Variable Capacitance Diodes, Artech House, 1974.

[15] M. P. J. Tiggelman, K. Reimann, F. V. Rijs, J. Schmitz, and R. J. E. Hueting, “On the Trade-Off Between Quality Factor and Tuning Ratio in Tunable High-Frequency Capacitors,” IEEE Transactions on Electron Devices, vol. 56, no. 9, pp. 2128–2136, 2009.

[16] SKYWORKS, Appl. 200824 Rev A, Aug 2008

[17] S. Gevorgian, Ferroelectrics in Microwave Devices, Circuit and Systems Physics, Modelling, Fabrication and Measurements, London: Springer, 2008

[18] K. Entesari and G. M. Rebeiz, “RF MEMS, BST, and GaAs varactor system-level response in complex modulation systems,” International Journal of RF and Microwave Computer-Aided Engineering, vol. 18, no. 1, pp. 86–98, 2007.

[19] J.-S. Fu, X. A. Zhu, J. D. Phillips, and A. Mortazawi, “Improving Linearity of Ferroelectric-Based Microwave Tunable Circuits,” IEEE Transactions on Microwave Theory and Techniques, vol. 55, no. 2, pp. 354–360, 2007.

[20] G. Rebeiz and J. Muldavin, “RF MEMS switches and switch circuits,” IEEE Microwave Magazine, vol. 2, no. 4, pp. 59–71, 2001.

[21] L. Dussopt and G. Rebeiz, “Intermodulation distortion and power handling in RF MEMS switches, varactors, and tunable filters,” IEEE Transactions on Microwave Theory and Techniques, vol. 51, no. 4, pp. 1247–1256, 2003.

[22] Analog Devices, “SP4T, MEMS Switch with Integrated Driver”, ADGM1004 Datasheet Rev B, 2018

[23] K. Kobayashi, A. Oki, D. Umemoto, S. Claxton, and D. Streit, “GaAs HBT PIN diode attenuators and switches,” 1993 IEEE MTT-S International Microwave Symposium Digest, pp. 151–154, 1993.

[24] Microsemi Corporation, THE PIN DIODE CIRCUIT DESIGNERS’ HANDBOOK, Microsemi, 1998.

[25] Microsemi Corporation, “GigaMite Surface Mount PIN & Limiter Diodes,” GMP4201-GML4701 datasheet, 2007.

[26] R. Caverly and G. Hiller, “Distortion in microwave and RF switches by reverse biased PIN diodes,” IEEE MTT-S International Microwave Symposium Digest, pp. 1073–1076, Jun. 1989.

[27] R. Caverly and G. Phaneuf, “Nonlinear and transient microwave and RF modeling of the PIN diode,” IEEE International Symposium on Circuits and Systems, pp. 2209–2214, 1989.

3 Background Theory of Patch Antennas

This section discusses the microstrip patch antenna modelling techniques and theory of varactor diodes for use in this investigation.

3.1 Microstrip Patch Antenna

The microstrip patch antenna is a common antenna type that is very versatile and is adaptable to many different configurations to suit the requirements of a system.

The main advantages of microstrip patch antennas are:

- Low profile; this make them suitable for applications requiring good aerodynamic performance e.g. Spacecraft, satellites
- Inexpensive
- Planar configuration allows for each integration with surface mount components

The main disadvantages of microstrip patch antennas are:

- Low bandwidth, caused by high Q-factor
- Low gain
- Low efficiency
- Excitation of surface waves

3.2 Modelling Techniques

This section will look at the main models used with microstrip patch antennas and assesses their effectiveness in designing antennas that are loaded with varactors.

3.2.1 Transmission-Line Model

The simplest model used to design patch antennas is the transmission-line model [1]. This represents the patch as a transmission line with characteristic impedance Z_c, that separates two radiation slots. A simple edge fed patch is shown in Figure 3.1a with a length, *L* and width, *W*.

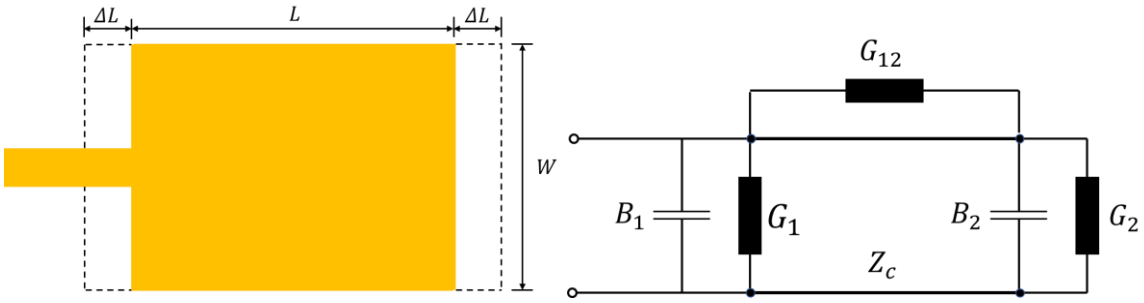

Figure 3.1 Transmission line model for patch antenna a) Top down view of edge fed microstrip patch antenna with extension from fringing E-Fields b) Equivalent circuit model (Adapted from [1])

As well as the physical patch being represented by a length *L*, the fringing fields at the radiating edges of a patch need to be considered in the model. This is done using an effective dielectric constant given by:

$$\varepsilon_{reff} = \frac{\varepsilon_r + 1}{2} + \frac{\varepsilon_r - 1}{2}\left[1 + 12\frac{h}{W}\right]^{-1/2} \tag{3}$$

where:

ε_r : Dielectric constant of substrate

h : Height of substrate, m

W : Width of patch, m

The fringing fields are now accounted for using the effective dielectric constant to calculate an effective increase in length, shown in Figure 3.1a denoted by ΔL.

This effective length is calculated using:

$$\Delta L = 0.412h\frac{(\varepsilon_{reff}+0.3)\left(\frac{W}{h}+0.264\right)}{(\varepsilon_{reff}-0.258)\left(\frac{W}{h}+0.8\right)} \tag{4}$$

The extra length contributed from the fringing fields needs to be removed to correctly calculate the required patch length for the desired frequency, this is done using:

$$L = \frac{\lambda_g}{2} - 2\Delta L \tag{5}$$

where:

λ_g : Wavelength in substrate, m

To calculate the input impedance of the patch with a microstrip edge feed, two radiating slots with admittance values are used to model the edge effects. These models consist of a conductance, G and susceptance, B as shown in Figure 3.1b.

Equations 6 and 7 are used to calculate the equivalent conductance and susceptance for a finite slot of width, W [1].

$$G_1 = \frac{W}{120\lambda_0}\left[1-\frac{1}{24}(k_0 h)^2\right] \qquad \frac{h}{\lambda_0} < \frac{1}{10} \tag{6}$$

$$B_1 = \frac{W}{120\lambda_0}\left[1-0.636\ln(k_0 h)\right] \qquad \frac{h}{\lambda_0} < \frac{1}{10} \tag{7}$$

where:

λ_0 : Free space wavelength, m

k_0 : Free space wavenumber

Assuming that the radiating slots can be modelled the same due to antenna symmetry.

$$Y_2 = Y_1, \; G_2 = G_1, \quad B_2 = B_1$$

There is a mutual conductance between the two radiating slots as shown in the equivalent transmission line model in Figure 3.1b. Equation 8 is used to calculate this mutual conductance.

$$G_{12} = \frac{1}{120\pi^2} \int_0^{\pi} \left[\frac{\sin\left(\frac{k_0 W}{2}\cos\theta\right)}{\cos\theta} \right] J_0(k_0 L \sin\theta) \sin^3\theta \, d\theta \tag{8}$$

The calculated conductances for the slots and mutual conductance between them, can now be used to find the input resistance using Equation 9.

$$R_{in} = \frac{1}{2(G_1 \pm G_{12})} \tag{9}$$

In Equation 9 the + sign denotes odd modes of the field distribution beneath the patch and the – sign denotes even mode distribution.

This model has its limitations in that it is only able to provide the resonant frequency and input resistance and will not provide a radiation pattern. The transmission line model is capable of modelling varactors on the radiating edge [2,3] but cannot model the antenna when varactors are placed on the non-radiating edges of the antenna.

3.2.2 Cavity Model

The cavity model treats a rectangular microstrip patch antenna as a rectangular cavity loaded with a dielectric material with a constant of ε_r, this is shown in Figure 3.2. The patch and ground plane are modelled as electric conductors, while the edges along the perimeter will be modelled as magnetic conductors which approximate an open circuit [1]. It is assumed that there is no variation of the electric field along the X-axis in Figure 3.2.

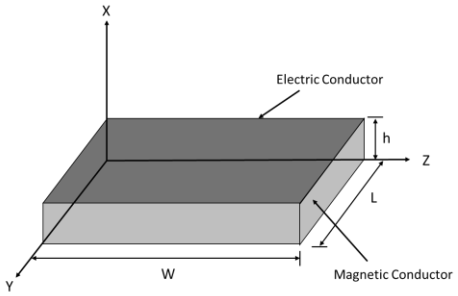

Figure 3.2 Cavity model of a microstrip patch antenna (Adapted from [1])

The resonant frequency of the antenna based on the modes supported in the cavity are given by [1]:

$$(f_r)_{mn} = \frac{1}{2\pi\sqrt{\varepsilon\mu}}\sqrt{\left(\frac{m\pi}{W}\right)^2 + \left(\frac{n\pi}{L}\right)^2} \tag{10}$$

Where m = 0, 1 , 2... and n = 0, 1, 2… and m=n≠0.

The cavity model can calculate the radiation patterns of patch antennas including higher order modes, unlike the transmission line model [4]. This model, while more capable that the transmission line model, is unable to support the addition of varactor diodes. Therefore, it is not suitable for the investigations reported in this thesis.

3.2.3 Commercial Modelling Packages

As neither of the most commonly used models for microstrip patch antennas are suitable for this investigation, the commercial simulation package CST is to be used [5]. Powerful commercially available electromagnetic simulation packages such as CST, HFSS and Sonnet can model more complex shapes of microstrip antennas, such as those shown in Figure 3.3a. This approach is also more accurate and widely used than both the transmission line and cavity model.

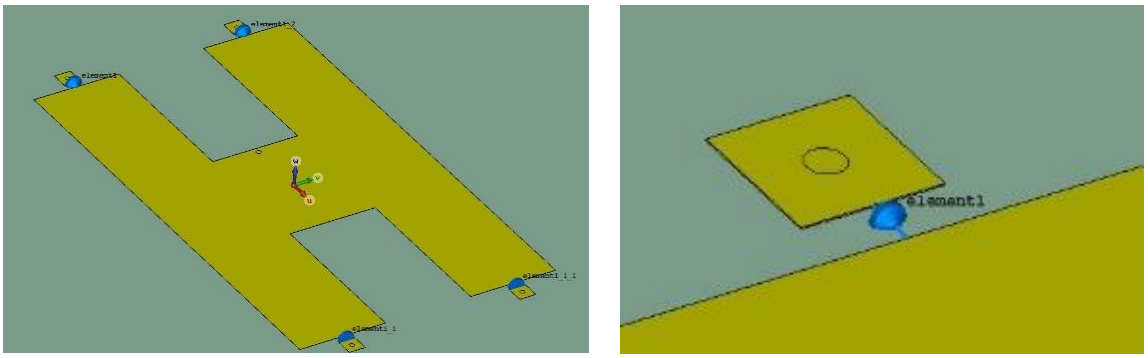

(a) (b)

Figure 3.3 Models generated in CST a) H-shaped varactor loaded microstrip patch antenna b) Varactor modelled in CST

These packages can also deal with tunable components placed on both the radiating and non-radiating edges. A varactor is modelled as a capacitance, inductance and resistance and is inserted into the model as shown in Figure 3.3b. The two ends of varactor diode equivalent model are attached to the section of the patch where the anode and cathode are to be soldered.

3.3 Varactor Diode

The varactor diode is a type of diode that exploits the PN junction to achieve the capacitance tuning range against a reverse bias voltage.

3.3.1 Formation of a PN Junction

A varactor diode is formed by creating a PN junction by combining two regions of semiconductor materials, P-type and N-type. N-type semiconductors are a material that has been doped with an electron donor element. This allows the formation of electrons as the majority carriers and holes as minority carriers. P-type semiconductors are a material that have been doped with electron acceptor elements. This allows for the formation of holes as the majority carriers and electron as minority carriers.

When these two types of material are combined, a junction is formed between the two regions of materials. Electrons from the N-type region will diffuse across into the P-type region and combine with holes. This leaves positively charged ions behind. At the same time, holes from the

P-type material will be diffusing across to the N-type region and combine with free electrons. This will leave negatively charged ions behind. This process will cause a region to form where there is an absence of mobile charge carriers. This region is called the depletion region, which is composed of unneutralized ions held in the lattice and is shown in Figure 3.4.

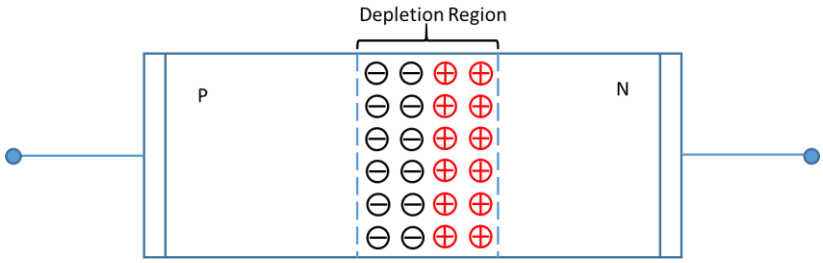

Figure 3.4 Formation of depletion layer between P- and N-type semiconductors (Adapted from [6])

These unneutralized ions in the depletion region form a dipole layer at the junction interface and represent a storage of charge [7]. Across the depletion region a junction voltage, called the built-in potential opposes the charge carriers across the junction.

3.4 Reverse Bias

The reverse bias is the configuration where a positive DC voltage is applied to the cathode relative to the voltage applied to the anode of the diode.

3.4.1 Physical Model

Applying a positive bias is applied to the N-type material relative to the voltage at the P-type will increase the contact potential difference of the unbiased PN junction. This reverse biasing will increase the width of the depletion region and decrease the junction capacitance, this is shown in Figure 3.5.

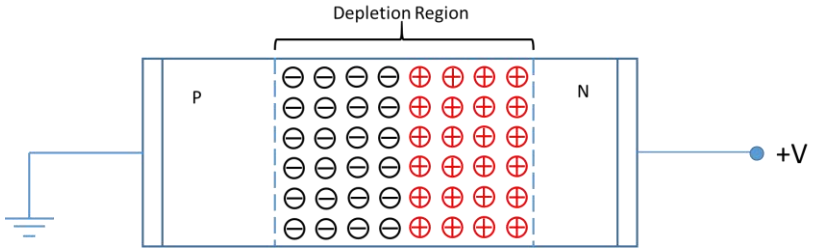

Figure 3.5 Physical model of a reverse biased PN junction showing enlargement of depletion layer (Adapted from [6])

The reverse bias mode of the varactor is the configuration that is desired for frequency tuning of RF and microwave components such as VCOs and phase shifters [8].

A more detailed model and equivalent circuit model for a reverse biased varactor is shown in Figure 3.6.

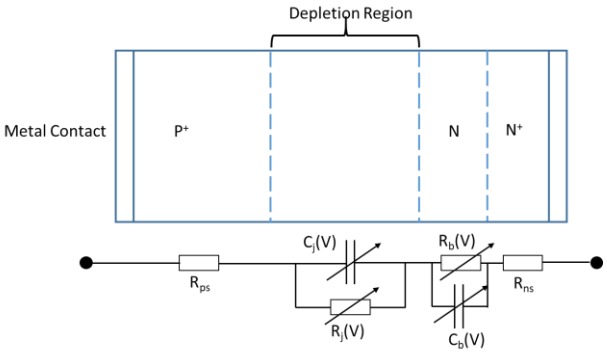

Figure 3.6 Physical and circuit equivalent model of reverse biased varactor (based on [7])

The most significant source of loss in a diode comes from the base region [7]. In the physical model this is shown by the N-type section and in the circuit, this is represented by the resistor R_b. The source of loss in this region are caused by the doping concentrations, these need to be at a low enough value to allow the depletion region to expand into the base and give the variation in capacitance [9]. To reduce losses, the doping concentrations could be increased in the base region, but this comes at a cost of reducing the capacitance tuning capability and lowering the breakdown voltage of the diode [7]. These design parameters need to be traded off for optimal performance and must to be considered when choosing a diode for a specific application.

3.4.2 Quality Factor

The quality factor of varactor diodes is defined using a small-signal equivalent series model as shown in Figure 3.7a. The model in Figure 3.7a neglects the inductance and capacitance from the diode packaging and the series resistance of the diode is lumped into R_s [7].

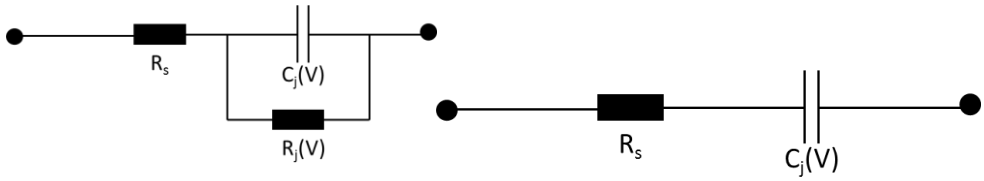

(a) (b)

Figure 3.7 Equivalent circuit model a) small-signal model b) High frequency equivalent model (adapted from [7])

At high frequencies, where $R_j(V) >> 1/C_j(V)\omega \approx R_s$ [7], the circuit reduces to a series equivalent circuit model shown in Figure 3.7b, where the quality factor is defined as:

$$Q(V) = \frac{1}{\omega C_j(V) R_s(V)} \tag{11}$$

As discussed in Section 2.3.1.1 the quality factor of varactor diodes reduces as the frequency of operation increases. When the reverse bias voltage increases, the series resistance decreases which leads to an improved quality factor [10].

3.4.3 Doping Gradient

The two most commonly seen types of varactor diode, and the ones investigated in this thesis are the abrupt and hyperabrupt. These terms refer to the doping levels of the semiconductor regions and are controlled during the wafer fabrication process [10]. Figure 3.8 shows simple models for the abrupt and hyperabrupt doping concentration.

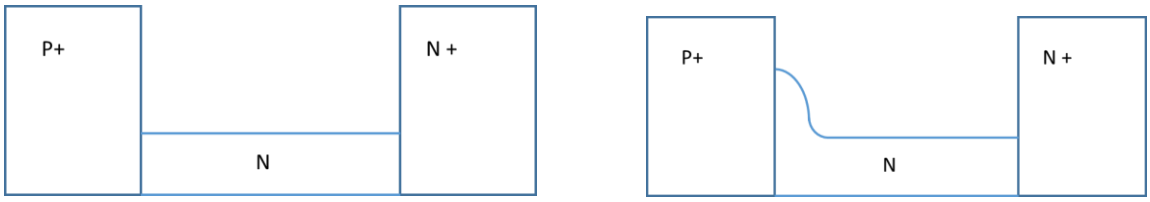

(a) (b)

Figure 3.8 Varactor doping profiles a) Abrupt b) Hyperabrupt (Adapted from [10])

The hyperabrupt doped varactor has a benefit over the abrupt varactor when being used for tuning VCOs. The gradient allows for a more linear tuning against bias voltage over a small frequency range. This removes the need to linearizer circuitry [11]. An example of how a hyperabrupt diode can improve VCO linearity is shown in Figure 3.9.

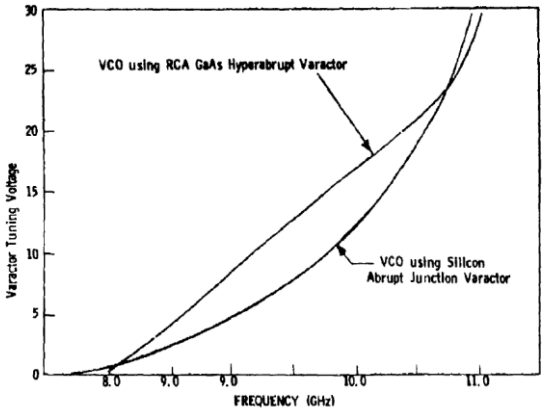

Figure 3.9 Graph showing improvement in linear tuning using hyperabrupt varactor compared to abrupt varactor[11]

This hyperabrupt doping profile allows for a lower bias voltage for the same change in capacitance of an equivalent abrupt diode. The capacitance against reverse bias voltage is given by the Equation 12.

$$C(V) = \frac{K}{(\phi + V)^n} \tag{12}$$

where:

K = Zero-bias capacitance, pF

ϕ = Contact potential, V

V = External bias voltage, V

n = Junction exponent

The contact potential is dependent on the material used to fabricate the diode. For silicon the value is 0.7V and for gallium arsenide it is 1.3V [10]. The junction exponent for diodes depends on the type of doping. For an abrupt diode the value is 0.5 and for hyperabrupt diodes it is a value greater than 0.5 [6].

3.4.4 Nonlinear Modelling

In the reverse bias mode of operation, the varactor will exhibit a nonlinear time-dependent capacitance as the RF signal modulates the bias point, this is shown in Figure 3.10.

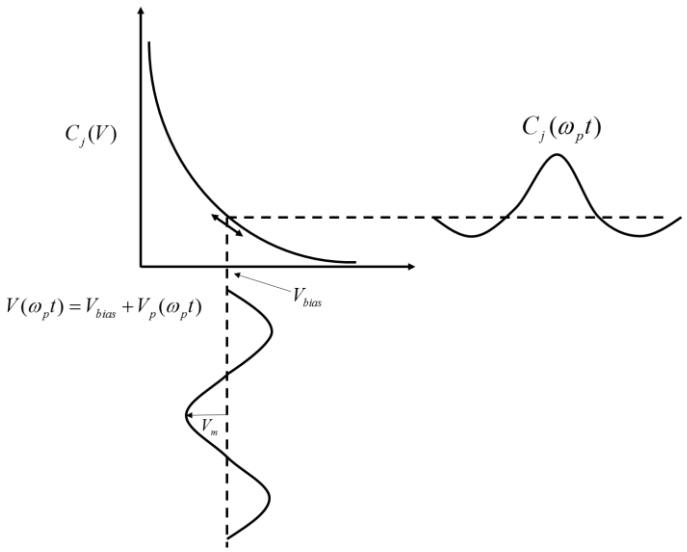

Figure 3.10 Example of a reverse biased varactor C-V curve being driven about the bias point by a RF signal and the resulting capacitance modulation (Adapted from [7])

When the diode is driven with a small enough RF signal it is assumed to be linear. However, when the RF voltage is large enough, the modulation of the C-V curve is used to perform nonlinear operations such as parametric amplification and mixing [12, 13]. It is this reverse bias C-V relationship that has been most extensively investigated for nonlinear modelling of tunable microwave components [14].

3.5 Forward Bias

3.5.1 Physical Model

The second mode in which varactors can operate is the forward bias region, this is where the N-type semiconductor is negatively biased relative to the P-type semiconductor. Applying the forward bias reduces the width of the depletion layer as shown in Figure 3.11.

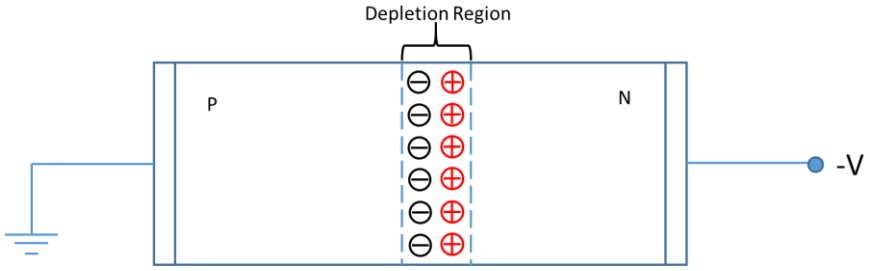

Figure 3.11 Forward bias model of PN junction (Adapted from [6])

When the voltage is applied to the PN junction it causes the diffusion of electrons; the minority carriers in the N-region into the P- region, and minority holes in the P-region to diffuse into the N-region. This diffusion of minority carriers across the depletion layer allows for the conduction of current.

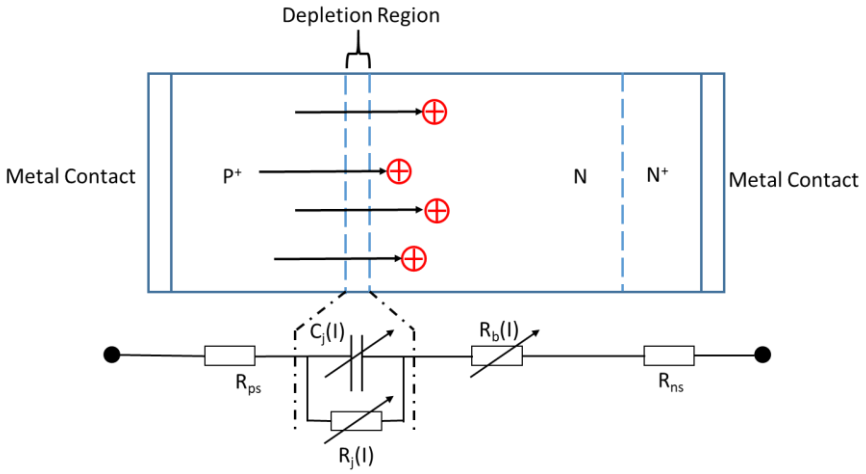

Figure 3.12 Physical and circuit equivalent model of forward biased varactor (Adapted from [7])

The injected minority carriers across the depletion layer, as shown in Figure 3.12, give rise to charge stored in the base layer and a resultant capacitance. There are two scenarios in which this capacitance can be generated.

3.5.1.1 Applied Forward DC Bias

An applied DC voltage biasing the diode into the forward conduction region with an RF superimposed signal.

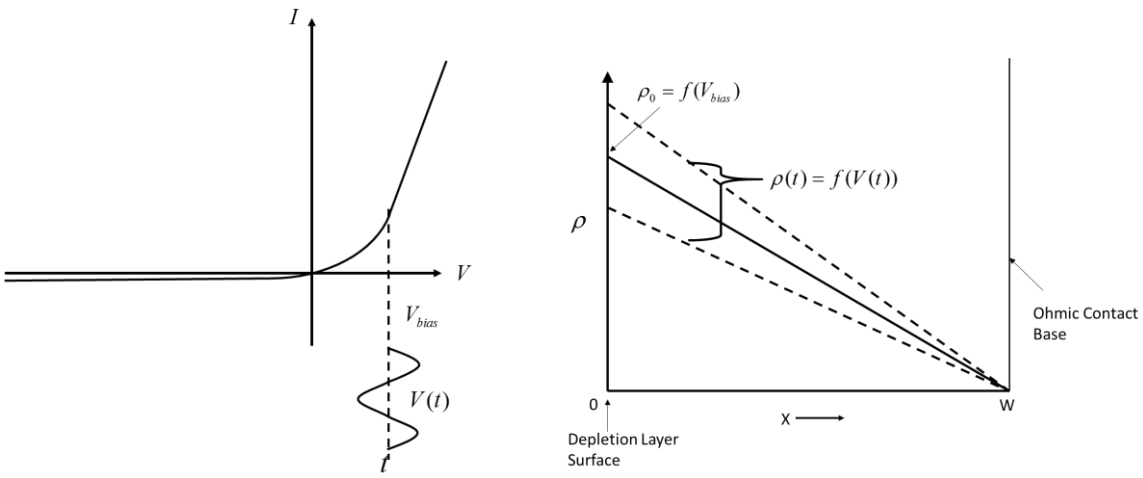

(a) (b)

Figure 3.13 Applied forward DC bias configuration a) Bias point of varactor diode b) Charge distribution in the base region (Adapted from [7])

Applying a forward V_{bias} across the diode as shown in Figure 3.13a, forms an equilibrium charge distribution ρ_0 across the base region as shown in Figure 3.13b. The depletion junction becomes a source of charge and the ohmic contact acts as a sink. It is this equilibrium charge distribution that represents a storage of charge. When the driving RF signal, *V(t),* is applied the diode it is superimposed onto the bias voltage. This causes the charge distribution to modulate as indicated by the dotted lines. This modulation of stored charge from an applied RF signal is the source of capacitance and it is of greater value than that of the depletion layer capacitance [7].

3.5.1.2 No DC Bias and large Applied RF Signal

The second mode in the forward bias region that causes capacitance is applying a large RF signal and no V_{bias} voltage, this is shown in Figure 3.14a. The RF signal causes the diode to swing from reverse bias to forward bias. This is different to the case shown in 3.5.1.1 where the diode is always in the forward conduction mode.

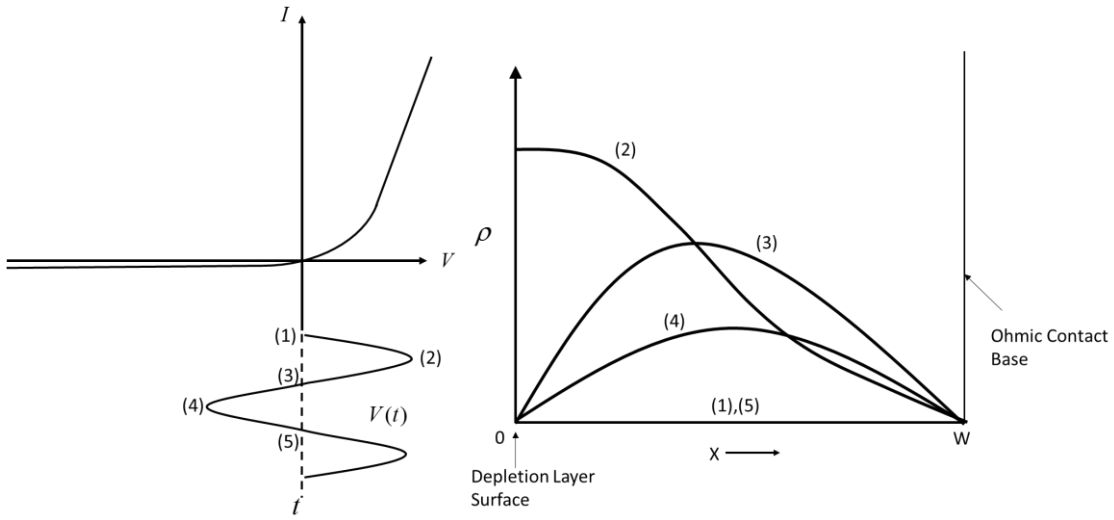

(a) (b)

Figure 3.14 Varactor with 0V applied V_{bias} and a large RF signal a) Bias point b) Charge distribution in the base region as RF signal goes through a cycle (Adapted from [7])

When the diode alternates between the forward and reverse bias cycles it causes charge to be stored in the base region. The major parts of a conduction cycle are shown in Figure 3.14a and 3.14b, they are broken down into:

1) At the start of the applied RF signal there is no charge in the base region as it has not been forward biased.

2) At the peak point of the applied RF signal the greatest injection of current is found at the depletion layer.

3) At this point there is no more RF signal driving the diode into the forward conduction part of the cycle. Therefore, as the RF applied signal starts to go negative, the junction will act as a sink as well as the ohmic contact at the base.

4) The applied RF signal is now biasing the diode into the reverse region and the charge in the base region has reduced significantly.

5) The process repeats itself again as per the stages 1-4.

This process will vary dependent upon the material properties of the diode as well as the operating conditions. It serves to give a general description of the large signal case. With the injection of charge into the forward bias region and the subsequent recovery of this charge, it creates a change in charge with a change in voltage. This creates an effective junction capacitance that is in addition to the junction capacitance of the depletion layer.

It is possible to stop the diode from being forward and reverse biased during a single RF cycle by biasing the diode suitably into the reverse bias region. However, this will remove the greatest tuning range of the diode on the C-V curve which occurs at the lower bias voltages.

3.5.2 Nonlinear Model

When the diode is operated with a 0V DC bias voltage and a large RF signal there is an associated nonlinear behaviour. The minority carriers in the base region do not instantaneously diffuse back across the junction. This causes a reverse current associated with a reverse recovery time τ_{rr} [15]. A simplistic example is shown in Figure 3.15, illustrating the reverse recovery time period. In Figure 3.15 a positive voltage pulse is applied to the diode which injects a current of minority carriers as shown by the positive current. As the applied voltage pulse changes to a negative voltage, and reverse biases the varactor diode, the current switches from positive to a negative current. This negative current exists for the time that is takes for the minority carriers to migrate back across the junction.

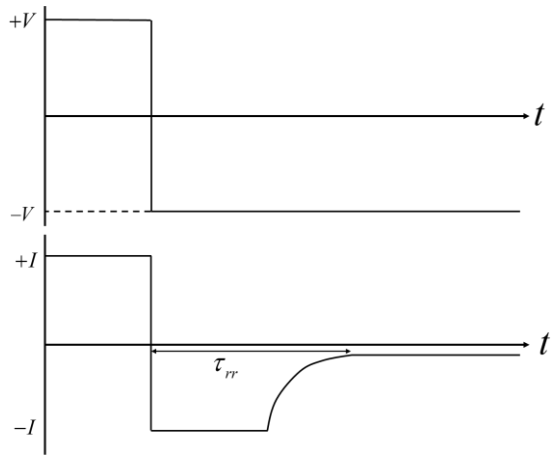

Figure 3.15 Reverse recovery times associated with diffusion of minority carriers (Adapted from [16])

The reverse recovery time of a diode is dependent on many parameters such as the amplitude of forward bias current, the frequency of the driving signal, the mobility of the carriers and the duty cycle of the signal [17].

As the charge is migrating back across the junction the diode is in a low impedance state. Once the charge is removed the diode flips into a high impedance state [6]. This process of removing the charge from the base region and transitioning between a low and high impedance state

creates a signal that is rich in harmonics and is utilised in the RF field for comb generators [18,19].

This process of forward and reverse biasing a varactor diode in an RLC circuit is shown in Figure 3.16a. This is of interest in the study of nonlinear dynamics and chaos [20].

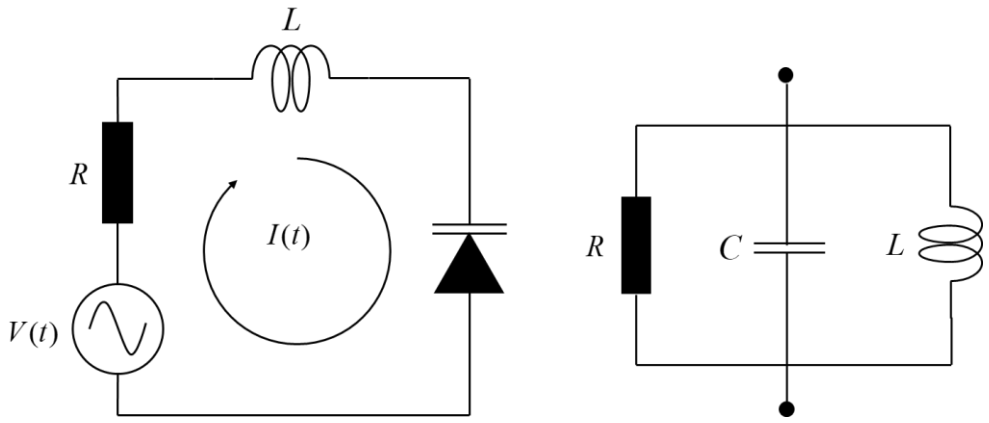

Figure 3.16 Equivalent circuits a) RLC resonator using varactor diode for investigating nonlinear behaviour (Adapted from [20]) b) Equivalent circuit of patch antenna (Adapted from [21])

This draws interesting parallels between the investigations in this thesis, as a patch antenna can be modelled as an RLC circuit at resonance although in a parallel configuration as shown in Figure 3.16b. A varactor therefore could be included in this model, which may produce conditions similar to those used in investigation of chaos [21].

3.6 References

[1] C. Balanis, Antenna theory. New York: Wiley-Interscience, 2005.

[2] C. Kalialakis and P. S. Hall, “Analysis and experiment on harmonic radiation and frequency tuning of varactor-loaded microstrip antennas," IET Microw. Ant. and Prop., vol. 1, no. 2, pp. 527-535, 2007.

[3] S. Yong, “Design and Analysis of Pattern Null Reconfigurable Antennas,” Ph.D dissertation, Dept. Electr. Comput. Eng., Univ. Illinois at Urbana-Champaign, Urbana, IL, 2012.

[4] A. Mohammad, H. Subhi, A. Ahmad, and S. Juma, “Cavity model analysis of rectangular microstrip antenna operating in TM03 mode,” 2006 2nd International Conference on Information & Communication Technologies, pp. 2218–2223, 2006.

[5] “Computer Simulation Technology,” CST. [Online]. Available: https://www.cst.com/. [Accessed: 19-May-2019].

[6] M. Norwood and E. Shatz, “Voltage variable capacitor tuning: A review,” Proceedings of the IEEE, vol. 56, no. 5, pp. 788–798, 1968.

[7] K. E. Mortensen, Variable Capacitance Diodes, Artech House, 1974.

[8] A. Keerti, J. Xiang, and A.-V. Pham, “High power linearized RF phase shifter using anti-series diodes,” IEEE Microwave and Wireless Components Letters, vol. 16, no. 4, pp. 200–202, 2006.

[9] M. P. J. Tiggelman, K. Reimann, F. V. Rijs, J. Schmitz, and R. J. E. Hueting, “On the Trade-Off Between Quality Factor and Tuning Ratio in Tunable High-Frequency Capacitors,” IEEE Transactions on Electron Devices, vol. 56, no. 9, pp. 2128–2136, 2009.

[10] SKYWORKS, Appl. 200824 Rev A, Aug 2008

[11] D. D. Mawhinney and J. J. Napoleon, “Hyperaprupt Varactor Voltage-Controlled Oscillators” RCA Labs., Princeton, NJ, USA, Oct. 1977.

[12] S. C. Cripps, “Elastic Reactance [Microwave Bytes],” IEEE Microwave Magazine, vol. 16, no. 1, pp. 21–25, 2015.

[13] M. Hines, “The Virtues of Nonlinearity-Detection, Frequency Conversion, Parametric Amplification and Harmonic Generation,” IEEE Transactions on Microwave Theory and Techniques, vol. 32, no. 9, pp. 1097–1104, 1984.

[14] M. El-Tanani and G. Rebeiz, “A Two-Pole Two-Zero Tunable Filter With Improved Linearity,” IEEE Transactions on Microwave Theory and Techniques, vol. 57, no. 4, pp. 830–839, 2009.

[15] M. A. van Wyk and W. -H. Steeb, “CHAOS IN ELECTRONICS,” Springer, 1997.

[16] W. Ko, “The reverse transient behavior of semiconductor junction diodes,” IRE Transactions on Electron Devices, vol. 8, no. 2, pp. 123–131, 1961.

[17] R. M. D. Moraes and S. M. Anlage, “Unified model and reverse recovery nonlinearities of the driven diode resonator,” Physical Review E, vol. 68, no. 2, 2003.

[18] J. Moll, S. Krakauer, and R. Shen, “P-N Junction Charge-Storage Diodes,” Proceedings of the IRE, vol. 50, no. 1, pp. 43–53, 1962.

[19] R. Mouw and F. Coale, “Microwave Applications of the Step Recovery Diode,” PTGMTT International Symposium Digest, pp. 176–180, May 1961.

[20] R. W. Rollins and E. R. Hunt, “Exactly Solvable Model of a Physical System Exhibiting Universal Chaotic Behavior,” Physical Review Letters, vol. 49, no. 18, pp. 1295–1298, 1982.

[21] F. Abboud, J. Damiano, and A. Papiernik, “Simple model for the input impedance of coax-fed rectangular microstrip patch antenna for cad,” IEE Proceedings H Microwaves, Antennas and Propagation, vol. 135, no. 5, pp. 323–326, 1988.

4 Test Setup

This chapter discusses the experimental methods used to assess the different performance metrics of the frequency reconfigurable antennas.

4.1 Frequency Tunability

A vector network analyzer is used to assess the frequency tunability. A bias tee is used to apply DC bias; it is connected to the end of the VNA cable and a SOLT calibration is applied to remove systematic errors. A maximum bias voltage of 29.5V was used as the maximum rating of the bias tee was 30V. This ensures there was no risk of damaging the test equipment. This means the full tuning range of some of the varactor diodes investigated was not used. The typical C-V curve of a varactor is almost flat near the maximum bias voltage therefore this will not contribute any significant error in the tunability measurements. The tunability is calculated using Equation 13 [1].

$$Tunability = \frac{2(f_{high} - f_{low})}{f_{high} + f_{low}} \times 100 \tag{13}$$

where:

f_{high} : Resonant frequency at maximum bias value, Hz

f_{low} : Resonant frequency at 0V bias voltage, Hz

4.2 Two-Tone Testing

The two-tone test is the most commonly used test for assessing the nonlinearity of microwave components. Two tones with frequencies f_1 and f_2 are applied to the device under test, the nonlinear behaviour causes them to mix and generate intermodulation products. Figure 4.1 shows a general output power measurement of a nonlinear device when two tones are applied, and intermodulation products are generated.

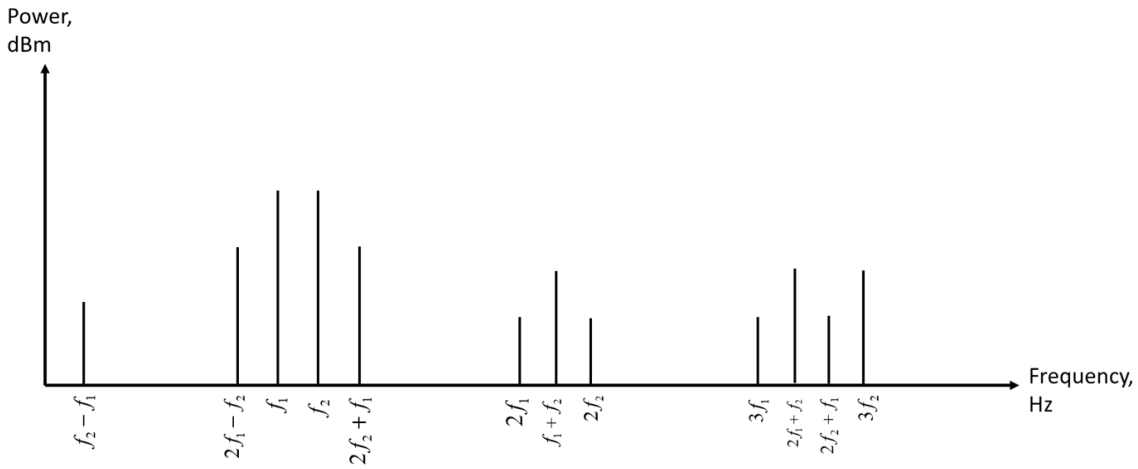

Figure 4.1 Representative two-tone output from a nonlinear device (Adapted from [2])

The most important intermodulation products are $2f_2 - f_1$ and $2f_2 + f_1$ as they will fall within the passband of the system and can enter adjacent channel users as shown in Figure 1.2b.

To qualify the performance of a device, the power levels of the applied fundamental tones and the generated third-order intermodulation products in the passband are measured and plotted on a graph. A general example is shown in Figure 4.2.

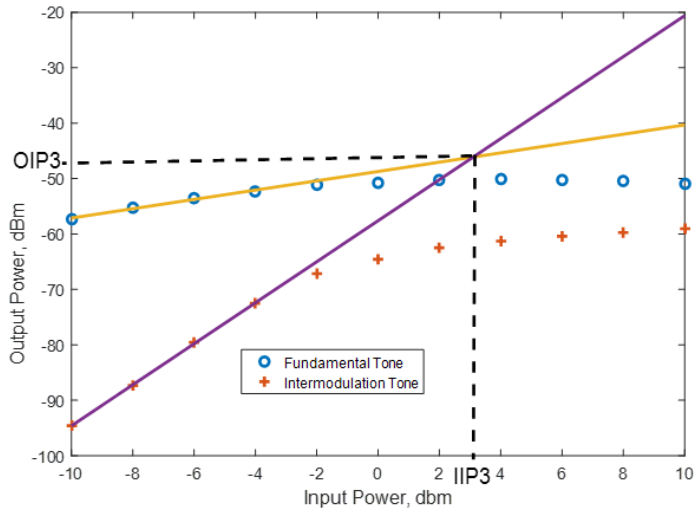

Figure 4.2 Graph showing intercept point between third-order intermodulation products and fundamental tones

Lines are fitted to measured data points and where they intercept is defined as either output intercept point (OIP3) or input intercept point (IIP3) depending on which axis is used. In this thesis the IIP3 point is used; the greater the value the IIP3 the more linear the device.

4.2.1 Two-Tone Setup

Figure 4.3 shows the two-tone test setup used for characterising the nonlinearity of the antennas.

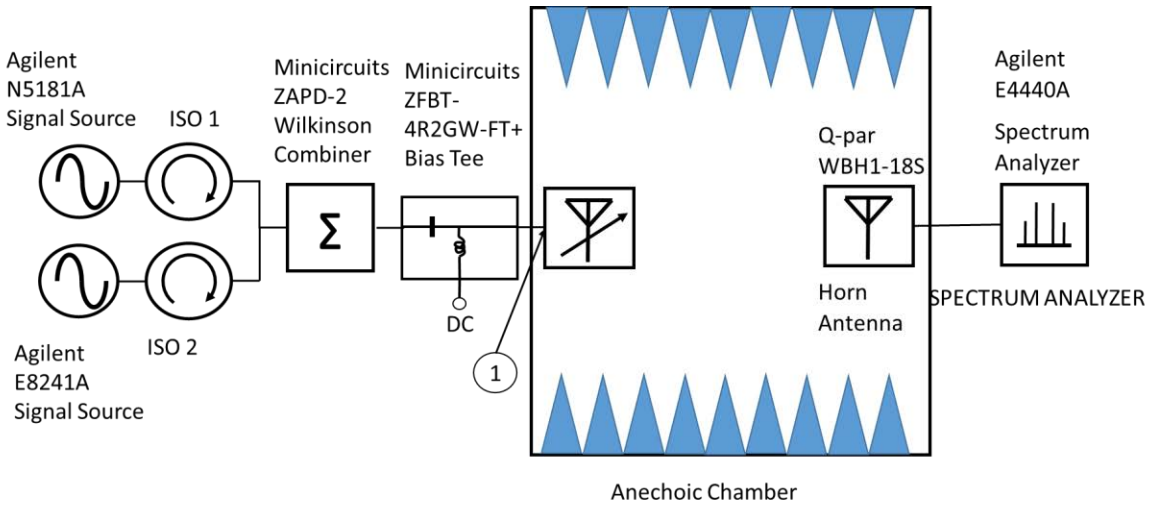

Figure 4.3 Two-tone test setup used for measuring IIP3 point

As shown in Figure 4.3, the testing was performed in the anechoic chamber to remove any unwanted interference and any multipath effects that could occur in a laboratory setting. The distance between the antenna under test and the reference antenna was set at 2.5m.

To remove the losses of the system contributed by the cables, isolators, combiner and bias tee, Point 1 in Figure 4.3 is connected directly to the spectrum analyzer. The losses of the system were then measured and then calibrated out by adjusting the output power levels at the signal sources accordingly. Therefore, both tone power levels at the antenna input will be accurately known.

Isolators were included, when available, for the frequency range of interest. Their function is to reduce any reflected signal from impedance mismatches in the setup and stop them from entering

the front end of the signal sources. Such a reflected signal could lead to mixing and produce intermodulation products which would corrupt the measurements.

The settings used on the spectrum analyzer are listed in Table 4.1.

Table 4.1 Spectrum analyzer settings used for two-tone testing

Setting	Value
Resolution Bandwidth	10kHz
Span	4MHz
Averaging	20 samples

Small values of resolution bandwidth and high averaging values were required as the generated intermodulation products power levels were near the noise floor of the spectrum analyzer.

4.2.2 Fitting of Lines

The fitting of the line to the data points is crucial in accurately determining the IIP3 point. If the line is fitted to data points that appear in the noise floor or once the device under test has entered gain compression it will add error into the calculated IIP3 point. An example of poorly fitted line to the measured data is given in Figure 4.4.

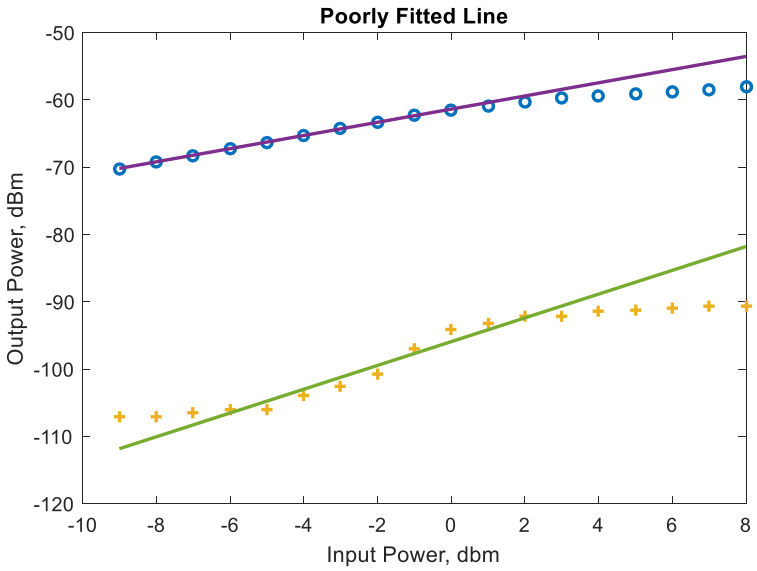

Figure 4.4 Poorly fitted lines for IIP3 calculation

Figure 4.4 shows the points in the noise floor and in gain compression have not been removed from the fitting process. By using this poorly fitted line, the value of IIP3 point will be artificially increased as the gradient of the fitted line is too shallow.

4.2.3 Two–Tone Spacing

There are no specific rules on the tone spacing for testing the nonlinearity of microwave components, so a review of the literature was performed. A table of the papers reviewed is given in Appendix A and shows the spread of the tone spacings that can be used. In this thesis a tone spacing of 1MHz was chosen, this ensures that they will both be within the operating bandwidth of the antennas under test.

4.2.4 Calibration of Reflection Coefficient

In this thesis it is the comparison of different tunable antenna configurations that is of interest. In order to make this investigation valid the power accepted by the antennas should be the same. Therefore, the variation in reflection coefficient of the different antennas needs to be calibrated out.

This is performed using Equation 14 [3].

$$P_{Incident} = \frac{P_{accepted}}{1-|S_{11}|^2} \tag{14}$$

where:

$P_{Incident}$: Power applied to the input connector, W

$P_{accepted}$: Desired power accepted by the antenna, W

S_{11} : Magnitude of reflection coefficient, linear units

By calibrating out the difference in the reflection coefficient of the antennas and the losses in the test setup, the available power levels accepted into the antennas is reduced. To combat the loss,

the use of amplifiers was considered to increase the power levels. However, due to the drift in gain with temperature the incident power levels were not consistent so they could not be used.

4.2.5 Calibration of Reflection Coefficient in CST

To gain an understanding of the behaviour of the antennas it is necessary to look at the voltage levels across the varactors on the antennas modelled in CST, as shown in Figure 3.3. When the antennas are simulated, they will not have the exact same reflection coefficient values. To calibrate this out a similar procedure is undertaken as discussed in Section 4.2.4.

Equation 14 is used to calibrate out the difference in reflection coefficient from the simulated response. To compare the antennas a value of 0.001W is chosen for $P_{accepted}$ and is used in all simulations.

Once the required $P_{Incident}$ value is known for the simulated reflection coefficient, the port signal amplitude for the CST ports needs to be scaled for the simulation. Equation 15 shows the amount of power accepted into a model in CST for a given amplitude of the signal source feeding the model [4].

$$P_{incident}^{port} = \frac{1}{2}\sum_{n=1}^{N}(Ampl.)_n^2 \tag{15}$$

where:

N : Number of ports in the model

Ampl. : Amplitude of the signal at port.

As the antenna models only have a single port it is necessary to set N=1. Then re-arranging Equation 15 to give Equation 16 gives the amplitude. Entering the value required for $P_{incident}^{port}$ will give the required signal source amplitude in CST for $P_{accepted}$ =0.001W in the simulation.

$$Ampl. = \sqrt{P_{stim}^{port} \times 2} \tag{16}$$

4.3 Radiation Measurements

The radiation measurements for the AUT were performed in an anechoic chamber to reduce multipath effects. The measurement planes are shown in Figure 4.5; the E-Plane is aligned with the E-fields and the H-plane with the H-fields of the patch.

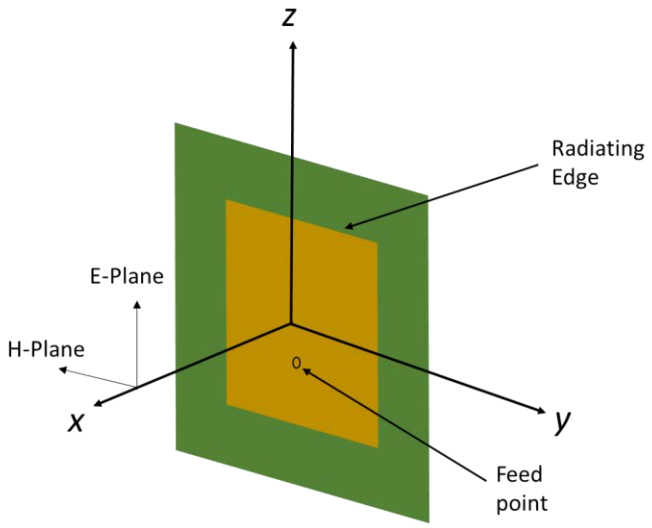

Figure 4.5 Measurement planes for patch antennas

4.3.1 Radiation Pattern and Gain

To perform the radiation measurements a full two-port calibration was performed to remove any losses in the cables. A wideband horn antenna with known gain was used as a reference antenna. To measure the gain of the AUT the gain transfer method was used [5]. The ideal measurement setup is shown in Figure 4.6 where the boresights are lined up correctly.

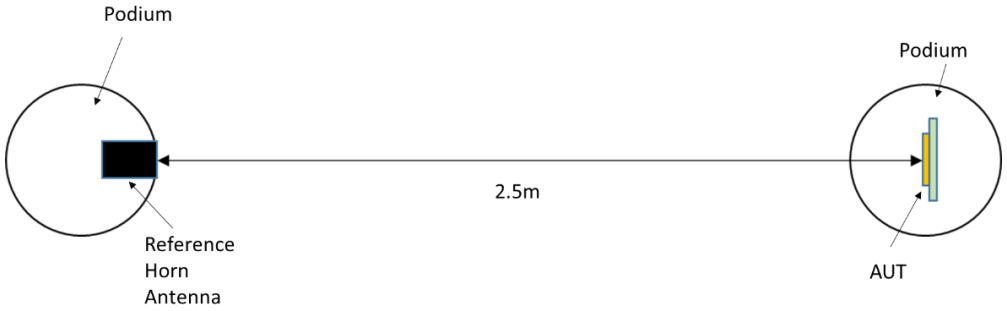

Figure 4.6 Top down view of an ideal measurement setup of antenna radiation pattern and gain measurements

The chamber used for the measurements is versatile as it allows podiums to be removed. This versatility comes with its own problems; the user has to align the podiums to the best of their ability. If they are not correctly aligned there can be an angle between the antennas as shown in Figure 4.7.

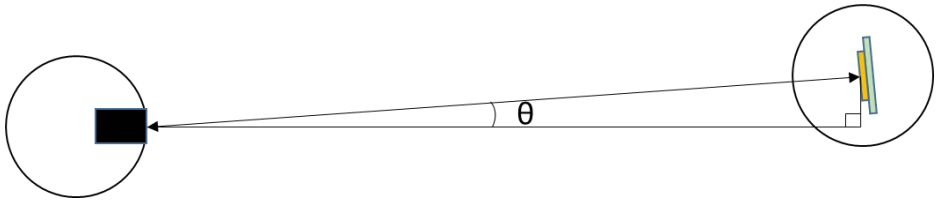

Figure 4.7 Top down view of measurement setup with errors

With this deviation, alignment of the antennas can cause errors in the gain measurements. If the boresights are not aligned it will artificially reduce the gain. Every effort was made to ensure that the podiums were aligned.

4.4 Conclusion

The measurement techniques used in this thesis are standard tests and make use of common laboratory equipment. There are areas of the testing that require care such as the setup of the antenna measurements and ensuring the loss of the system is removed from the two-tone testing.

4.5 References

[1] A. Petosa, “Frequency agile antennas for wireless communications – A Survey,” 2010 14th International Symposium on Antenna Technology and Applied Electromagnetics & the American Electromagnetics Conference, 2010.

[2] D. D. Weiner and J. F. Spina, Sinusoidal Analysis And Modeling of Weakly Nonlinear Circuit. New York, N.Y: Van Nostrand Reinhold, 1980.

[3] P. A, Rizzi, Microwave Engineering Passive circuits, New Jersey: Prentice Hall, 1988.

[4] CST Help Guide, CST, 2017.

[5] “IEEE Standard Test Procedures for Antennas,” ANSI/IEEE Stand. 149-1979, 1979.

5 Investigation of Varactor Loaded Microstrip Patch Antenna at Different Frequencies

5.1 Introduction

This chapter is an investigation into the performance of frequency tunable microstrip patch antennas at different frequencies. The aims were to investigate if the linearity performance of frequency reconfigurable antennas have a dependence on frequency; the influence the substrate properties is also investigated at each frequency point.

5.2 Design

To undertake this investigation a total of six antennas were fabricated on two different substrates, Cer-10 and TLC30. The thicknesses were 0.64mm and 0.78mm for the Cer-10 and TLC30 substrates respectively. Table 5.1 shows the electrical parameters of the substrates.

Table 5.1 Electrical properties of TLC30 and Cer-10 substrates

Substrate	Dielectric Constant	Loss Tangent @ 10GHz
TLC30 [1]	3.0±0.05	0.0030
Cer-10 [2]	9.5±0.50	0.0035

Three different frequencies of operation at 0V bias were chosen, these were 1.4GHz, 1.6GHz and 1.8GHz. This frequency range was chosen to reduce the difficulty in the design and fabrication of the antennas which arises from using two different substrates. Cer-10 with its high dielectric constant dramatically reduces the size of the patch at frequencies above 2GHz, which increases the difficulty in matching the input probe. Whereas using TLC30 as a substrate for the patch antenna at frequencies below 1.4GHz results in the patch becoming large and difficult to attach onto the antenna mount. The patches are designed with all the edges to be the same length, this removed one variable from the investigation.

The varactor diode chosen for this investigation was the SKYWORKS SMV1405 abrupt diode in the SC-079 package [3]. This package type was chosen as it has physical tabs for the anode and cathode that allow for soldering using a fine pitch soldering iron rather than reflow soldering. This diode has a capacitance range of 2.67pF to 0.63pF over a bias voltage range of 0 to 30V. Figure 5.1 shows the layout of the metallisation pattern used for this investigation. The varactor is mounted onto the radiating edge. The cathode is soldered onto the patch and the anode to a ground pad which connects to the ground plane using a via.

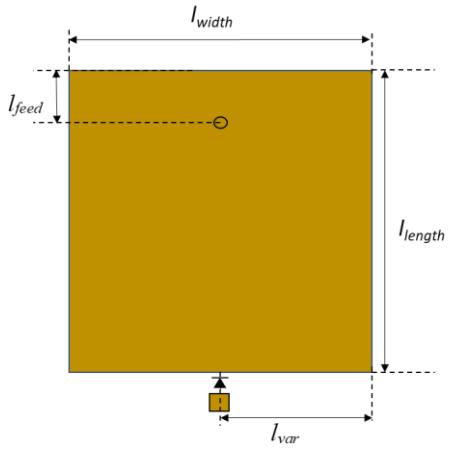

Figure 5.1 Metallisation pattern for antennas on TLC30 and Cer-10

The dimensions for the antennas fabricated on TLC30 and Cer-10 are given in Tables 5.2 and 5.3 respectively.

Table 5.2 Dimensions for antennas on TLC30

Antenna	l_{width} (mm)	l_{length} (mm)	l_{var} (mm)	l_{feed} (mm)
1.40 GHz	58.00	58.00	29.00	17.40
1.60 GHz	49.50	49.50	24.75	14.85
1.80 GHz	41.50	41.50	20.75	6.91

Table 5.3 Dimensions for antennas on Cer-10

Antenna	l_{width} (mm)	l_{length} (mm)	l_{var} (mm)	l_{feed} (mm)
1.40 GHz	35.00	35.00	17.50	5.83
1.60 GHz	29.30	29.30	14.65	7.33
1.80 GHz	25.50	25.50	12.75	6.38

5.3 Simulated and Measured Results

5.3.1 Measured Reflection Coefficient

The measured reflection coefficient for all antennas investigated in this chapter are given in Figure 5.2. Figure 5.2d includes the simulated response of the antenna on TLC30 at 1.6GHz, the number of bias voltage points has been reduced from 5V steps to 10V to make the plot clearer.

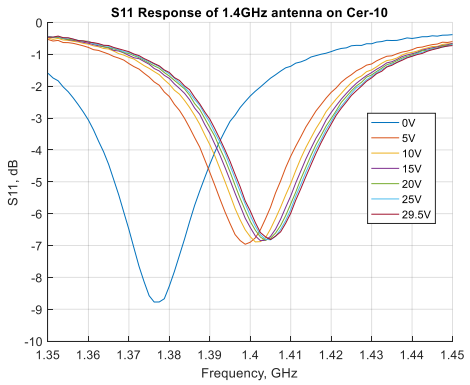

(a)

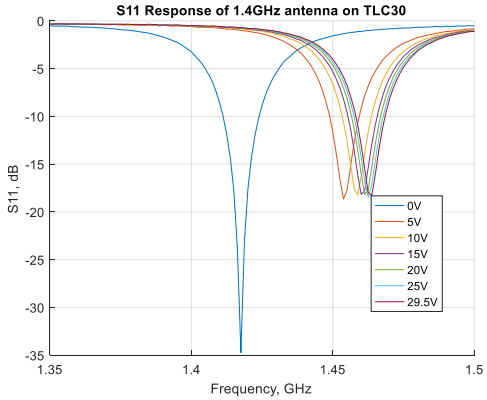

(b)

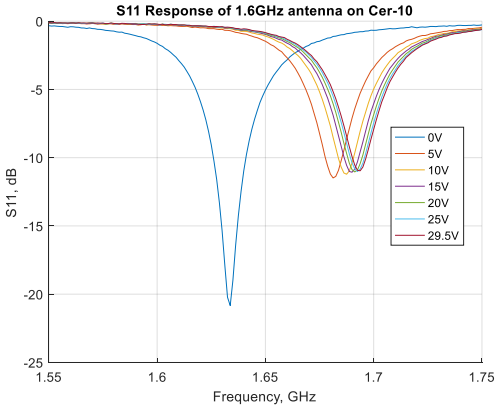

(c)

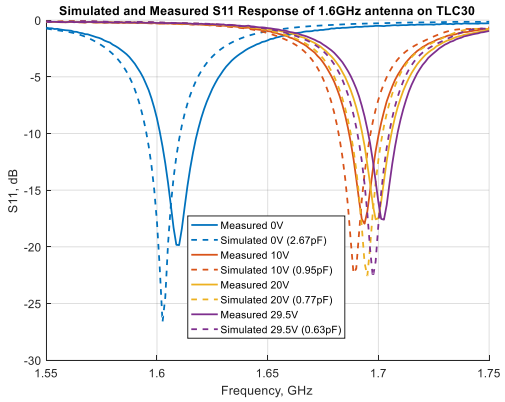

(d)

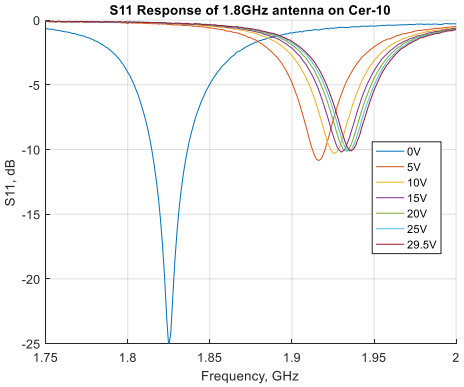

(e)

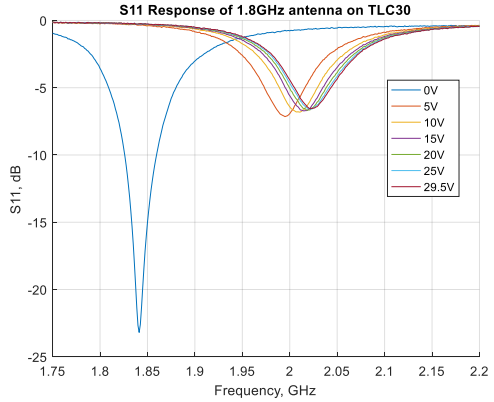

(f)

Figure 5.2 Measured and S_{11} responses for antennas (a) 1.4GHz Cer-10 (b) 1.4GHz TLC30 (c) 1.6GHz Cer-10 (d) Simulation response included 1.6GHz TLC30 (e) 1.8GHz Cer-10 (f) 1.8GHz TLC30

The measurements in Figure 5.2 show the impedance match for each antenna changes as it tunes through the frequency range; as the frequency increases the impedance match degrades, this is common to antennas fabricated on both substrates. The origin of the change in impedance match is the change in spatial distribution of the E- and H-fields around the patch. Simulated E-fields for 2.67pF and 0.63pF varactor capacitance values loading the 1.4GHz patch on TLC30 are shown in Figure 5.3a and 5.3b respectively.

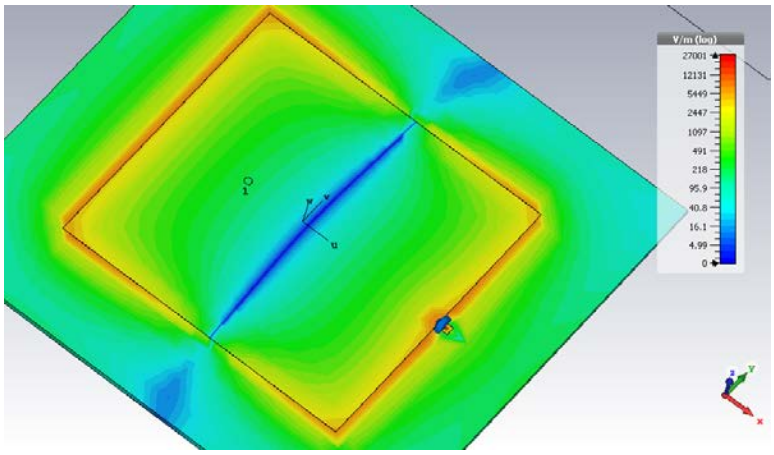

(a)

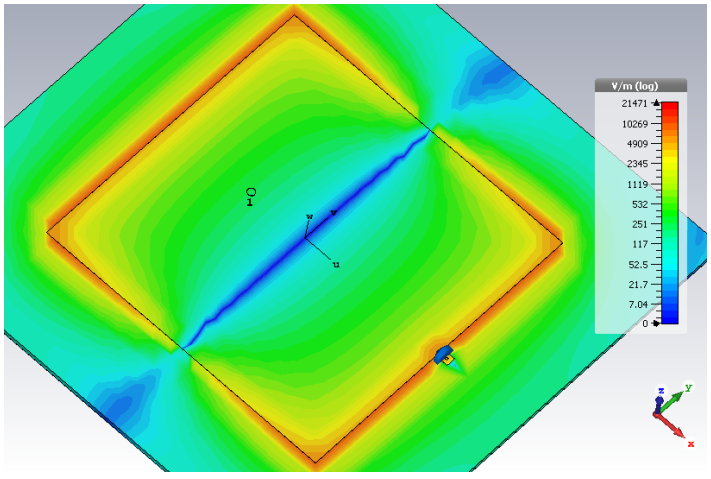

(b)

Figure 5.3 E-field distribution (a) 2.67pF varactor capacitance (b) 0.63pF varactor capacitance corresponding to bias voltages of 0V and 30 V respectively. The feed point is indicated by the circle on each plot, the varactor is the located on the edge perpendicular to the positive u axis

When the varactor is biased to 2.67pF the E-field is skewed towards the radiating edge loaded with the varactor; this was the configuration for which the feed point was matched in the simulations. Changing the varactor capacitance value to 0.63pF reduces the loading effect on the patch, this produces a more symmetric E-field symmetric distribution that would be found from an unloaded patch.

The SMA connector is used as the feed mechanism for these investigations as a DC voltage bias needs to be applied to the varactor using a bias tee. Alternative methods of coupling in which the matching could be improved across the frequency range of operation could be either proximity coupling or slot fed coupling; these are not suitable though because of the need to apply the bias.

5.3.2 Tunability

The measured and simulated values for the different antennas are given in Tables 5.4, 5.5, 5.6 and 5.7 for the antennas fabricated on TLC30 and Cer-10 respectively.

Table 5.4 Measured tunability, for antennas on TLC30 at different frequencies. At 0V the nominal capacitance of the varactor is 2.67pF. At 29.5V the capacitance is 0.63pF

Antenna	Frequency at 0V (GHz)	Frequency at 29.5V (GHz)	Tunability (%)
1.4 GHz	1.42	1.47	3.25
1.6 GHz	1.61	1.71	5.89
1.8 GHz	1.84	2.03	9.78

Table 5.5 Simulated tunability, for antennas on TLC30 at different frequencies. At 0V the nominal capacitance of the varactor is 2.67pF. At 29.5V the capacitance is 0.63pF

Antenna	Frequency at 0V (GHz)	Frequency at 29.5 (GHz)	Tunability (%)
1.4 GHz	1.40	1.45	2.95
1.6 GHz	1.60	1.70	5.48
1.8 GHz	1.80	1.99	10.10

Table 5.6 Measured tunability, for antennas on Cer-10 at different frequencies. At 0V the nominal capacitance of the varactor is 2.67pF. At 29.5V the capacitance is 0.63pF

Antenna	Frequency at 0V (GHz)	Frequency at 29.5V (GHz)	Tunability (%)
1.4 GHz	1.38	1.41	2.08
1.6 GHz	1.63	1.69	3.60
1.8 GHz	1.82	1.94	5.88

Table 5.7 Simulated tunability, for antennas on Cer-10 at different frequencies. At 0V the nominal capacitance of the varactor is 2.67pF. At 29.5V the capacitance is 0.63pF

Antenna	Frequency at 0V (GHz)	Frequency at 29.5V (GHz)	Tunability (%)
1.4 GHz	1.38	1.41	2.36
1.6 GHz	1.60	1.67	3.90
1.8 GHz	1.79	1.91	6.35

5.3.2.1 Tolerance Investigation

The discrepancy between the simulated and measured resonant frequencies comes from the variation in the materials used to fabricate the antennas and the manufacturing process. The datasheets for TLC30 and Cer-10 state the tolerances of the dielectric constant and are given in Table 5.1, any variation from the nominal value will have an impact on the resonant frequency. When the antenna is being etched it is left in etchant to remove the excess metal leaving behind the desired design; if the substrate is left in too long the patch can be over-etched and the patch will be too small. Conversely the patch can be removed from the etchant too soon and the patch will be slightly too large. An estimation used for the manufacturing tolerance here is ±0.2mm. The varactor diode will also have a variation in the capacitance value, this will be from the manufacturing of the varactor. The datasheet does not specify a tolerance on the capacitance value, so it is assumed a maximum tolerance of ±5%, this is lower than other documented tolerance values [2]. Table 5.8 shows the tolerance values used for the patch simulation at 1.4GHz on TLC30.

Table 5.8 Parameters used in simulation to investigate effects of tolerances on resonant frequency of antenna. The antenna investigated was on TLC30 substrate at 1.4GHz

	Dielectric Constant	Patch Length (mm)	Varactor capacitance (pF)	Resonant Frequency (GHz)
Minimum resonance tolerances	3.05	58.2	2.8035	1.392
Maximum resonance tolerances	2.95	57.8	2.5365	1.430

Looking at the simulated values for the maximum and minimum resonant frequency shown in column 5 of Table 5.8. The effect of these small tolerance variations can influence the resonant frequency of the antenna and it is these slight variations in the materials and fabrication techniques that cause the discrepancy between the CST model and the fabricated antenna.

5.3.3 Radiation Patterns

Radiation patterns for the antennas that are designed to resonate at 1.6GHz at 0V on both substrates are shown in Figure 5.4 and 5.5. The other patterns are omitted as they are similar in nature and are a standard radiation patterns for a patch antenna.

5.3.3.1 TLC30 Patches

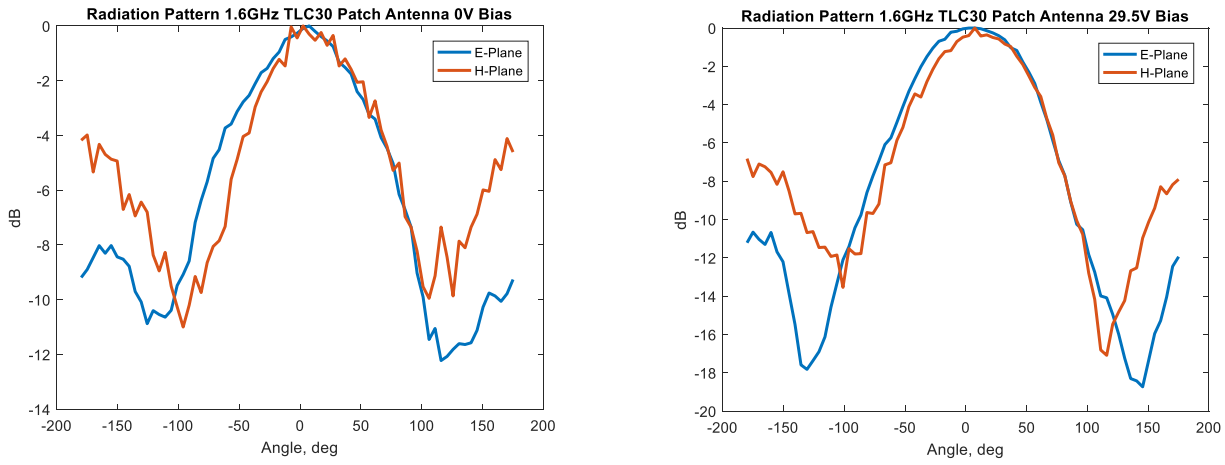

(a) (b)

Figure 5.4 Radiation pattern cuts for antennas fabricated on TLC30 radiating at 1.6GHz a) 1.61GHz with 0V bias b) 1.71GHz with 29.5V bias

5.3.3.2 Cer-10 Patches

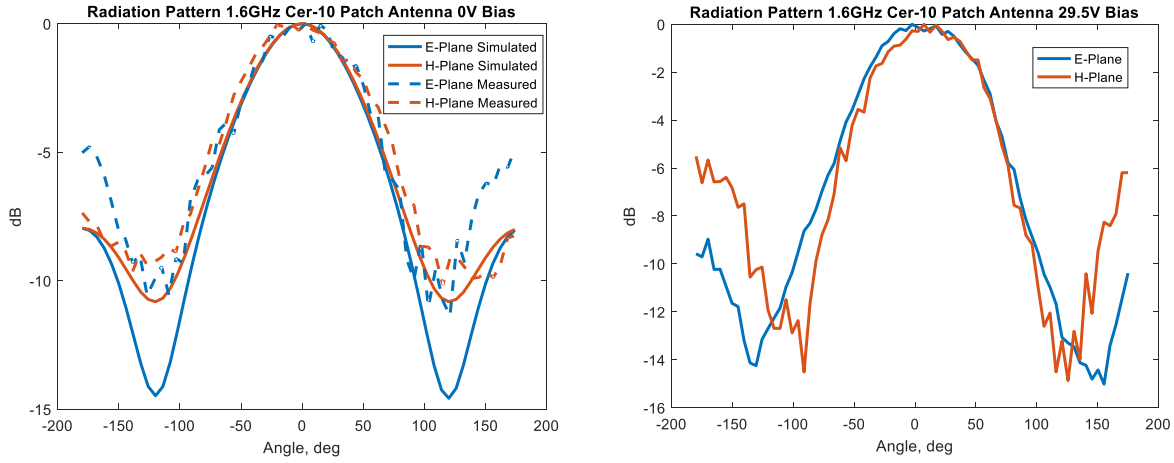

(a) (b)

Figure 5.5 Radiation pattern cuts for antennas fabricated on Cer-10 radiating at 1.6GHz a) 1.63GHz with 0V bias b) 1.69GHz with 29.5V bias

Figure 5.5a shows the simulated pattern overlaid on the measured response. There is close agreement between the two, except at angles greater than 90° where greater deviation between the measured and simulated patterns is seen. This deviation at greater angles is likely to have come from the non-ideal conditions caused by the anechoic chamber to measure the patterns unlike the ideal modelling conditions used in CST. The simulated patterns are excluded from the rest of this radiation patterns shown in thesis as they all matched the measured patterns in a similar way as shown in Figure 5.5a.

The measured radiation patterns for the antennas show measurement uncertainty as indicated by the jagged nature. This measurement uncertainty comes from the poor gain of both the reference horn and antennas under test at these frequencies. Although the patterns exhibit this measurement uncertainty when the gain of the patch antennas is poor, the overall shape of the patterns is clearly that of a patch antenna.

The jagged nature of the patterns could be reduced by either using a reference horn antenna with greater gain at the frequency of interest or reducing the intermediate bandwidth of the VNA. The

intermediate bandwidth of the VNA could not be reduced any further in measurements of the patterns shown here, this was caused by the long sweep time of the VNA would not have finished within the time period allowed by the automated turntable before it rotated around to the next measurement angle.

5.3.4 Gain

The measured and simulated peak gain values are given in Table 5.9.

Table 5.9 Measured gain values of antennas on TLC30 and Cer-10 at different frequencies

Frequency (GHz)	Gain (dBi)			
	TLC30		Cer-10	
	Simulated	Measured	Simulated	Measured
1.4	+2.30	+1.63	-2.16	-2.24
1.6	+1.98	+1.17	-0.90	-1.22
1.8	+0.37	+1.02	-1.51	-0.99

5.3.5 IIP3 Measurements

The third order intercept points were measured and shown in Table 5.10; plots of the measurements are given in Figure 5.6.

Table 5.10 Measured IIP3 points of antennas at 0V bias on TLC30 and Cer-10 at different frequencies

Frequency (GHz)	TLC30 (dBm)	Cer-10 (dBm)
1.4	+7.4	+2.8
1.6	+2.8	+1.7
1.8	-0.4	-0.6

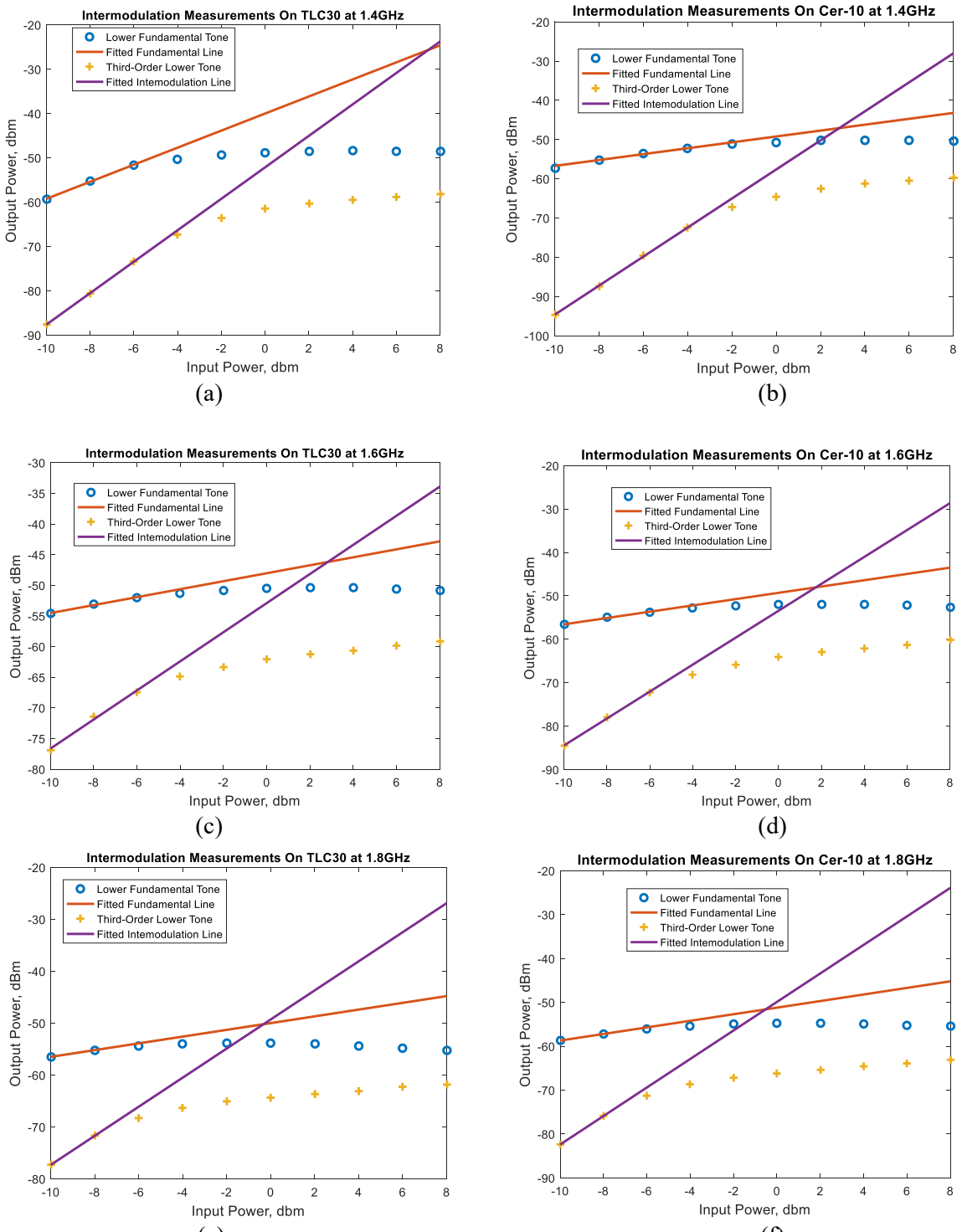

Figure 5.6 Measured Intermodulation products at 0V bias a) 1.4GHz TLC30 b) 1.4GHz Cer-10 c) 1.6GHz TLC30 d) 1.6GHz Cer-10 e) 1.8GHz TLC30 f) 1.8GHz Cer-10

5.4 Discussion

Comparing the measured tunability of the antennas fabricated on TLC30 shown in Table 5.4 to the tunability of those made on Cer-10 given in Table 5.6 it is shown that the TLC30 antennas have a greater tuning range; this is true across all the frequency points investigated. To understand this an analysis was performed by looking at the equivalent extracted capacitance of the six different patches. The capacitance of the patches is extracted using the procedure in [3]. The extracted values are shown in Tables 5.11 and 5.12 for the patches on TLC30 and Cer-10 respectively.

Table 5.11 Extracted capacitance and reactance of TLC30 patches

Frequency (GHz)	Extracted capacitance (pF)	Extracted Reactance X_{patch} (Ω)	Varactor reactance at 0V bias X_{var} (Ω)	X_{patch}/X_{var}	Measured Tunability (%)
1.4	120.52	0.94	42.58	0.022	3.25
1.6	88.38	1.13	37.26	0.030	5.89
1.8	62.64	1.41	33.12	0.043	9.78

Table 5.12 Extracted capacitance and reactance of Cer-10 patches

Frequency (GHz)	Extracted capacitance (pF)	Extracted reactance X_{patch} (Ω)	Varactor reactance at 0V bias X_{var} (Ω)	X_{patch}/X_{var}	Measured Tunability (%)
1.4	160.50	0.71	42.58	0.017	2.08
1.6	113.28	0.88	37.26	0.024	3.60
1.8	86.34	1.02	33.12	0.031	5.88

Looking at Tables 5.11 and 5.12 as the design frequency at 0V bias increases the extracted capacitance of the patches goes down. This is expected; in a simple parallel plate model, the area of the patch is directly proportional to the capacitance and the frequency of operation is inversely proportional to the square root of capacitance. The reactance of the patch and varactor is calculated using the extracted capacitance of the patch and capacitance of the varactor at 0V bias at the design frequency. Column 5 in each table shows the ratio of the extracted reactance of the

patch and that of the varactor. It is clear that larger values of this ratio are correlated with greater measured tunability (Column 6).

The significance of lower patch capacitance enabling higher tunability can also be illustrated from the extent to which the patches are reduced in size, compared to a patch with the same design frequency and no varactor loading. CST was used to extract the size of the patches for the same design frequencies as the varactor loaded antennas for both the substrates and at all frequency points, the results are shown in Tables 5.13 and 5.14.

Table 5.13 Difference in patch area between antennas on TLC30 with and without varactors

Antenna	Area with varactor (mm^2)	Area without varactor (mm^2)	Area reduction due to varactor (%)
1.4 GHz	3364	3600	6.5
1.6 GHz	2450	2756	11.1
1.8 GHz	1722	2180	21.0

Table 5.14 Difference in patch area between antennas on Cer-10 with and without varactors

Antenna	Area with varactor (mm^2)	Area without varactor (mm^2)	Area reduction due to varactor (%)
1.4 GHz	1225	1218	0.6
1.6 GHz	858	924	7.1
1.8 GHz	650	729	10.8

Figure 5.7 shows a plot of the percentage reduction in the patch area due to varactor loading for both the antennas on Cer-10 and TLC30 against tunability.

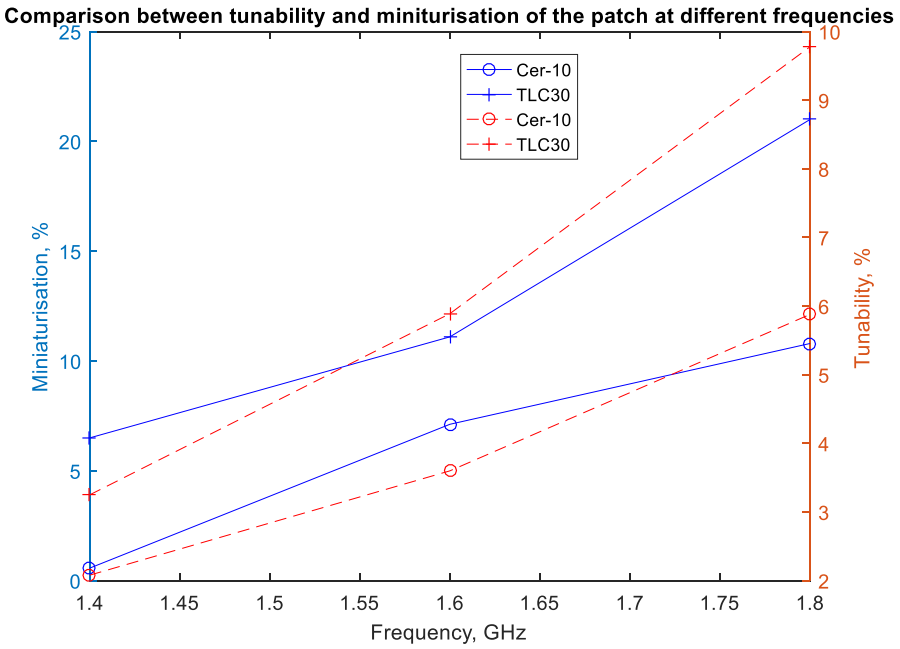

Figure 5.7 Plot showing miniaturisation due to varactor loading against tunability

Figure 5.7 shows the TLC30 patches undergo a greater reduction in size due to the loading of the varactor compared to the Cer-10 patches at each frequency. This greater area reduction corresponds to a greater tuning range.

The next parameter looked at is the gain, as shown in Table 5.9. The first point to observe is the higher gain of the antennas fabricated on TLC30 compared with those fabricated on Cer-10. This is true across the entire design frequency range. This result is expected as the lower dielectric constant of TLC30 gives larger antenna dimensions which will improve radiation efficiency and improve directivity [4].

The trend in Table 5.9 shows that the gain of the antennas fabricated on TLC30 decreases as the design frequency of the patches increases, whereas the gain for antennas on Cer-10 increases. One possible reason for this behaviour is different reflection coefficient values between the antennas causing a difference in measured gain. However, the data suggest this is not the cause as Figures 5.2b, 5.2d and 5.2f for the antennas fabricated on TLC30 show that the impedance

match does degrade between 1.4GHz and 1.6GHz but between 1.6GHz and 1.8GHz it improves again.

The losses in the varactors will be the same for both antenna types at the same design frequency, they can therefore be ruled out as the origin of this difference in gain behaviour between the two antenna types.

Turning to an example from the literature, Figure 5.8 shows the radiation efficiency as a function of frequency for antennas with no varactor loading on two different substrates with dielectric constant similar to those used in the present work.

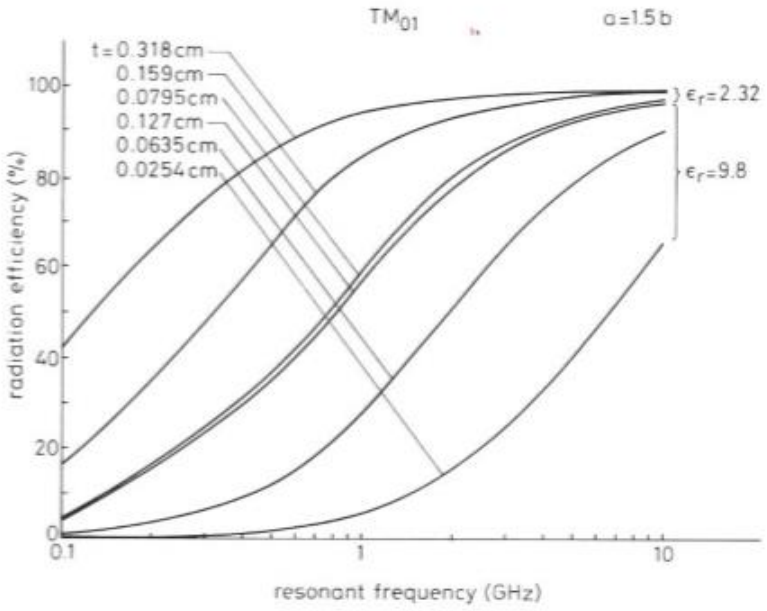

Figure 5.8 Radiation efficiency against resonant frequency of rectangular patch antennas [4]. Though these experiments were performed on rectangular rather than square patches, it is expected that the effect of the dielectric constant will be comparable.

Looking at Figure 5.8 the radiation efficiency of antennas on lower permittivity substrates saturates as the fundamental resonant frequency goes above 1GHz. In contrast, for patch antennas fabricated on higher permittivity substrates the radiation efficiency increases rapidly above 1GHz. An increasing radiation efficiency will give an increase in gain for a given directivity as shown by Equation 17 [4].

$$G = \eta D \tag{17}$$

where:

G : Gain, dBi

η : Radiation Efficiency

D : Directivity, dBi

However, improvements in radiation efficiency need to be traded off against the effects of miniaturisation due to varactor loading. Figure 5.9 shows the calculated miniaturisation of the antennas against the measured gain values.

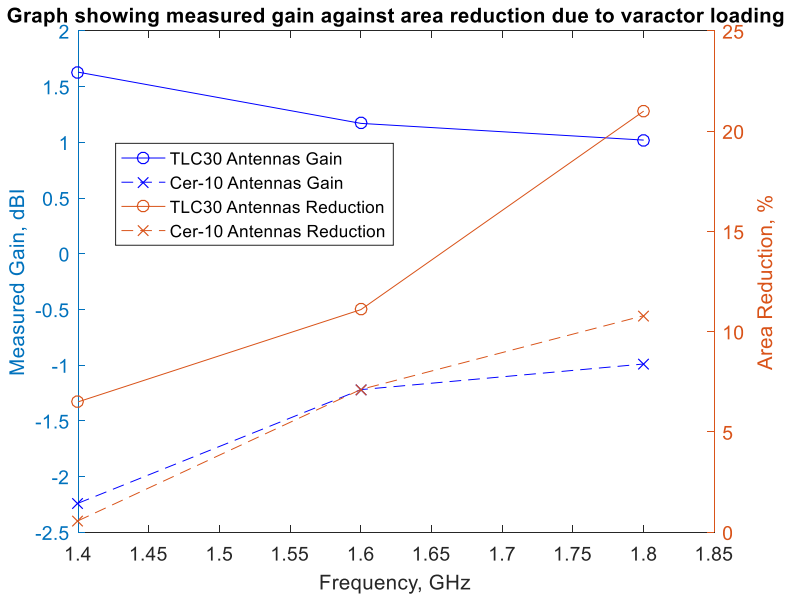

Figure 5.9 Plot showing measured gain of antennas against area reduction calculated in Tables 5.13 and 5.14

On comparing Figures 5.8 and 5.9, it is suggested here that for antennas on the high permittivity substrate, the rate of radiation efficiency increase with operating frequency has a greater effect on the gain than the reduction in electrical size from varactor loading. However, for antennas on lower dielectric constant substrates, the radiation efficiency improvements do not outweigh the effects of miniaturisation from the varactor loading as frequency of operation increases.

The measured gain of the antennas in Table 5.9 is shown to be lower than the varactor loaded patch antennas given in [5] which are of a similar design. The measured gain of the antenna on TLC30 operating at 1.4GHz is +1.63dBi whereas in [5] the antenna with a SMV1233 diode with 0V bias has a gain of +3.66dBi at 1.75GHz. It should be noted that the antenna design in [5] has the varactor located within the patch as shown in Figure 2.11 and not on the radiating edge which could account for the improved gain over the antennas investigated here.

The last property to be investigated was the linearity of the patches. The third-order intercept points measured for the antennas are given in Table 5.10. Where it is shown that as the frequency of operation increases the antennas become more nonlinear, as indicated by a reduced value of IIP3. This reduction in the IIP3 point is common to both antennas fabricated on both TLC30 and Cer-10.

Comparing the IIP3 points of the antennas on the different substrates the antennas fabricated on Cer-10 show lower values across the frequency points investigated compared to those on TLC30. It was expected that the antennas with the greatest tunability would behave more nonlinearly. However, the TLC30 antennas had the greater tuning range across all frequencies and show higher IIP3 points than those on Cer-10.

Comparing the measured IIP3 point shown in Table 5.10 with the measured IIP3 +5.5dBm of the patch antenna loaded with a SMV1233 varactor and using a 0V bias given in [5], only the antenna on TLC30 operating at 1.4GHz is superior in performance. There are many factors which could account for the superior IIP3 value of the antenna in [5] over the antennas investigated in this work here. Some of these factors are the different location of the varactor within the patch antenna, the different varactor capacitance value and the frequency of operation.

To look at why the antennas have these nonlinear performance characteristics, the peak RF voltage amplitude across the varactors was extracted in CST. The reflection coefficient of the simulated antennas was accounted for using the procedure discussed in Chapter 4. This keeps the incident signal level at the feed point of the simulated antennas the same irrespective of the substrate. The extracted voltages across the varactors and the reflection coefficient at resonance of the patch are shown for all the antennas are given in Tables 5.15 and 5.16 and are plotted against the measured IIP3 points in Figure 5.10.

Table 5.15 Extracted peak RF voltage amplitude across varactors TLC30 antennas

Antenna	Voltage (V)
1.4GHz	0.76
1.6GHz	0.84
1.8GHz	0.91

Table 5.16 Extracted peak RF voltage amplitude across varactors Cer-10 antennas

Antenna	Voltage (V)
1.4GHz	0.66
1.6GHz	0.77
1.8GHz	0.83

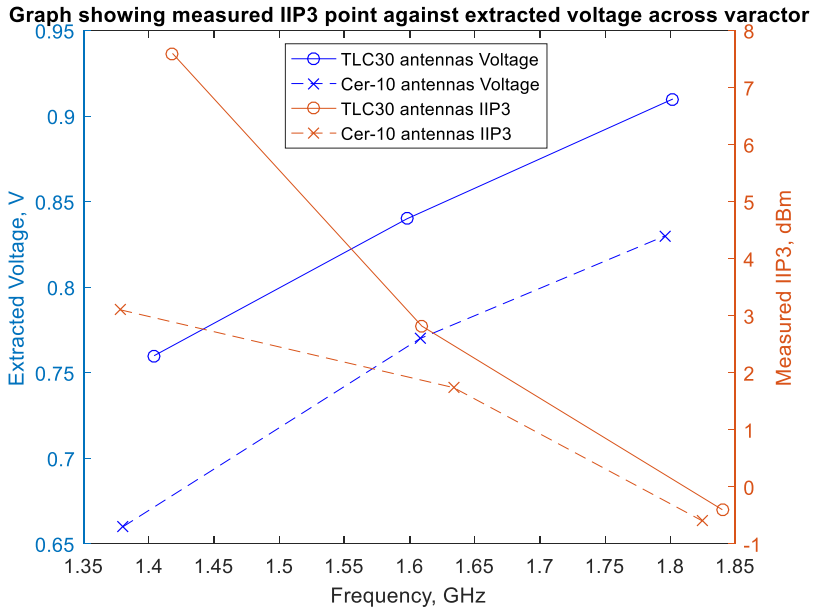

Figure 5.10 Plot showing the extracted peak RF voltage amplitude against measured IIP3 points of antennas on TLC30 and Cer-10 substrates

Figure 5.10 shows that the amplitude of the RF voltage across the varactors in the antennas fabricated on TLC30 were greater than those on the Cer-10 substrate at equivalent design frequencies. This was an unexpected result as a larger RF voltage driving the diode would be expected to produce a more nonlinear antenna. This was indicated by antennas in transmit mode having poorer linearity than those in receive mode [6]. However, the antennas on TLC30 had superior linearity performance, as judged from the IIP3 point.

One factor to consider is the varactors are operating at the 0v bias point in these IIP3 investigations. Therefore, the varactors will likely be switching between being forward and reverse bias as discussed in Section 3.5.1.2 in Chapter 3. This operation mode of a varactor diode is shown in Figure 5.11.

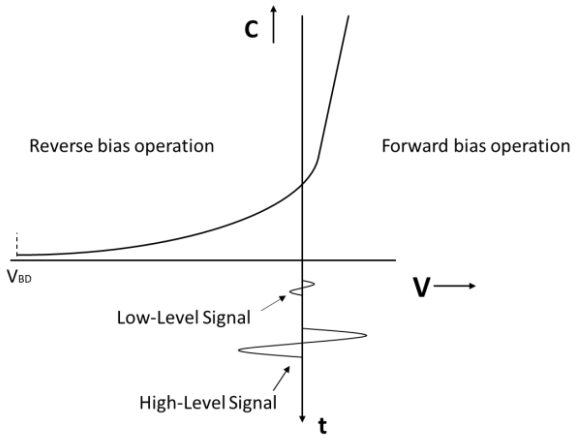

Figure 5.11 Varactor operating in forward and reverse bias (Adapted from [7])

There is no simple way of modelling the nonlinearity of the varactor diode in this investigation, as it is operating in both forward and reverse bias during a single cycle. It is proposed here that a larger RF signal biases the varactor further into the forward bias region which has a larger capacitance as shown in Figure 5.11. In this region the diode will act more like a short circuit and the diode will behave more linearly. Further work is needed to verify this hypothesis.

The simplest method of improving the nonlinear performance would always be to operate the varactors at a higher bias voltage. This would bias the varactors in a more linear part of the C-V curve and maintain a reverse bias throughout the RF cycle. The compromise of using the diodes at higher bias voltages is that the tunability would be reduced.

5.5 Conclusion

This chapter has looked at six different antennas fabricated on two different substrates that operate at three different frequencies.

The key points from the analysis presented in this chapter are:

1. The tunability is greater in antennas fabricated on lower permittivity substrates, because they underwent the largest reduction in area due to varactor loading.

2. The tunability is greatest when the ratio of varactor reactance to patch reactance is largest.

3. The IIP3 is highest when fabricated on a low permittivity substrate and at 1.4GHz and gives the most linear antenna.

4. The gain is highest when using a low permittivity substrate at 1.4GHz as it has the largest surface area.

5. Antennas with the largest tunability do not necessarily have the lowest IIP3 point.

5.6 References

[1] Taconic, “TLC low Cost RF Substrate,” TLC30 datasheet.

[2] Taconic, “orcer cεr-10,” Cer-10 datasheet.

[3] SKYWORKS, “SMV1405 to SMV1430 Series: Plastic Packaged Abrupt Junction Tuning Varactors,” SMV1405 datasheet, Jan. 2016

[2] A. P. Godse and U. A. Bakshi, Basic Electronics. Technical Publications Pune, 2009.

[3] F.Abboud, J. Damiano, and A.Papiernik, “Simple model for the input impedance of coax-fed rectangular microstrip patch antenna for CAD,” Proc. Inst, Electr. Eng., vol. 135, no. 5, pp. 323-326, 1988.

[4] J. R. James and P. S. Hall, Handbook of Microstrip Antennas Volume 1, London: Peter Peregrinus, 1989.

[5] S. Yong, “Design and Analysis of Pattern Null Reconfigurable Antennas,” Ph.D dissertation, Dept. Electr. Comput. Eng., Univ. Illinois at Urbana-Champaign, Urbana, IL, 2012.

[6] J.-B. Yan, S. Yong, and J. T. Bernhard, “Intermodulation and Harmonic Distortion in Frequency Reconfigurable Slot Antenna Pairs,” IEEE Transactions on Antennas and Propagation, vol. 62, no. 3, pp. 1138–1146, 2014.

[7] K. E. Mortensen, Variable Capacitance Diodes, Artech House, 1974.

6 Investigation into Placement of Varactors on Microstrip Patch Antenna

6.1 Introduction

This chapter investigates the effect of varactor positioning on the tunability, linearity and radiation characteristics of patch antennas. It was reported in [1] that placing the varactors on the non-radiating edge of the patch antennas produced a highly tunable patch, this chapter determines whether this achieves superior performance than varactors placed on the radiating edges of a patch.

6.2 Design

Six antennas were fabricated on TLC30 substrate and each were loaded with four SMV1405 varactors. The varactors had the same parameters as detailed in Section 5.1. The design frequency was 1.8GHz with a 0V bias voltage applied to the varactors. Three of the antennas had four varactors loaded on the radiating edge; this is defined as the edge where the E-fields have a constant amplitude along the edge. The radiating edge can be seen in Figure 6.1a where the E-field magnitudes have the same colour along the whole length of the edge.

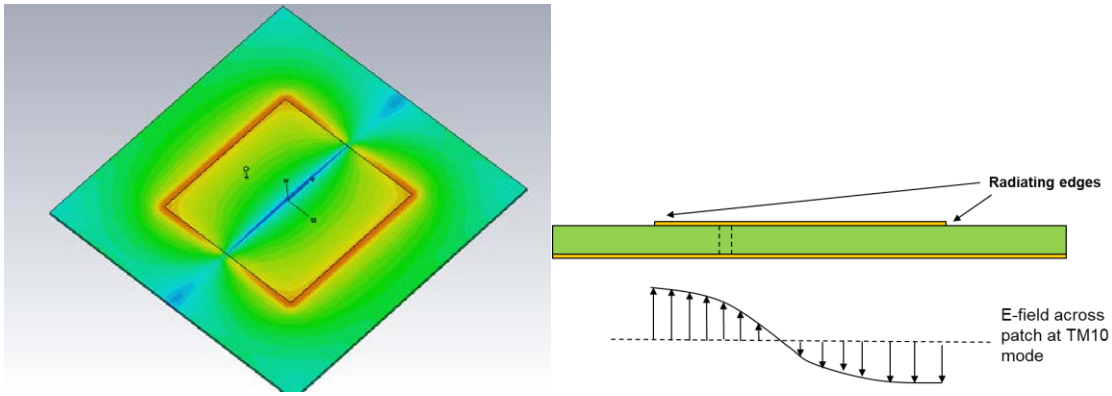

(a) (b)

Figure 6.1 E-field distribution for patch antenna in TM_{10} mode a) E-fields from CST b) Cross-section of E-field amplitude across patch

The remaining three antennas had the four varactors on the non-radiating edge, this is defined as the edge of the patch where the E-fields have a varying amplitude. The non-radiating edges are shown in Figure 6.1a where the E-field magnitude goes to a 0 V/m at the midpoint, shown here by the colour blue. The E-field distribution across the patch is shown in Figure 6.1b. The four varactors are placed at three different locations on each edge. They are located in either one third, quarter or sixth of the patch length from the edge. The radiating and non-radiating edges of the patches are kept the same length. Figure 6.2a shows the layout of the antennas with the varactors loading the radiating edge and Figure 6.2b shows the varactors on the non-radiating edge.

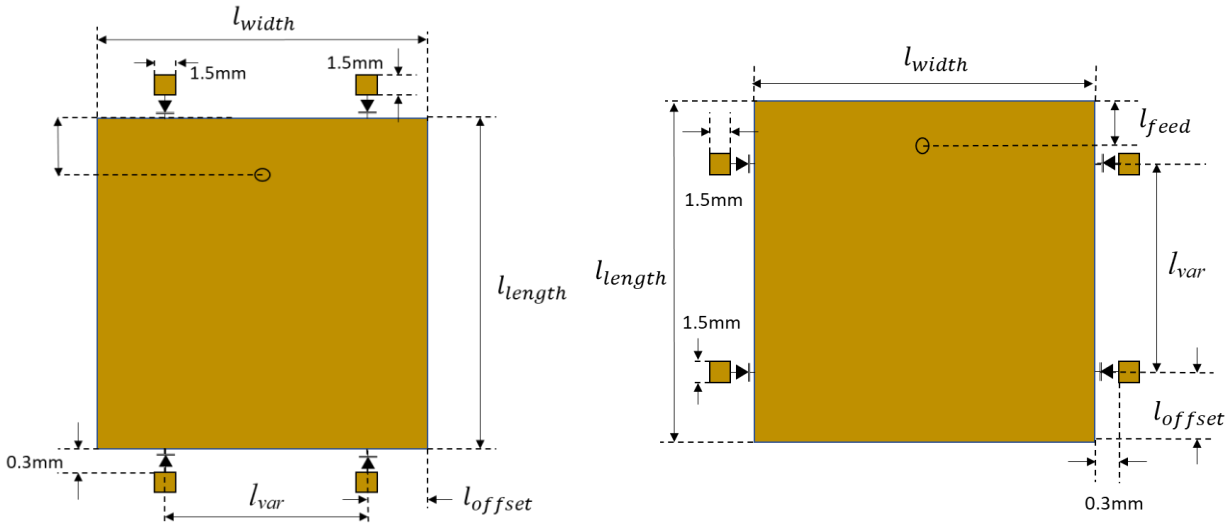

(a) (b)

Figure 6.2 Layout of patches (a) Varactors loading radiating edge (b) Varactors loading non-radiating edge

The dimensions for the antennas are given in Tables 6.1 and 6.2 for the antennas with the varactors on the radiating edge and non-radiating edge respectively.

Table 6.1 Dimensions for antennas with varactors on radiating edges

Antenna	l_{width} (mm)	l_{length} (mm)	l_{offset} (mm)	l_{var} (mm)	l_{feed} (mm)
1	28.00	28.00	9.33	9.34	0.67
2	28.00	28.00	7.00	14.00	0.67
3	28.00	28.00	4.67	18.66	0.67

Table 6.2 Dimensions for antennas with varactors on non-radiating edge

Antenna	l_{width} (mm)	l_{length} (mm)	l_{offset} (mm)	l_{var} (mm)	l_{feed} (mm)
4	43.00	43.00	14.33	14.34	1.02
5	38.00	38.00	9.50	19.00	0.90
6	33.00	33.00	5.50	22.00	0.78

The fabricated antennas are shown in Figure 6.3.

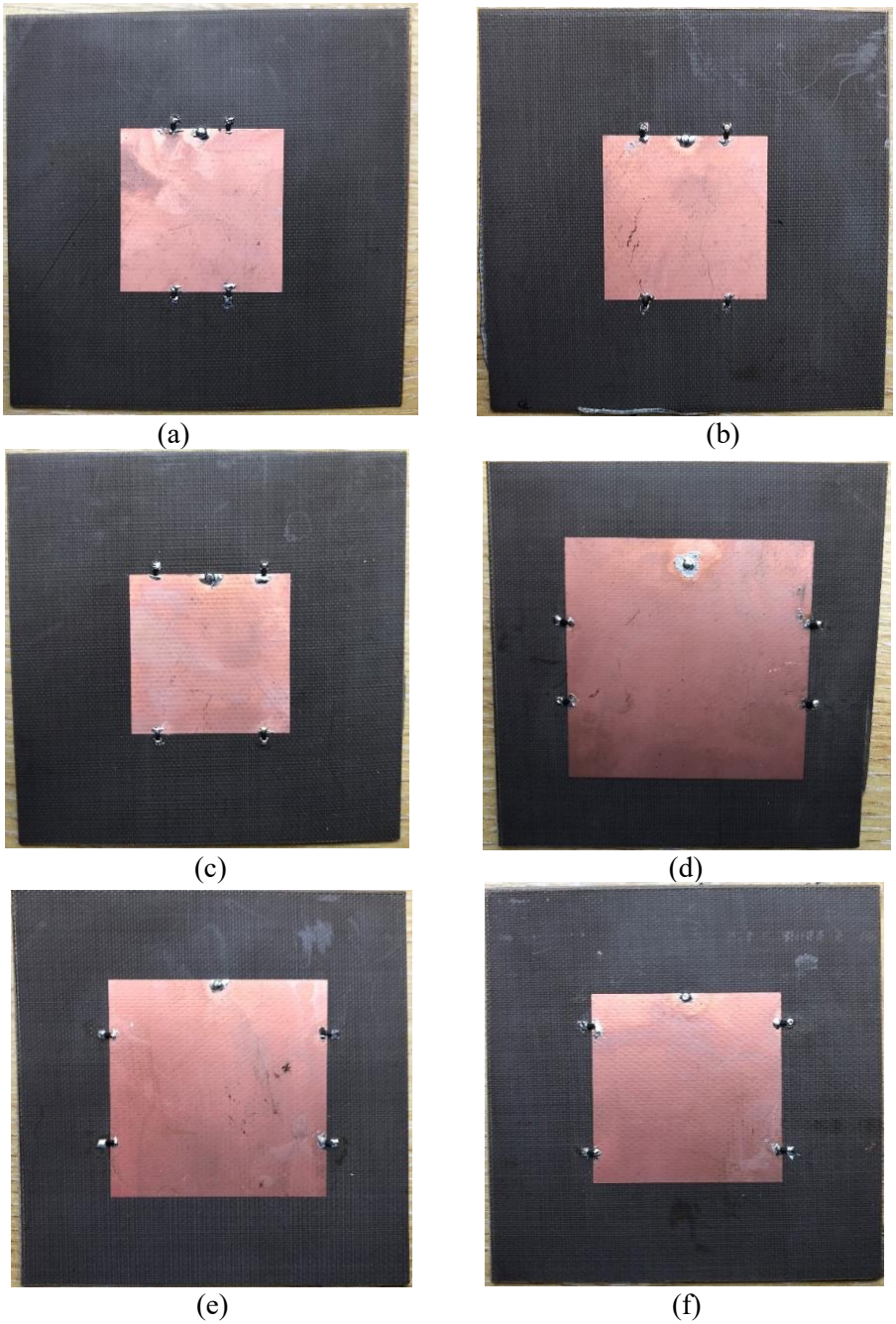

Figure 6.3 Pictures of fabricated antennas a) Antenna 1 b) Antenna 2 c) Antenna 3 d) Antenna 4 e) Antenna 5 f) Antenna 6

As the varactors on the non-radiating edge are moved out towards the radiating edge, and the length l_{offset} decreases, the patch length, l_{length} reduces in size to keep the same resonant frequency. The patches with the varactors loading the radiating edge have the same patch length $l_{length,}$ irrespective of the varactor placement along the edge.

The feed point for all six antennas is located very closely to the edge, irrespective of whether the varactors are located on the radiating or non-radiating edges, this is similar to that found in [1].

6.3 Simulation and Measured Results

6.3.1 Measured Reflection Coefficient

The measured reflection coefficient of the antennas is shown in Figures 6.4. For all the antennas except antennas 3 and 6 the reflection coefficient performance degrades as they are tuned up in frequency.

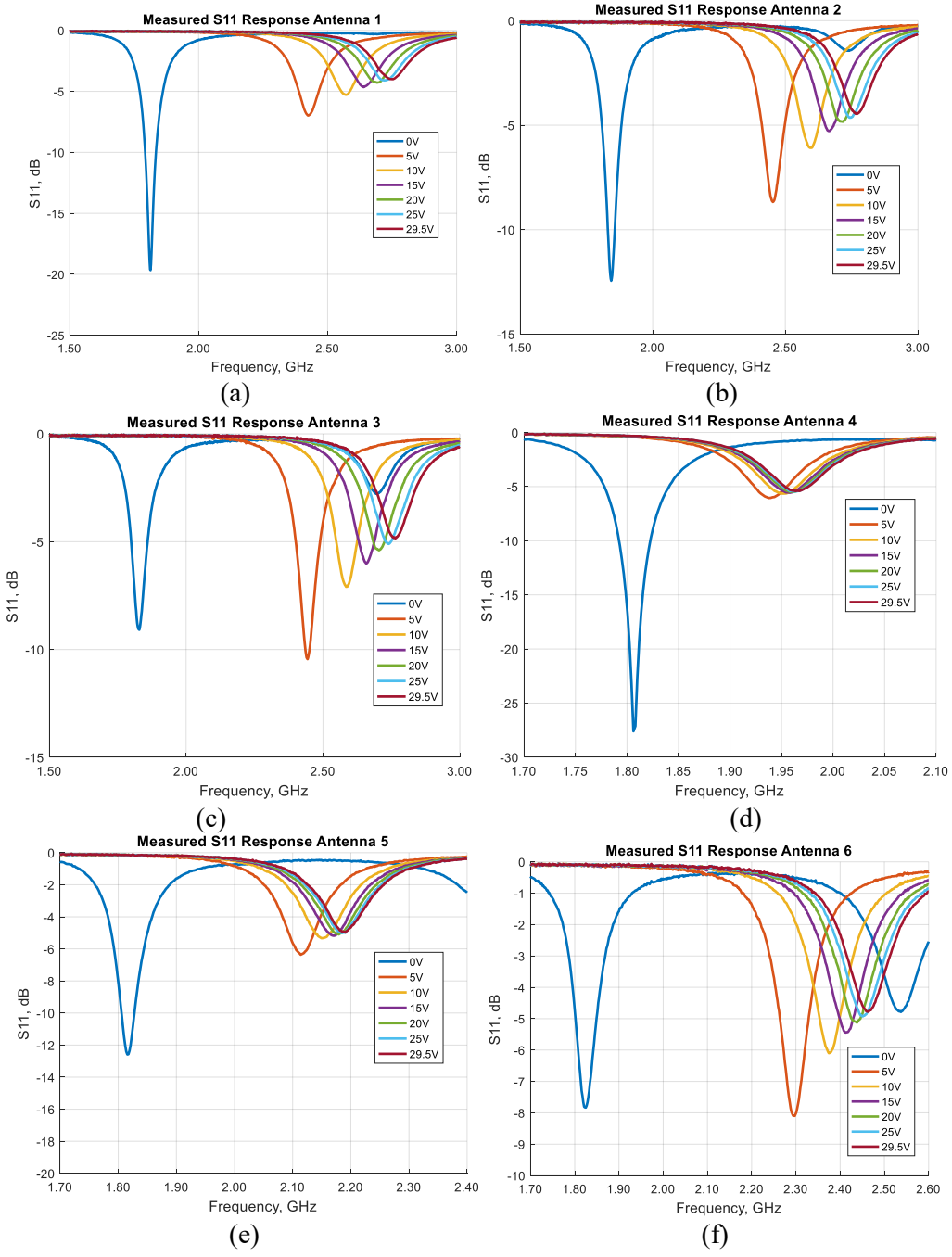

Figure 6.4 Measured S_{11} response of antennas a) Antenna 1 b) Antenna 2 c) Antenna 3 d) Antenna 4 e) Antenna 5 f) Antenna 6

6.3.2 Tunability

The measured tunability for the antennas with varactors on the radiating edge and non-radiating edge are given in Tables 6.3 and 6.5 respectively. The simulated tunability are given in Tables 6.4 and 6.6.

Table 6.3 Measured tunability for antennas with varactor loading on radiating edge. At 0V the nominal capacitance of the varactor is 2.67pF. At 29.5V the capacitance is 0.63pF

Antenna	Frequency at 0V (GHz)	Frequency at 29.5V (GHz)	Tunability (%)
1	1.81	2.75	41.60
2	1.84	2.77	41.00
3	1.83	2.77	41.00

Table 6.4 Simulated tunability for antennas with varactor loading on radiating edge. At 0V the nominal capacitance of the varactor is 2.67pF. At 29.5V the capacitance is 0.63pF

Antenna	Frequency at 0V (GHz)	Frequency at 29.5V (GHz)	Tunability (%)
1	1.80	2.66	38.57
2	1.82	2.66	37.50
3	1.81	2.66	38.03

Table 6.5 Measured tunability for antennas with varactor loading on non-radiating edge. At 0V the nominal capacitance of the varactor is 2.67pF. At 29.5V the capacitance is 0.63pF

Antenna	Frequency at 0V (GHz)	Frequency at 29.5V (GHz)	Tunability (%)
4	1.81	1.96	8.36
5	1.82	2.19	18.72
6	1.83	2.46	29.74

Table 6.6 Simulated tunability for antennas with varactor loading on non-radiating edge. At 0V the nominal capacitance of the varactor is 2.67pF. At 29.5V the capacitance is 0.63pF

Antenna	Frequency at 0V (GHz)	Frequency at 29.5V (GHz)	Tunability (%)
4	1.81	1.96	7.96
5	1.81	2.16	17.63
6	1.81	2.39	27.62

6.3.3 Radiation Patterns

Radiation patterns for antennas 1 and 2 are shown in Figure 6.5a and 6.5b respectively. The other patterns are omitted as they are similar in nature and are a standard radiation pattern for a patch antenna.

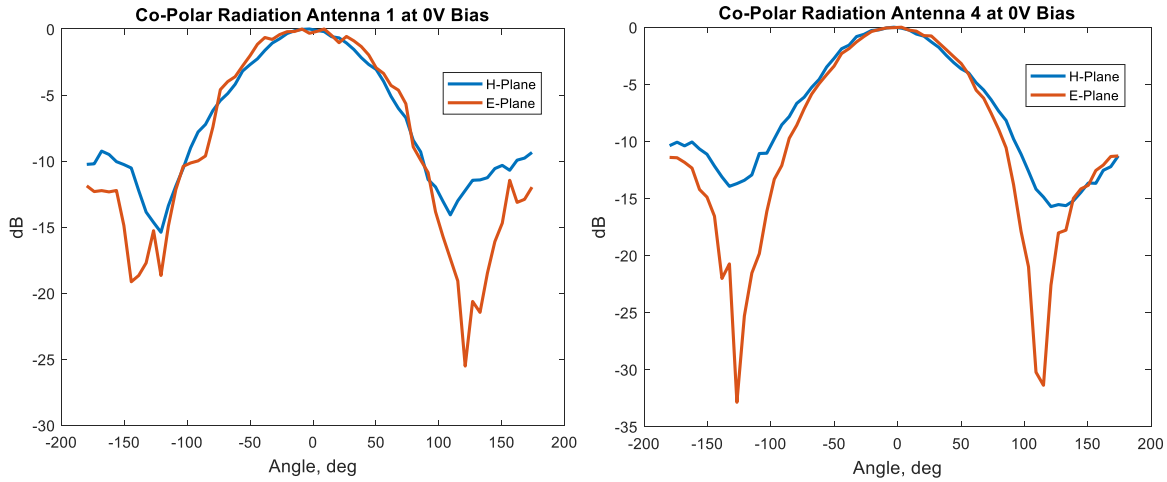

(a) (b)

Figure 6.5 Measured radiation patterns at 0V bias voltage a) Antenna 1 at 1.81GHz b) Antenna 4 at 1.81GHz

6.3.4 Gain

The measured and simulated gain values for the antennas are given in Table 6.7.

Table 6.7 Simulated and measured gain values of antennas with varactor loading on radiating and non-radiating edge

Antenna	Gain (dBi)	
	Simulated	Measured
1	-3.2	-6.1
2	-3.1	-6.0
3	-3.2	-6.5
4	+0.7	-1.6
5	-2.1	-4.4
6	-3.5	-7.4

6.3.5 IIP3 Measurements

The measured IIP3 point is shown in Table 6.8, plots of the measured data are given in Figure 6.6.

Table 6.8 Measured IIP3 points of antennas at 0V bias with varactor loading on radiating and non-radiating edge

Antenna	IIP3 (dBm)
1	+2.9
2	+1.7
3	+1.1
4	+2.6
5	+2.4
6	+1.9

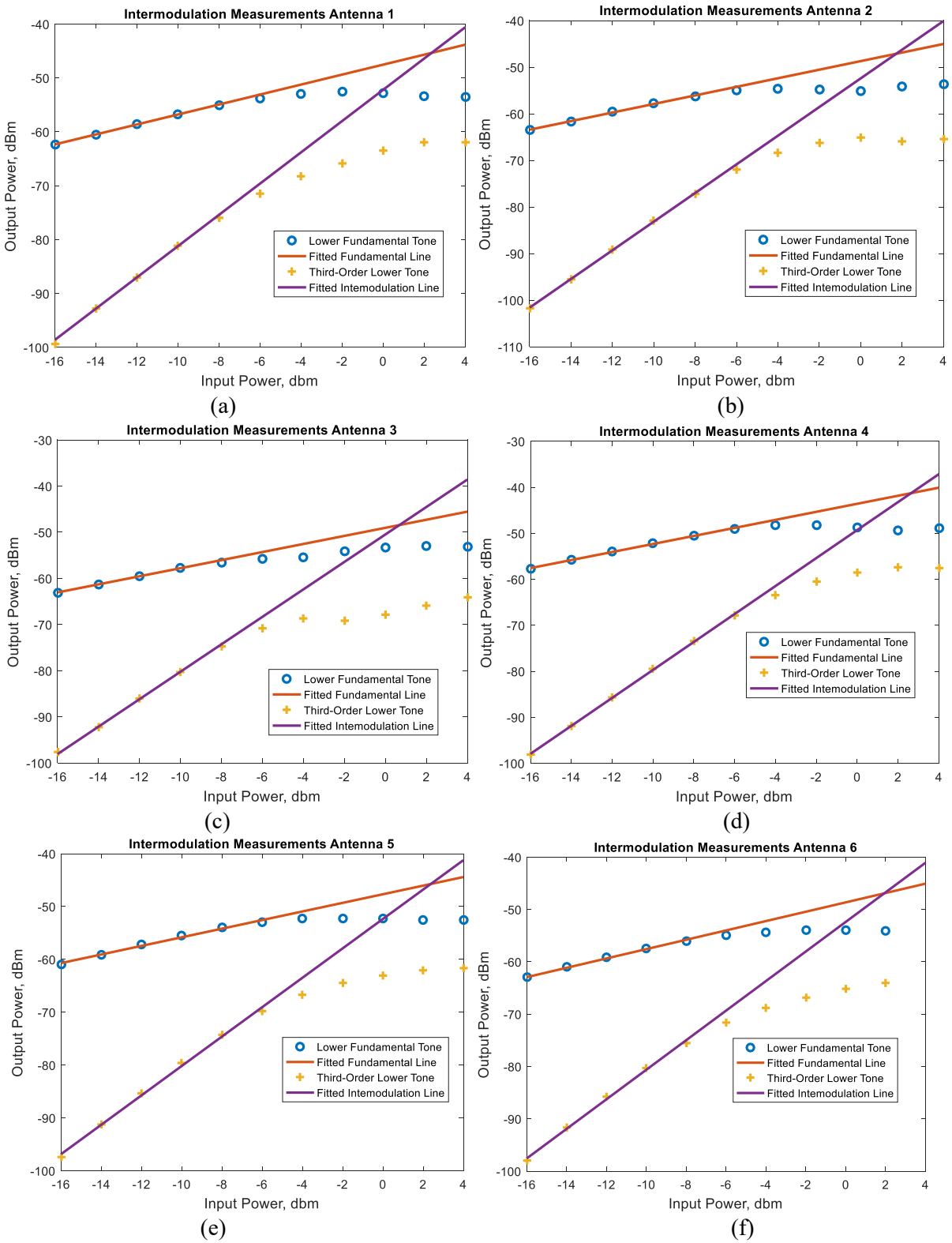

Figure 6.6 Measured intermodulation products at 0V bias a) Antenna 1 b) Antenna 2 c) Antenna 3 d) Antenna 4 e) Antenna 5 f) Antenna 6

6.4 Discussion

Any configuration of the varactors on the radiating edge achieve a higher tunability compared to those achieved by placement on the non-radiating edge, as shown by the measurements in Tables 6.3 & 6.5. The tunability achieved by placing varactors on the radiating edge is similar whatever the separation distance l_{var} between the varactors. Table 6.1 shows that the patches with the varactors on the radiating edge all have the same dimensions, this gives the same area reduction as shown in Table 6.9. It was shown in Chapter 5 that the area reduction of a patch antenna is related to the tunability.

Table 6.9 Patch area reduction due to varactors compared to an antenna on the same substrate with no varactor loading

Antenna	Area Reduction (%)
1	64.0
2	64.0
3	64.0
4	14.2
5	33.7
6	50.0

The varactor placement along the non-radiating edges of the patches effects the tunability of the antennas, unlike the placement of varactors on the radiating edge. Table 6.2 shows that as the distance l_{var} increases and l_{offset} reduces, both tunability and the area reduction increase, this is shown by the data in Tables 6.5 and 6.9.

Figure 6.7 shows a plot of taking the separation distance l_{var} of the non-radiating patches as a percentage of patch length of an antenna with no varactors. This is then plotted against the area reduction calculated in Table 6.9. It is shown that as the separation distance, $l_{var,}$ between the varactors tends to the unloaded patch length a greater tunability is achieved.

The varactor separation distance, $l_{var,}$ can never obtain the same length as the unloaded patch lengths due to the size reduction of the varactor loading. This shows that moving the varactors further apart on the non-radiating edge increases area reduction of the patch and subsequently improves tunability.

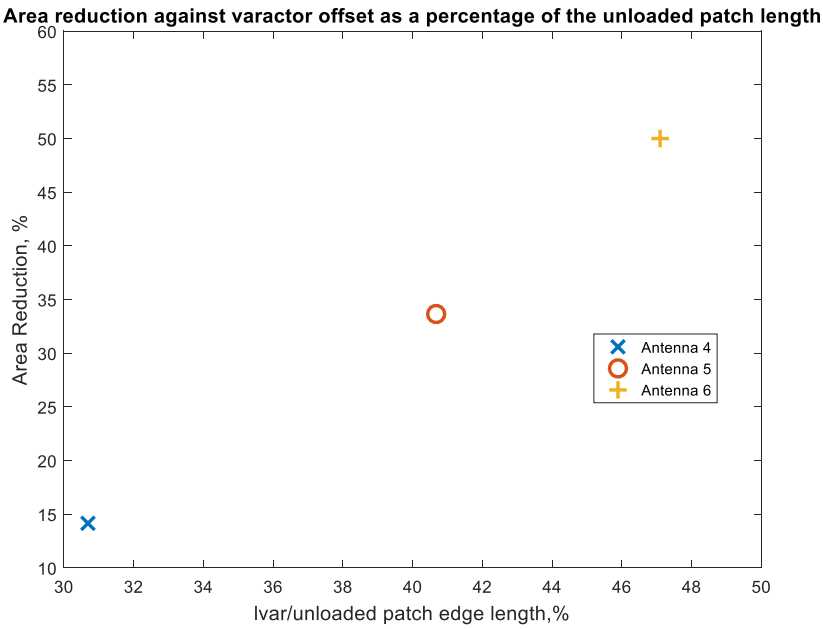

Figure 6.7 Plot showing patch area reduction against varactor spacing as a percentage of unloaded patch length for varactors on the non-radiating edge

Looking at Figure 6.1b, the amplitude of the E-field distribution along the non-radiating edge increases towards the radiating edge. Therefore, antennas with varactors on the non-radiating edge will see an increase in the E-field across each varactor as l_{offset} decreases. This causes the varactor loading to have a greater impact and reduction of the patch area. With the placement of the varactors on the radiating edge there was shown very little variation in the tunability, this is explained by looking at Figure 6.1b. The E-field distribution is constant across the radiating edge so the varactors have the same loading effect and area reduction.

The gain of the antennas improves for the varactors on the non-radiating edge as the separation distance l_{var} between the varactors decreases and the patches increase in size. This is similar to

the results shown in Chapter 5. When comparing antennas on different substrates; the high dielectric constant substrates reduced the size of the patches and reduced the gain accordingly. The increase in gain here comes from the improvement of the radiation efficiency rather than a significant improvement in directivity, this is supported by the simulated values in Table 6.10.

Table 6.10 Simulated directivity and radiation efficiency measurements

Antenna	Directivity (dBi)	Radiation Efficiency (dB)
1	+6.0	-9.3
2	+6.0	-9.1
3	+6.0	-9.2
4	+6.5	-5.9
5	+6.3	-8.0
6	+6.2	-9.6

The varactors on the radiating edge had similar gain measurements for all three configurations, this results from the patches having the same size. There is no difference in the directivity and only slight difference in radiation efficiency as shown by the simulated values in Table 6.10. Table 6.7 shows that the measured gain values are lower than expected from the simulations. This has occurred from a systematic measurement error, however the trend of whether the gain increases, or decreases is the same as the simulated values.

Looking at the measured IIP3 points shown in Table 6.8 it is shown that the linearity performance of the antenna is dependent on the location of the four varactors. As the distance l_{var} between the varactors on the non-radiating edge decreases the IIP3 point of the antennas increases. Similarly, antennas with varactors located on the radiating edge show an improved linearity as l_{var} decreases.

The peak RF voltage across the varactors in each configuration was extracted using the procedure discussed in Chapter 4. Comparing the extracted voltages in Table 5.15 of a single

SMV1405 varactor and those in Table 6.11 it is shown that the peak RF voltage across the four varactors is less than for a single varactor.

Table 6.11 Extracted peak RF voltage amplitude across varactors in CST

Antenna	Peak voltage (V)
1	0.56
2	0.55
3	0.55
4	0.46
5	0.53
6	0.55

When the varactors are located on the radiating edge, the extracted RF voltage across the varactors is almost constant, as seen with antennas 1, 2 and 3. This is expected as the E-field distribution on the radiating edge of a patch antenna is constant across the length as shown in Figure 6.1a. The extracted voltages therefore do not explain why the patches with varactors on the radiating edge have different IIP3 points.

Looking at Figure 6.6a-c the intermodulation measurements for the antennas 1, 2 & 3 all show a dip in the measured power levels; this is seen in both the fundamental and third-order intermodulation products. The dip becomes apparent at a lower applied power level in the fundamental tones than in the intermodulation products. The dip occurs at the highest applied power level for antenna 1, where the varactors with the smallest separation distance l_{var}; antenna 1 also has the highest IIP3 value of the configurations of varactors placed on the radiating edge. Antenna 3 has the dip occurring at the lowest applied power level and has the lowest IIP3 value. Another RF application where this dip can be seen in power limiter circuits that use Schottky diodes [2]. Figure 6.8 shows a typical power in against power out for a limiter circuit with the dip shown.

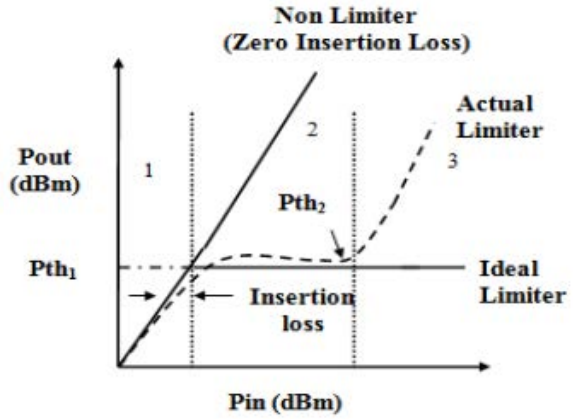

Figure 6.8 Input power against output power for power limiter that exhibits a dip in output power levels [2]

In the design of power limiters an antipodal configuration can be utilized where pairs of diodes are shunted, this configuration is shown in Figure 6.9.

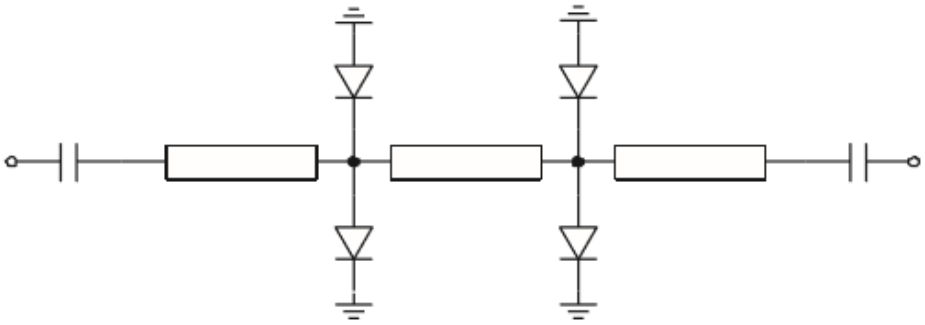

Figure 6.9 Schematic of symmetrical 5th order antipodal limiter [3]

The configuration of the diodes for antennas 1,2 & 3 have the same configuration here except they are separated by the patch with an electrical length of 180 degrees at resonance.

It is proposed that the varactors are acting as a power limiter between the applied signal at the input of the antenna and the radiated signal. It is unknown at present why the spatial differences along the radiating edge has an effect in changing the IIP3 point whilst having the same RF voltage driving each varactor.

The extracted voltages across the varactors on the non-radiating edges do show an increase in amplitude as l_{var} increases. This increase in voltage across the varactors is expected as the magnitude of the E-Field magnitude increases towards the radiating edge as shown in Figure 6.1b. The measured IIP3 points decrease as the varactors separate and the peak RF voltages increase, this behavior is different to that seen in Chapter 5 for patches loaded with a single varactor; it is not known as to why the behaviour is different and further investigation is needed.

6.5 Conclusion

This chapter has looked at the effect of varactor placement on a patch antenna from a frequency tunability, gain and linearity.

The key points from the analysis presented in this chapter are:

1. The greatest frequency tunability is found when the varactors are placed on the radiating edge and the separation distance between the varactors makes marginal difference to the tuning range.
2. The separation distance between the varactors on the non-radiating edge affects the tuning range. The greater the separation distance the greater the tuning range.
3. The worst gain performance is seen when the varactors are placed on the radiating edge this is because the reduction in patch area is at its greatest. In this configuration it was found there is little difference in the gain depending on the separation distance of the varactors.
4. When the varactors are on the non-radiating edge the best gain performance is observed then they are most closely spaced because the patch is largest giving the best radiation efficiency.
5. The IIP3 performance was found to be the best when the varactors are closely spaced on the non-radiating edge, this comes from having the lowest driving RF voltage. As the varactors move apart the linearity performance degrades due to increased RF driving voltage.

6. When the varactors are placed on the radiating edge there is geometry dependent factor that effects the linearity performance. This is indicated by the RF voltage being the same across all the varactors whilst having a variation in the measured IIP3 values.

6.6 References

[1] E. Nishiyama, T. Itoh, "Widely Tunable Stacked Microstrip Antenna Using Varactor Diodes", APMC, 2008.

[2] B. Bhatt, S. C. Bera, "Behaviour of Schottky diode's Dynamic Resistance", International Conference on Electrical Electron. and Optimization Techniques, pp. 1802-1807, 2016.

[3] Plextek Ltd, “Technology Overview Broadband, Low-Loss Limiter MMICs” Plextek, Essex, UK, 2014. [Online]. Available: https://www.plextekrfi.com/publications/publications-from-plextek-rfi/

7 Investigation into the Number of Varactors Loading a Microstrip Patch Antenna

7.1 Introduction

This chapter investigates how the number of varactors loading a patch effect the tunability, linearity and radiation characteristics.

7.2 Design

In this investigation three antennas were fabricated on Cer-10 substrate and loaded with SMV1405 varactors as detailed in Chapter 5. The design frequency was 1.4GHz with a 0V bias voltage applied across the varactors. The antennas had either one, two or three varactors loading the radiating edge. Therefore, the antennas in this chapter will be referred to as single, double or triple relating to the number of varactors attached to the patch. The separation distance between the varactors and the edges of the patch was kept equal and the edges of the patches are kept the same length. The dimensions of the antennas are given in Figure 7.1 and the fabricated antennas are shown in Figure 7.2.

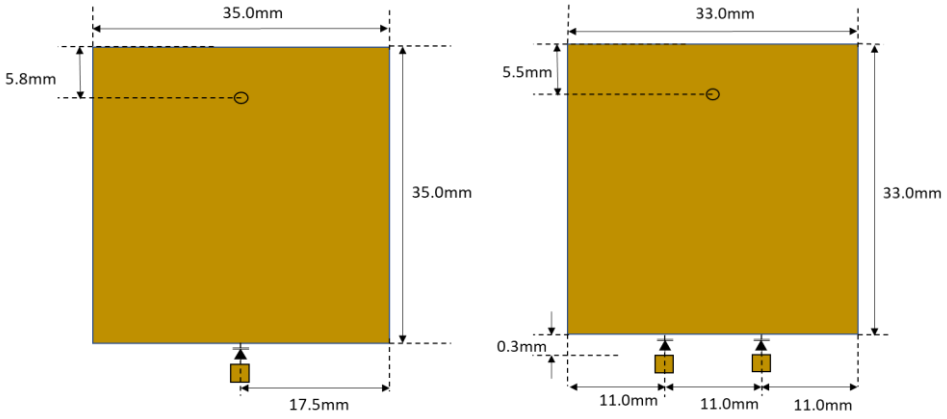

(a) (b)

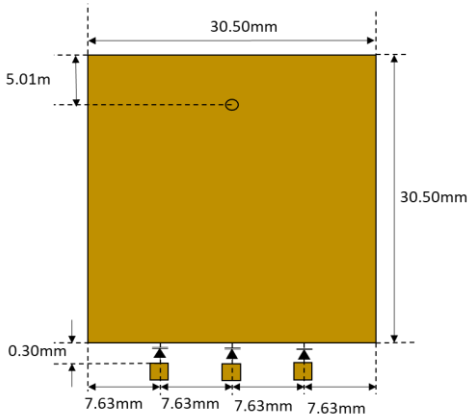

(c)

Figure 7.1 Layout of patches a) Single b) Double c) Triple

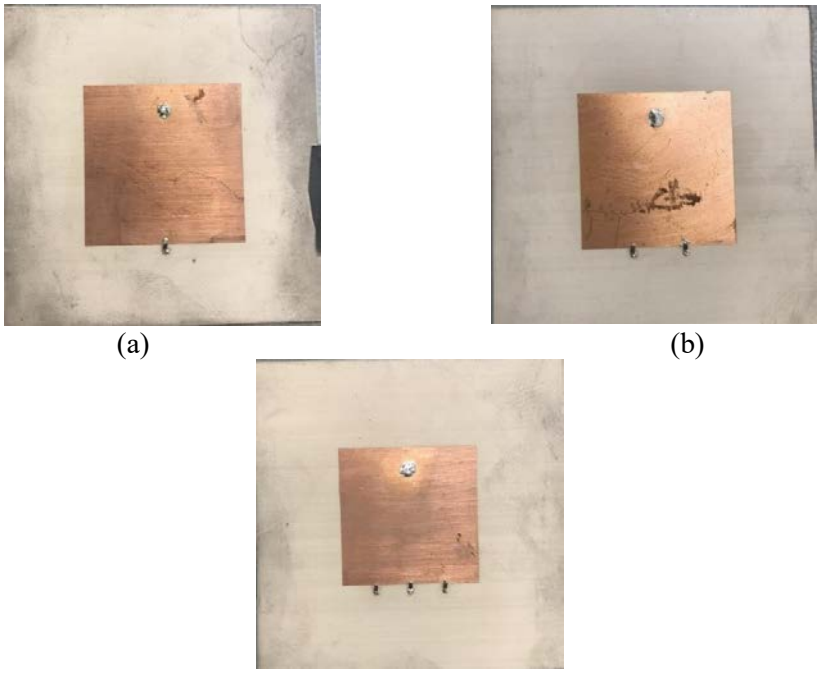

(a) (b)

(c)

Figure 7.2 Fabricated antennas a) Single b) Double c) Triple

7.3 Simulation and Results

7.3.1 Measured Reflection Coefficient

The measured reflection coefficient of the antennas is shown in Figure 7.3.

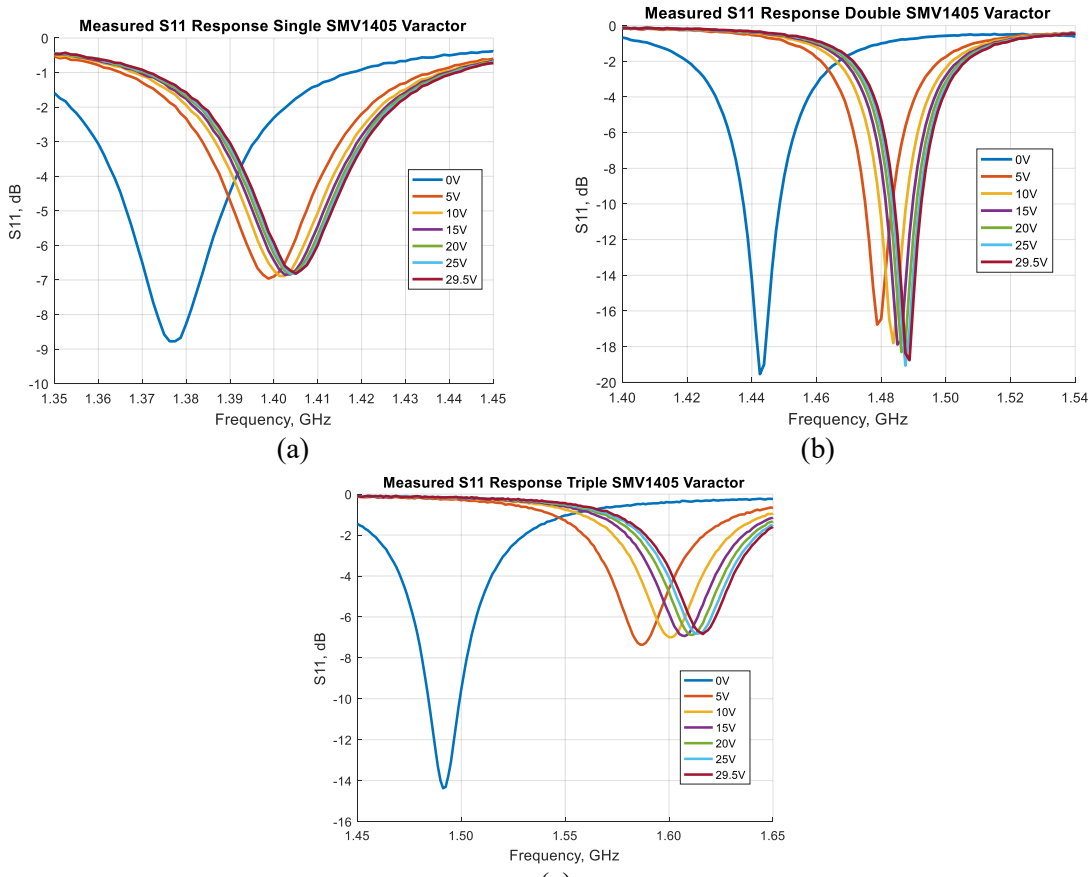

Figure 7.3 Measured S_{11} response of antennas a) Single b) Double c) Triple

7.3.2 Tunability

The measured tunability for the antennas with varying varactor loading given in Tables 7.1.

Table 7.1 Measured results for antennas with multiple number of varactors. At 0V the nominal capacitance of the varactor is 2.67pF. At 29.5V the capacitance is 0.63pF

Antenna	Frequency at 0V (GHz)	Frequency at 29.5V (GHz)	Tunability (%)
Single	1.38	1.41	2.01
Double	1.44	1.49	3.14
Triple	1.49	1.62	7.88

All antennas were designed to be closer to 1.4GHz rather than the spread shown here in the measured values listed in Table 7.1. It was found from simulation that the dielectric constant of Cer-10 was different from the nominal value as given in Table 5.1. Each of the antennas has a different configuration of varactor loading, this causes them to be shifted in frequency by a different amount from design frequency of 1.4GHz. Using the correct extracted dielectric constant value of 9, the simulated frequencies shown in Table 7.2 are now closely matched to those given in Table 7.1.

Table 7.2 Simulated results for antennas with multiple number of varactors, using correct dielectric constant value of 9. At 0V the nominal capacitance of the varactor is 2.67pF. At 29.5V the capacitance is 0.63pF

Antenna	Frequency at 0V (GHz)	Frequency at 29.5V (GHz)	Tunability (%)
Single	1.38	1.41	2.15
Double	1.42	1.49	4.73
Triple	1.48	1.59	7.62

There is still a small variation, however this will likely have come from the other manufacturing tolerances as discussed in section 5.3.2.1.

7.3.3 Radiation Patterns

Radiation patterns for the single and triple antenna are shown in Figure 7.4a and 7.4b respectively.

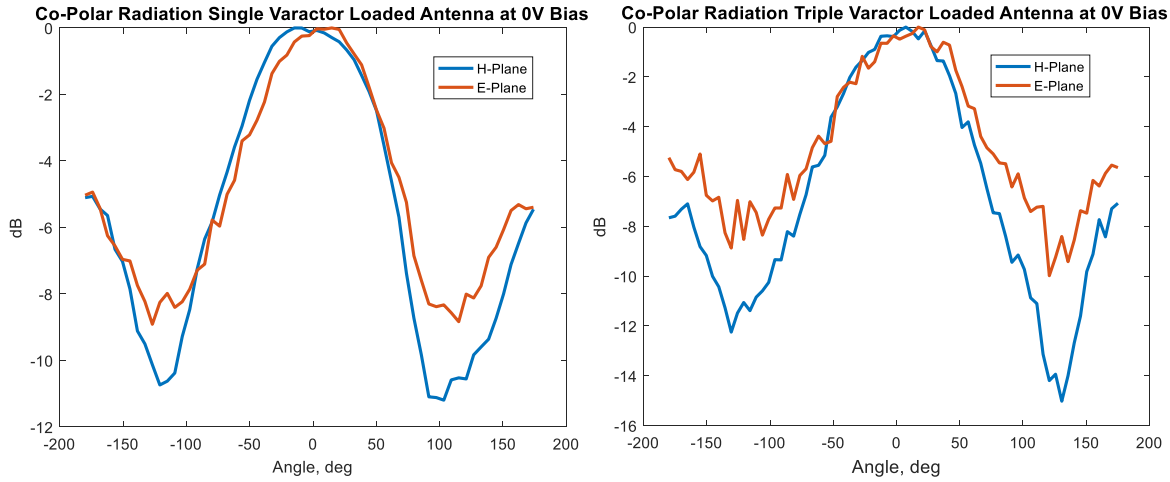

(a) (b)

Figure 7.4 Measured radiation patterns at 0V bias a) Single antenna 1.38GHz b) Triple antenna at 1.49GHz

7.3.4 Gain

The measured and simulated gain values for the antennas are given in Table 7.3.

Table 7.3 Simulated and measured gain values for antennas with different number of varactors

Antenna	Gain (dBi)	
	Simulated	Measured
Single	-1.8	-2.2
Double	-1.8	-3.2
Triple	-1.9	-3.7

7.3.5 IIP3 Measurements

The measured IIP3 points are given in Table 7.4 and the measured data plots are given in Figure 7.5.

Table 7.4 Measured IIP3 points at 0V bias for antennas with different number of varactors

Antenna	IIP3 (dBm)
Single	+2.8
Double	+3.0
Triple	+5.9

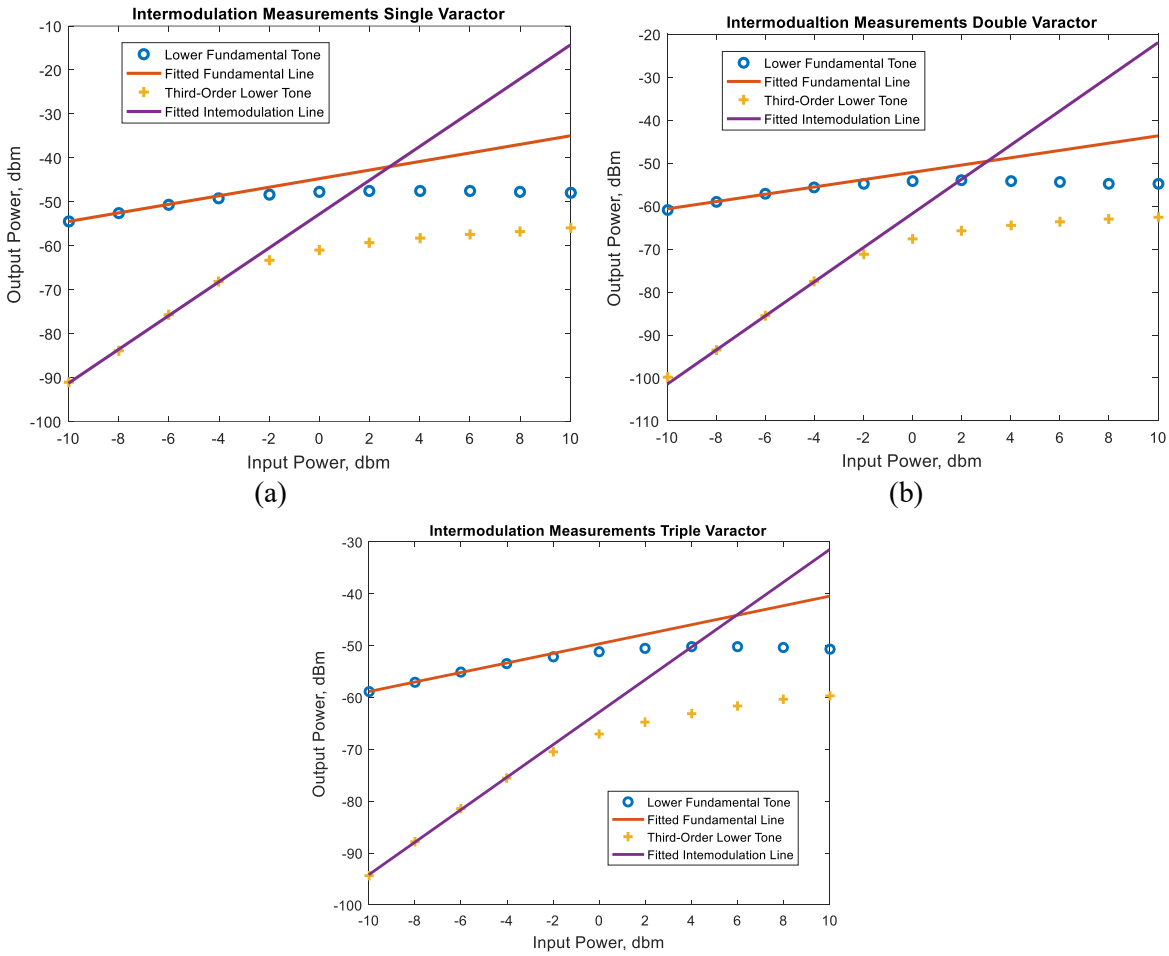

Figure 7.5 Measured intermodulation products at 0V bias a) Single b) Double c) Triple

7.4 Discussion

The antenna that achieved the best tunability is the triple antenna as shown by the measurements in Table 7.1. It is the triple antenna that has the largest area reduction as shown in Table 7.5, these results support the previously seen relation between tunability and reduction in the surface area of the patch.

Table 7.5 Patch area reduction of antennas due to varactor loading compared to unloaded patch

Antenna	Area Reduction (%)
Single	0.57
Double	10.59
Triple	23.60

Chapter 5 showed that as design frequency is increased, so does the tunability of a varactor loaded antenna. In this investigation the design frequencies at 0V of the three antennas are not the same as shown in Table 7.1. To remove the influence of frequency on the tunability of the patch antennas they were re-simulated. There is now confidence in the simulated results as the dielectric constant of the substrate has been identified and confirmed from looking at the simulated and measured values in Table 7.1 and 7.2. The re-simulated antennas with new dimensions are listed in Table 7.6.

Table 7.6 Simulated results for antennas with different varactor numbers using corrected dimensions

Antenna	Adjusted patch edge length (mm)	Frequency at 0V (GHz)	Frequency at 29.5V (GHz)	Tunability (%)
Single	34.5	1.40	1.43	2.12
Double	33.8	1.40	1.46	4.20
Triple	32.7	1.40	1.50	6.90

When the antennas have the same design frequency, the order of the tunability of the antennas as shown in Table 7.6 (column 5), is still the same as those found from using the measured antennas in Table 7.1. This gives confidence that the triple antenna does have the largest tuning range even with its higher starting frequency.

The peak RF voltage across the varactors was extracted in CST using the same procedure as detailed in Chapter 4. Figure 7.6 shows the labelling of the varactors and Table 7.7 shows the extracted peak RF voltages.

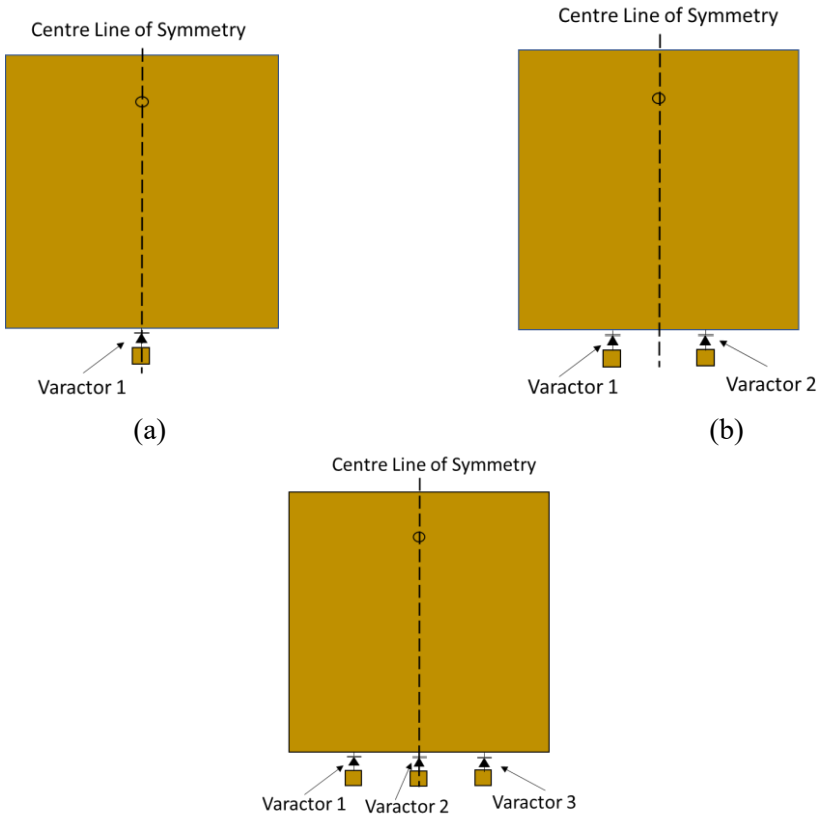

Figure 7.6 Varactor labels for fabricated antenans a) Single b) Double c) Triple

It was expected that the voltages across the varactors for the triple antenna would have the same value across all three varactors however this is not the case as shown by Table 7.7. The voltages are however symmetric about the centre line defined in Figure 7.6b-c.

Table 7.7 Extracted peak RF voltage amplitude across varactors for antennas with varying varactor loading

Antenna	Peak voltage (V)		
	Varactor 1	Varactor 2	Varactor 3
Single	0.65		
Double	0.61	0.61	
Triple	0.58	0.61	0.58

The E-field distribution on an unloaded patch will be the same magnitude across the radiating edge as shown in Figure 6.1a. Looking at the simulated E-fields of the patches in Figures 7.7, the locations of the varactors alter the E-field distribution across the radiating edge. The alterations of the E-field patterns from the varactor loading do not affect the radiation patterns as shown in measured radiation patterns in Figure 7.4a and 7.4b.

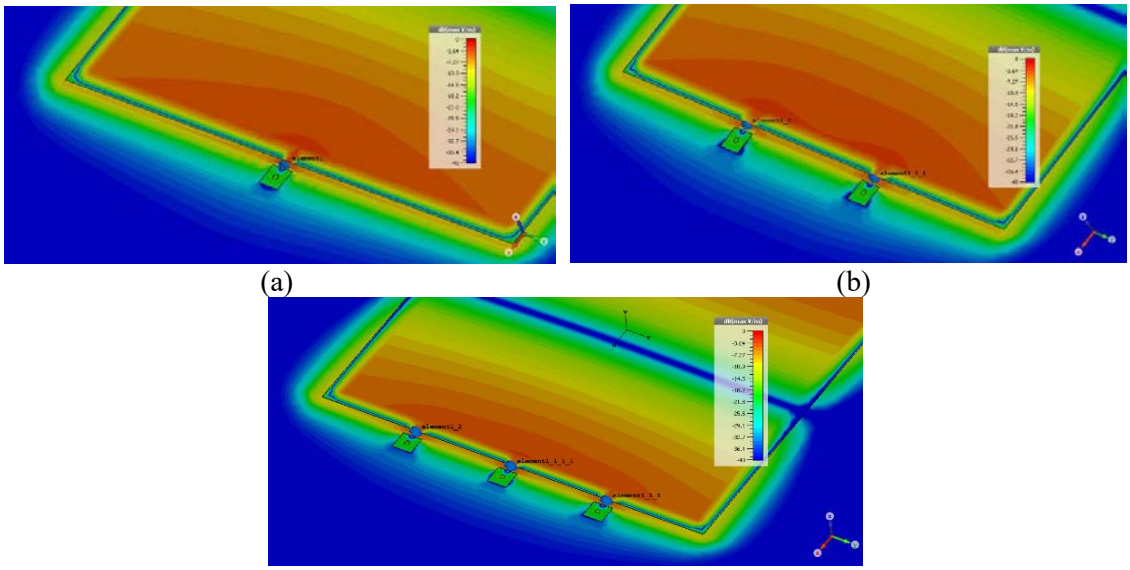

(a) (b)

(c)

Figure 7.7 Simulated E-Field distribution across radiating edge at 0V bias a) Single b) Double c) Triple

The extracted voltages and simulated E-fields on the triple antenna suggest that the centre varactor is providing the greatest loading effect on the patch. To test if a centrally placed varactor is the most influential, the three varactors on the triple and the two varactors on the double antenna are replaced with a single varactor in CST. The single varactor has the same total capacitance loading the radiating edge as either the double or triple antenna. The edges of the patches are tuned in length to achieve the same resonant frequency as the values given in Table 7.2. Table 7.8 shows the new patch lengths of the antennas with the combined capacitance values.

Table 7.8 Dimensions for antennas with a single varactor replacing multiple varactors. New simulated frequencies and tunability are shown.

Antenna	Total Capacitance at 0V (pF)	Total Capacitance at 29.5V (pF)	New patch length (mm)	Frequency at 0V (GHz)	Frequency at 29.5V (GHz)	Tunability (%)
Double	5.34	1.26	30.3	1.42	1.61	12.54
Triple	8.01	1.89	15.3	1.48	2.59	54.54

Looking at the new patch lengths in Table 7.8 and comparing them to the original lengths for double and triple antennas shown in Figure 7.1b-c, a reduction is found when using the single varactor. With the reduction in length and the subsequent area reduction greater tunability is achieved. The triple antenna shows a significant increase in the tunability when using a single varactor compared to three individual varactors with the same capacitance.

This shows that the distribution of the capacitance along a patch's radiating edge and not just the total capacitance value has a noticeable effect on the tunability. Therefore, if improved tunability is required, it is better to use a single varactor with a greater capacitance value rather than distributing the capacitance along a single edge.

Looking at Table 7.3 there is a difference between the measured gain of the antennas and the simulated values. The simulations suggest that the gain value of the patches should be the same irrespective of the varactor numbers. The measured gain however decreases as the patch size decreases which is like results seen in previous chapters. It was reported in [1] that loading a patch with multiple varactors along the radiating edge improves the gain of a patch. The measured values here in Table 7.3 show a different result, the gain decreases with the addition of more varactors. A difference between the work undertaken here and that in [1] is only one edge of the patch is loaded in this work, this may account for the discrepancy in results.

The most linear antenna tested here is the triple antenna as shown by the highest measured IIP3 point in Table 7.4. Therefore, by adding extra varactors each one behaves more linearly and

contributes to a higher IIP3 point, even though more nonlinear elements are added onto the patch.

With the addition of more varactors, and the reduction in peak RF voltage across the varactors seen in this investigation, it would suggest that the antennas loaded with four varactors in Chapter 6 would have higher IIP3 points than those seen in Table 7.4. However, Chapter 5 showed that the as the frequency of operation increases it causes a reduction in the IIP3 point of the antenna. This explains why the IIP3 point of the antenna loaded with four varactors operating at 1.8GHz in Chapter 6 is lower than the antenna loaded with three varactors operating at 1.4GHz presented here.

With multiple varactors investigated in this chapter there is not the same dip in the IIP3 measurement as shown in Chapter 6. This supports the findings that the varactor placement on the patches does have an inherent effect on the nonlinear performance characteristics.

7.5 Conclusion

This chapter has looked at the effect of the number of varactors loading a patch antenna and the effect on tunability, gain and linearity.

The key points from the analysis presented in this chapter are:

1. The linearity of the antennas is improved by adding multiple varactors onto the patch even though more nonlinear components are being added.

2. The tunability of the antennas is improved when more varactors are added as area reduction of the patch is greater.

3. The gain of the antennas is reduced as more varactors are loaded onto the antenna.

4. The location of the varactors influences the tuning range and it is more effective to put a single larger capacitance varactor on the edge rather than distributing the capacitance into multiple varactors.

7.6 References

[1] Z. Jin and A. Mortazawi, "An L-Band Tunable Microstrip Antenna Using Multiple Varactors," IEEE Antennas and Propagation Symposium, 2003, pp. 524-527.

8 Investigation into Abrupt and Hyperabrupt Diodes on a Microstrip Patch Antenna

8.1 Introduction

This chapter investigates the performance of microstrip patch antennas that are loaded with either hyperabrupt or abrupt diodes as the tunable component. The difference between these two types of diode, as discussed in Chapter 3, is the doping gradient of the varactors. This investigation will show if there is any significant difference or benefit in tunability, gain and linearity when using the two different types of diode.

8.2 Design

To investigate the different effects on performance between using abrupt and hyperabrupt varactor diodes, a total of four were chosen with the characteristics listed in Tables 8.1 and 8.2.

Table 8.1 Capacitance values for abrupt diodes

Varactor	Capacitance (pF)		Series resistance (Ω)
	0V bias	30V bias	
SMV1405 [1]	2.67	0.63	0.80
SMV1413 [1]	9.24	1.77	0.35

Table 8.2 Capacitance values for hyperabrupt diodes

Varactor	Capacitance (pF)		Series resistance (Ω)
	0V bias	15V bias	
SMV1231 [2]	2.35	0.47	2.50
SMV1234 [2]	9.63	1.32	0.80

All the diodes used in this investigation are in the SC-079 package type. They therefore all have a package inductance of 0.7nH. These diodes were chosen as they have similar capacitance values at 0V bias between the abrupt and hyperabrupt, this gives patches of a similar size. Figure 8.1 shows the plotted capacitance against reverse bias voltages for the four diodes, this clearly

shows the hyperabrupt varactors achieve a larger tuning range to the abrupt diodes for a lower bias voltage.

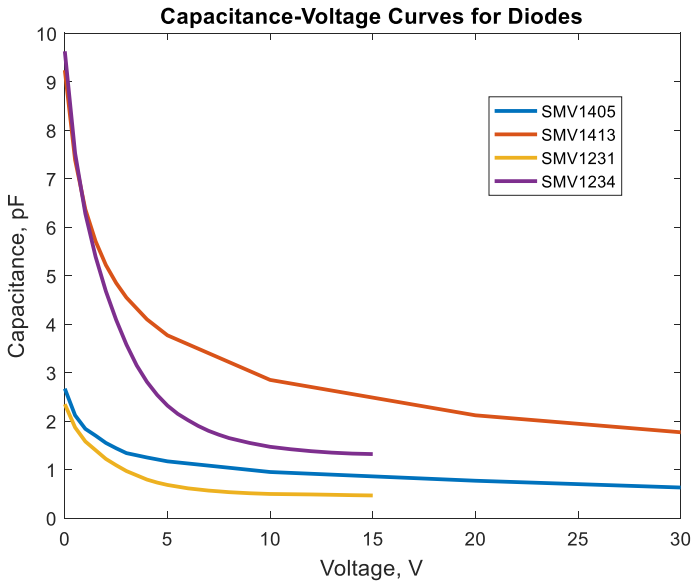

Figure 8.1 Plot showing capacitance against reverse bias voltage for abrupt (SM14xx) and hyperabrupt (SM12xx) diodes

This selection of diodes also allows an investigation into the difference in tunability, linearity and gain for varactors with different capacitance values of the same type.

Square patches are used with a single varactor loading the radiating edge as shown in Figure 8.2 with dimensions given in Table 8.3. The patches were fabricated using TLC30 substrate with thickness 0.78mm and have the electrical properties listed in Table 5.1. All the patches have a design frequency of 1.4GHz at 0V bias.

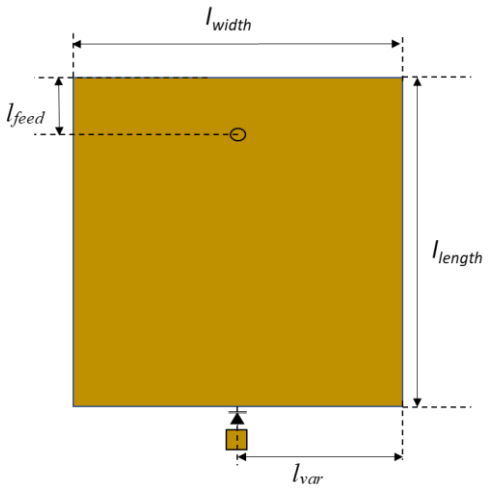

Figure 8.2 Layout of antennas with abrupt and hyperabrupt diodes

Table 8.3 Dimensions for patch antennas with varactors on radiating edges. The hyperabrupt diodes are numbered 12xx, the abrupt are numbered 14xx. The low capacitance diodes are the SMV1405 and SMV1231. The high capacitance diodes are the SMV1413 and SMV1234.

Antenna	l_{width} (mm)	l_{length} (mm)	l_{var} (mm)	l_{feed} (mm)
SMV1405	58.0	58.0	29.0	17.4
SMV1413	23.0	23.0	11.5	9.6
SMV1231	58.5	58.5	29.3	14.6
SMV1234	22.0	22.0	11.0	8.8

The fabricated antennas loaded with the SMV1405 and SMV1413 abrupt diodes are shown in Figure 8.3, the difference in patch size can be seen clearly.

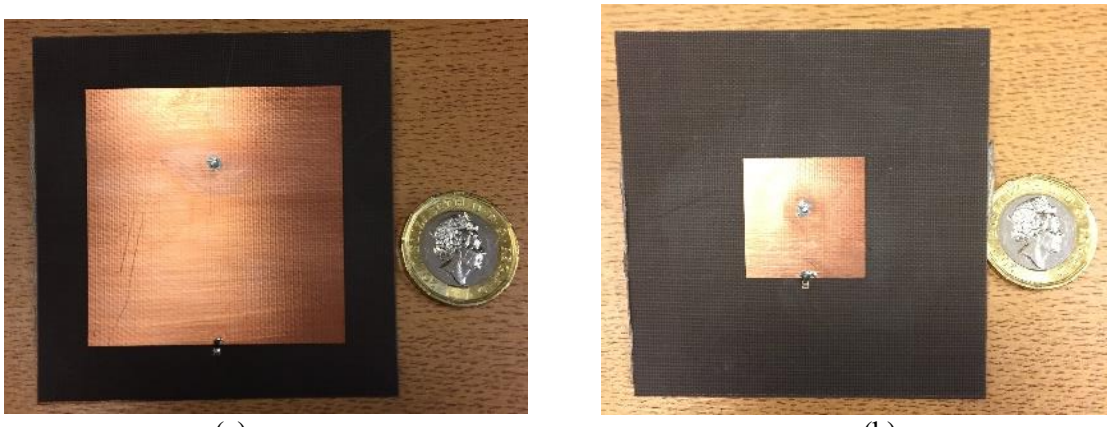
(a) (b)

Figure 8.3 Fabricated antennas with abrupt diodes a) Patch with SMV1405, low capacitance b) Patch with SMV1413, high capacitance

8.3 Simulation and Results

8.3.1 Measured Reflection Coefficient

The measured reflection coefficient of the antennas is shown in Figure 8.4.

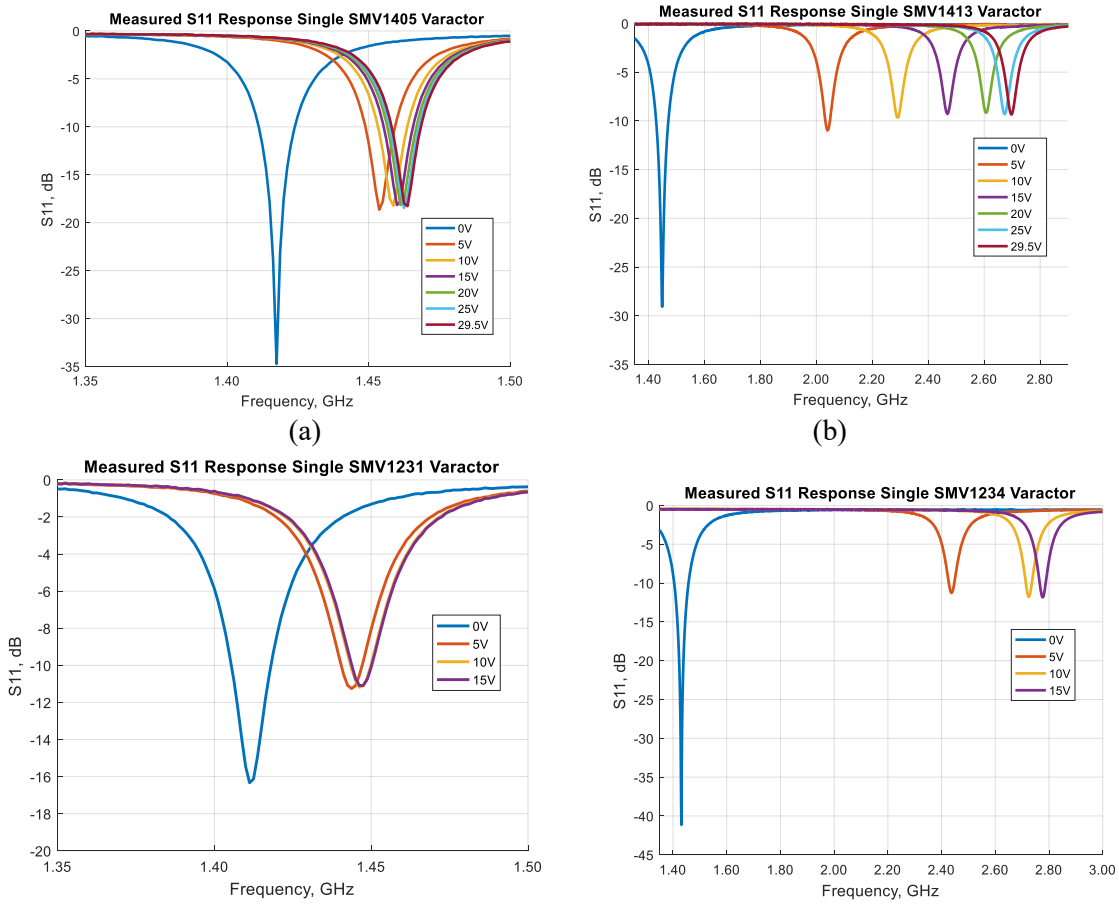

Figure 8.4 Measured S_{11} response of antennas a) SMV1405 b) SMV1413 c) SMV1231 d) SMV1234. Note (a) is low capacitance, abrupt, (b) is high capacitance, abrupt. (c) is low capacitance, hyperabrupt, (d) is high capacitance, hyperabrupt

8.3.2 Tunability

The measured and simulated tunability for the antennas loaded with abrupt and hyperabrupt diodes are given in Tables 8.4, 8.5, 8.6 and 8.7 respectively.

Table 8.4 Measured tunability for antennas with abrupt varactors. The high capacitance diode is the SMV1413. The low capacitance the SMV1405

Antenna	Frequency at 0V (GHz)	Frequency at 29.5V (GHz)	Tunability (%)
SMV1405	1.42	1.47	3.25
SMV1413	1.45	2.70	59.90

Table 8.5 Simulated tunability for antennas with abrupt varactors. The high capacitance diode is the SMV1413. The low capacitance the SMV1405

Antenna	Frequency at 0V (GHz)	Frequency at 29.5V (GHz)	Tunability (%)
SMV1405	1.40	1.45	2.95
SMV1413	1.40	2.63	61.20

Table 8.6 Measured tunability for antennas with hyperabrupt varactors. The high capacitance diode is the SMV1234. The low capacitance the SMV1231.

Antenna	Frequency at 0V (GHz)	Frequency at 15V (GHz)	Tunability (%)
SMV1231	1.41	1.45	2.48
SMV1234	1.44	2.78	63.60

Table 8.7 Simulated tunability for antennas with hyperabrupt varactors. The high capacitance diode is the SMV1234. The low capacitance the SMV1231.

Antenna	Frequency at 0V (GHz)	Frequency at 15V (GHz)	Tunability (%)
SMV1231	1.40	1.44	2.60
SMV1234	1.40	2.94	70.84

8.3.3 Radiation Patterns

The measured radiation patterns for the abrupt diodes are given in Figure 8.5a and 8.5b and the radiation patterns for the hyperabrupt diodes are given in Figure 8.5c and 8.5d.

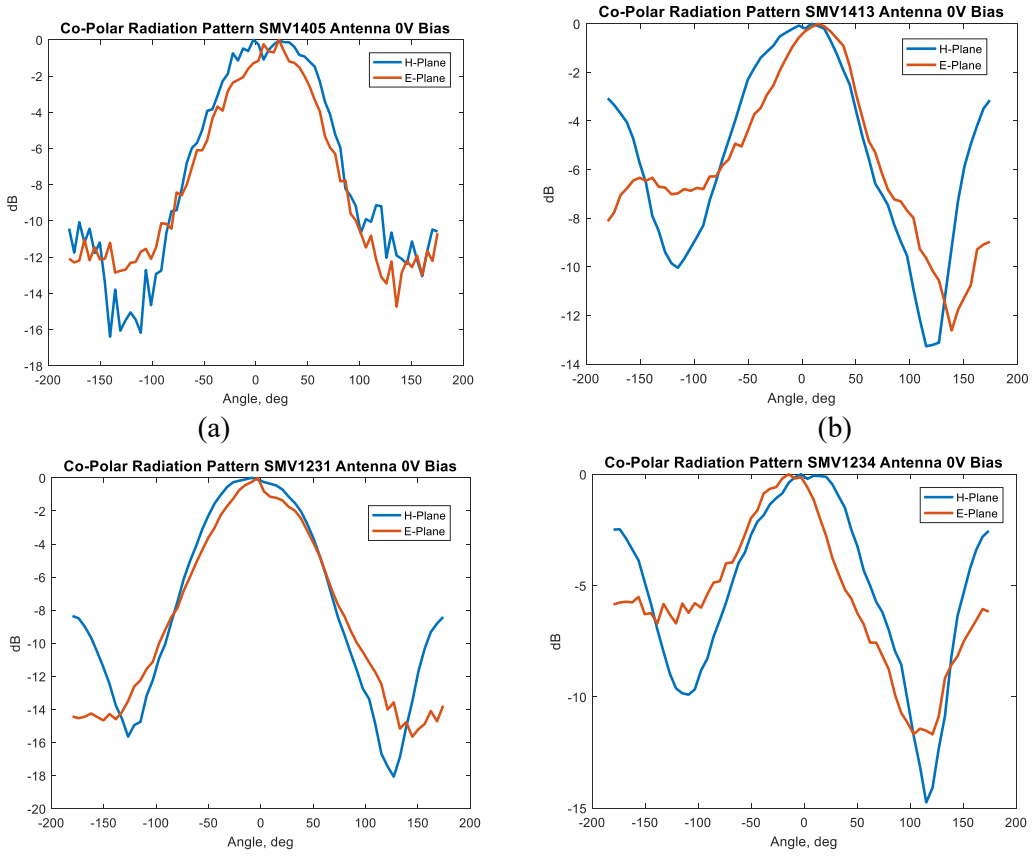

Figure 8.5 Measured radiation patterns at 0V bias a) SMV1405 at 1.42GHz 1 b) SMV1413 at 1.45GHz c) SMV1231 at 1.41GHz d) SMV1234 at 1.44GHz. Note (a) is low capacitance, abrupt, (b) is high capacitance, abrupt. (c) is low capacitance, hyperabrupt, (d) is high capacitance, hyperabrupt

Looking at Figure 8.5, the radiation patterns are those of standard patch antennas. There is a jump in the radiation pattern in Figure 8.5c, this sudden change is likely to have come from the patch shifting slightly on the stand. The patch is held on by double sided tape and can come loose due to the movement of the turntable.

8.3.4 Gain

The measured and simulated gain values for the antennas are given in Table 8.8.

Table 8.8 Simulated and measured gain values for antennas loaded with different varactor types. The hyperabrupt diodes are numbered 12xx, the abrupt are numbered 14xx. The low capacitance diodes are the SMV1405 and SMV1231. The high capacitance diodes are the SMV1413 and SMV1234.

Antenna	Gain (dBi)	
	Simulated	Measured
SMV1405	+2.4	+1.6
SMV1413	-14.6	-14.8
SMV1231	+0.6	+2.0
SMV1234	-16.9	-16.3

8.3.5 IIP3 Measurements

The measured IIP3 points in the anechoic chamber are given in Table 8.9 and the measurement plots in Figure 8.6

Table 8.9 Measured IIP3 points of antennas loaded with different varactor types at 0V bias. The hyperabrupt diodes are numbered 12xx, the abrupt are numbered 14xx. The low capacitance diodes are the SMV1405 and SMV1231. The high capacitance diodes are the SMV1413 and SMV1234.

Antenna	IIP3 (dBm)
SMV1405	+7.4
SMV1413	+5.5
SMV1231	+4.9
SMV1234	+9.1

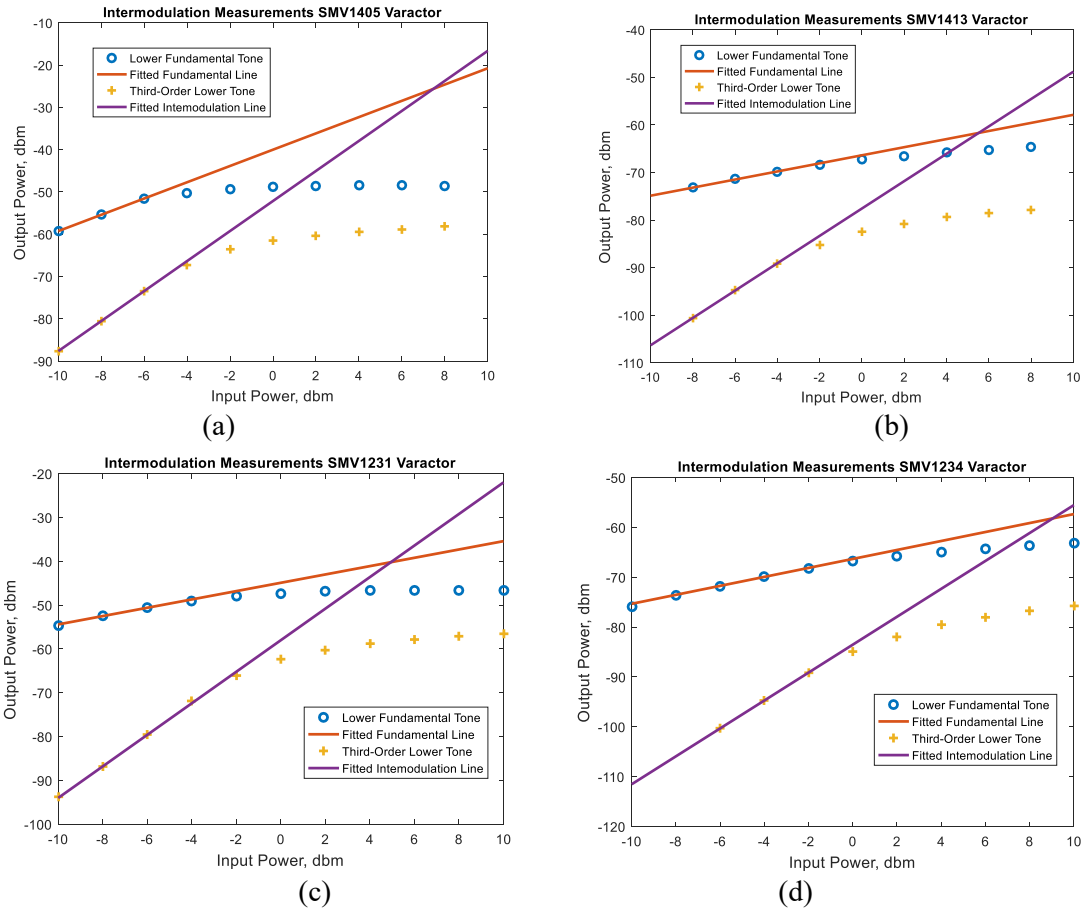

Figure 8.6 Measured intermodulation products at 0V bias a) SMV1405 b) SMV1413 c) SMV1231 d) SMV1234. Note (a) is low capacitance, abrupt, (b) is high capacitance, abrupt. (c) is low capacitance, hyperabrupt, (d) is high capacitance, hyperabrupt

8.4 Discussion

As seen with the other antennas investigated in this thesis, an antenna's tunability will be dependent on the capacitance of the varactor at 0V bias and the subsequent miniaturization of the patch. The amount that a patch is miniaturized is not only affected by the varactors capacitance but also dependent upon such factors as the location of the varactors and the substrate material used. In this chapter unlike the previous chapters, different types of varactors with similar capacitance values and different tuning ratios are being compared, as well as similar types of diodes with dissimilar capacitance values.

The tuning ratio of a varactor is defined as [3]:

$$\eta = \frac{C_{\max}}{C_{\min}} \tag{18}$$

where:

$C_{\max}$: Maximum capacitance value of varactor, pF

$C_{\min}$: Minimum capacitance value of varactor, pF

The tuning ratio of the varactors used here are listed in Table 8.10

Table 8.10 Calculated tuning ratio using values in datasheet. The hyperabrupt diodes are numbered 12xx, the abrupt are numbered 14xx. The low capacitance diodes are the SMV1405 and SMV1231. The high capacitance diodes are the SMV1413 and SMV1234.

Antenna	η
SMV1405	7.42
SMV1413	5.22
SMV1231	6.12
SMV1234	7.30

The first comparison to be made is between the two varactors with lower capacitance, the SMV1405 and SMV1231, to the higher capacitance varactors, the SMV1413 and the SMV1234. The antennas loaded with the greater capacitance diodes have the greatest miniaturization of the patch as shown by Table 8.11. This gives a greater tunability as was shown in previous chapters and the results in Tables 8.4 and 8.6.

Table 8.11 Calculated area reduction from varactor loading. The hyperabrupt diodes are numbered 12xx, the abrupt are numbered 14xx. The low capacitance diodes are the SMV1405 and SMV1231. The high capacitance diodes are the SMV1413 and SMV1234.

Antenna	Area Reduction (%)
SMV1405	6.5
SMV1413	85.3
SMV1231	5.0
SMV1234	86.5

The next comparison of tunability is between varactors with similar capacitance values. Looking first at the SMV1405 and the SMV1231, the tunability is greatest for the abrupt SMV1405 diode as shown from looking at Tables 8.4 and 8.6. The abrupt SMV1405 achieves its greater tunability over the hyperabrupt SMV1231 by having a larger starting capacitance and also the larger tuning ratio as shown in Table 8.10.

Similarly, when comparing the tunability of the antennas with the SMV1413 and the SMV1234 diodes, the superior tuning performance of the hyperabrupt SMV1234 diode comes from possessing the greater starting capacitance and subsequent miniaturization as well as the larger capacitance tuning ratio.

Of these two parameters, starting capacitance and tuning ratio, for achieving the greatest tunability the more critical is the starting capacitance. This can be seen by the SMV1405 having the largest capacitance ratio of the diodes but does not create an antenna with the greatest tunability as it does not have the greatest miniaturization of the patch.

In previous investigations in this thesis, the antennas all used the same varactor diodes. Therefore, any losses within the diodes are the same and any difference in measured gain is attributed to the patch size reduction due to the different loading effects of the varactors. In this investigation the hyperabrupt diodes have different losses to the abrupt diodes. This comes from the variation in the doping of the diodes which allow for a greater capacitance tuning value per applied DC bias voltage. The extracted losses of the diodes are given as a resistance value listed in Table 8.12.

To examine the effects that varactor diodes have on the radiation characteristics of the antenna the dissipated power in the different varactors was extracted using CST; the power levels accepted by the antennas were calibrated using the procedure outlined in Chapter 4. The

extracted power dissipation in the varactor, and the radiation efficiency for the different antennas is given in Table 8.12.

Table 8.12 Simulated radiation efficiency and power dissipation in varactors. The hyperabrupt diodes are numbered 12xx, the abrupt are numbered 14xx. The low capacitance diodes are the SMV1405 and SMV1231. The high capacitance diodes are the SMV1413 and SMV1234.

Antenna	$R_s(\Omega)$	Radiation efficiency (dB)	Power dissipated (mW)
SMV1405	0.80	-3.86	0.18
SMV1413	0.35	-18.56	0.82
SMV1231	2.5	-5.66	0.47
SMV1234	0.80	-21.20	0.92

Looking at the results in Table 8.12, greater power dissipation in the varactor leads to a lower the radiation efficiency which is an expected result. This result is true for both the low and high capacitance values and both types of diode. The measured gain of the hyperabrupt SMV1231 antenna is larger than that of the abrupt SMV1405 antenna which conflicts with the simulated results given in Table 8.8. The greater measured gain is likely to have come from a measurement error as discussed in Chapter 4.

Comparing the measured gain of the antennas shown in Table 8.8 to the antenna in [4] that uses a SMV1233 diode with 0V bias and layout as shown in Figure 2.11, the antenna in [4] has a measured gain value of +3.66dBi which is better than any of the antennas investigated in this chapter.

The expectation was that varactors with similar capacitance values would have similar linearity performance as they have related C-V curves as shown in Figure 8.1. However, this is not shown by the measured IIP3 points in Table 8.9. Comparing the SMV1413 and the SMV1234 diodes, whilst close in capacitance values at 0V, the hyperabrupt SMV1234 exhibits a higher IIP3 value. In contrast, the abrupt SMV1405 diode has a higher IIP3 value to that measured for the hyperabrupt SMV1231 diode.

To understand this, it is necessary to consider another factor that will be influential in the IIP3 point. The extracted RF voltages across the diodes using CST are different, as shown in Table 8.13. Therefore, even with similar C-V curves there is a different RF driving voltage modulating the capacitance for similar diodes.

Table 8.13 Extracted peak RF voltages across varactors in CST. The hyperabrupt diodes are numbered 12xx, the abrupt are numbered 14xx. The low capacitance diodes are the SMV1405 and SMV1231. The high capacitance diodes are the SMV1413 and SMV1234.

Antenna	Voltage (V)
SMV1405	0.76
SMV1413	0.44
SMV1231	0.66
SMV1234	0.27

Table 8.13 shows that the extracted voltage across the abrupt SMV1405 diode is greater than that across the SMV1231 diode. In this comparison the larger RF voltage amplitude across the SMV1405 gives a higher IIP3 point, shown in Table 8.9. Comparing next the high capacitance SMV1413 and the SMV1234 diodes, in this case the lower RF voltage across the hyperabrupt SMV1234 diode yields a higher measured IIP3 point shown in Table 8.9. These results show having a larger RF voltage across the varactor when they have a lower capacitance value will give improved IIP3 performance. In contrast, at higher capacitance values a lower RF voltage will improve IIP3 performance.

Another way to view the data is to consider the difference in the linearity performance between different capacitance values of the varactors within the two different types of diodes. When using abrupt diodes (SMV14xx), the lower the capacitance the greater the IIP3 point and the greater the RF voltage across the diode. Hyperabrupt diodes (SMV12xx) have the opposite relationship, the greater the capacitance the higher the IIP3 point, for this type of diode a lower RF voltage

yields better linearity which is the opposite to the abrupt diodes. It is difficult therefore to see any consistent behavior between the diodes based upon similar C-V curves, capacitance values at 0V, diode types or the magnitude of the RF voltage driving the diodes.

Comparing the measured IIP3 points shown in Table 8.9 with the measured IIP3 value of +5.5dBM given in [4] for a similar patch antenna with a SMV1233 hyperabrupt diode with 0V bias, only the SMV1231 diode investigated here has a lower IIP3 value.

In the previous investigations reported in this thesis, the same diode was used for the different configurations of antennas being compared. Therefore, the reverse and forward bias cycling effects of the diode were common between the antennas under investigation. In this study each of the diodes will have a different construction and doping gradient to achieve the different capacitance values and tuning characteristics.

To investigate the different effects of forward and reverse biasing a diode and its effect on nonlinearity an experiment could be implemented. The reverse recovery time of the different diodes could be measured as shown in Figure 3.15. These measurements could then be combined in a SPICE model of the diode. It would still be difficult to include hysteresis effects of the minority carriers not fully diffusing back across the base region and extracting the nonlinear performance.

8.5 Conclusion

This chapter has looked at the effect of abrupt, hyperabrupt diodes and different capacitance values of each on the tunability, gain and linearity of frequency tuned antennas.

The key points from the analysis are:

1. When using diodes with similar capacitance values at 0V the tuning ratio now needs to be taken into account.

2. The miniaturization of the patch due to the varactor capacitance at 0V is more influential in determining the tunability of a patch than the tuning ratio.

3. Diodes that have a greater series resistance, will increase the power dissipation in the diode and reduce the radiation efficiency of the antenna.

5. There was no consistent diode behaviour when investigating the linearity of the patches however, the most linear diode was the SMV1234 and the least linear diode was the SMV1231.

6. Further modelling techniques that investigate the forward and reverse bias effects on the different diodes are required and need to be combined with the three-dimensional modelling of the patch.

8.6 References

[1] SKYWORKS, "SMV1405 to SMV1430 Series: Plastic Packaged Abrupt Junction Tuning Varactors," SMV1405 TO SMV1430 VARACTORS, Jan. 2016.

[2] SKYWORKS, "SMV123x Series: Hyperabrupt Junction Tuning Varactors," SMV123x VARACTORS, June 2012.

[3] M. P. J. Tiggelman, K. Reimann, F. V. Rijs, J. Schmitz, and R. J. E. Hueting, "On the Trade-Off Between Quality Factor and Tuning Ratio in Tunable High-Frequency Capacitors," IEEE Transactions on Electron Devices, vol. 56, no. 9, pp. 2128–2136, 2009.

[4] S. Yong, "Design and Analysis of Pattern Null Reconfigurable Antennas," Ph.D dissertation, Dept. Electr. Comput. Eng., Univ. Illinois at Urbana-Champaign, Urbana, IL, 2012.

9 Investigation of Microstrip Patch Antenna Using Common Cathode Varactors

9.1 Introduction

This chapter looks at the effects of loading a tunable patch antenna with either a single common cathode pair of varactors or two pairs of common cathode varactors. The gain, tunability and linearity are measured and discussed.

9.2 Design

9.2.1 Common Cathode Varactor Pair Theory

It has been shown that a topology of two varactors with a common cathode connection, Figure 9.1, has improved linearity compared to a single varactor [1,2]. The requirement for this topology is that the power law exponent of the diode is n=0.5 as defined in Equation 12. This corresponds to an abrupt diode. Having the cathodes of two abrupt diodes connected together will reduce the modulation of the combined C-V curves by an applied RF signal compared to a single varactor [3].

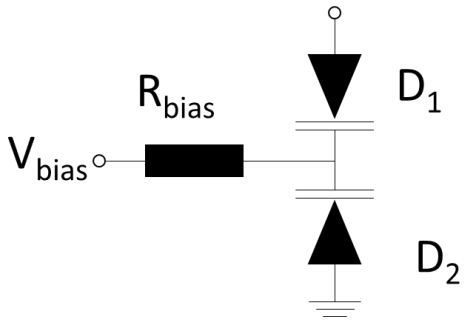

Figure 9.1 Common cathode varactor diode configuration

Common cathode varactor diodes have been used to improve linearity in different RF components such as phase shifters [4], filters [5] and bandpass resonators [6]. To the best of the author's knowledge this is the first use of common cathode pairs in frequency reconfigurable antennas. A design frequency of 1.4GHz was chosen as Chapter 5 showed lower frequencies have improved linearity.

The varactor chosen for this investigation was the SMV1413 in the SC-079 package with the characteristics listed in Table 8.1. This diode was chosen because it achieved the greatest tuning range of any abrupt diode investigated in this thesis. Due to the back-to-back configuration, the capacitance will be halved compared to that of a single diode. The antennas are fabricated on Taconic's RF-35 substrate with a thickness of 0.76mm, dielectric constant of 3.5 and a loss tangent of 0.0018.

Two configurations are investigated here; a single pair of common cathode diodes and two pairs of common cathode diodes. The single and double common cathode patch layouts are given in Figure 9.2a and 9.2b respectively and the dimensions are listed in Table 9.1.

Based on the findings in Chapter 7 the two pairs of common cathodes should have greater tunability and improved linearity performance.

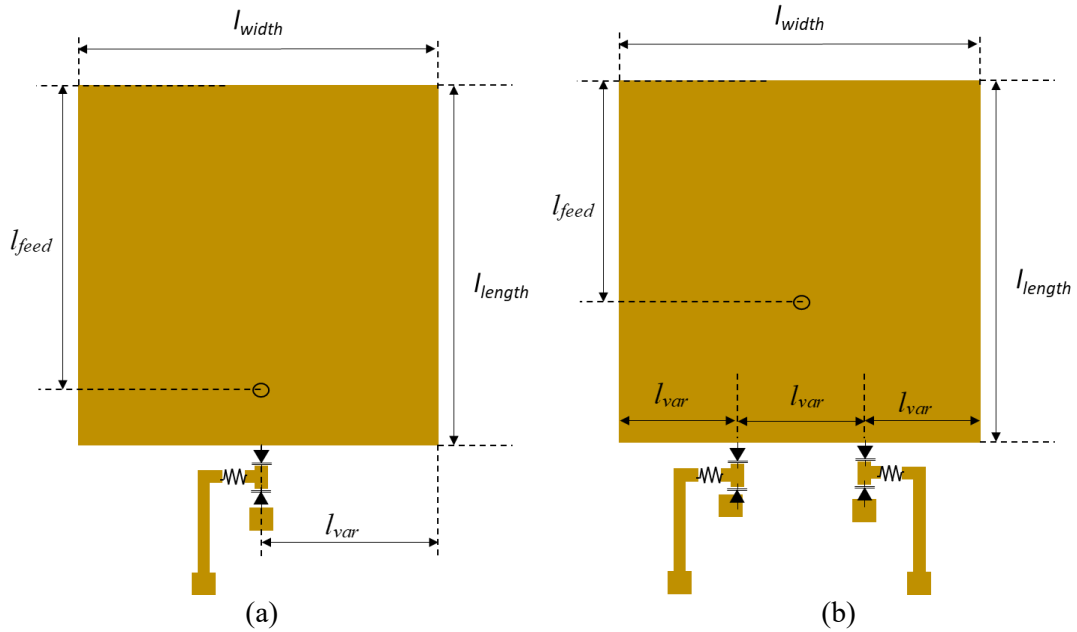

(a) (b)

Figure 9.2 Dimensions of tunable antenna using common cathode pairs (a) Antenna with single pair of common cathode diodes (b) Antenna with two pairs of common cathode diodes

Table 9.1 Dimensions for two different configurations of SMV1413 tunable common cathode patches

Antenna	l_{width} (mm)	l_{length} (mm)	l_{var} (mm)	l_{feed} (mm)
Single common cathode pair	14.50	14.50	7.25	9.75
Double common cathode pair	20.00	20.00	6.67	9.50

9.2.2 Common Cathode Bias Structure

The previously investigated varactor-tuned antennas use a bias tee to apply the DC bias voltage to the varactors. In the common cathode configuration, it is not possible to use the bias tee to apply a bias voltage to the cathodes as they are no longer attached to the antenna, therefore extra bias structures are required. The bias structure used to apply a DC bias voltage to the common cathode varactor pairs is shown in Figure 9.3a and an overall diagram showing the complete bias system in the measurement setup is shown in Figure 9.3b.

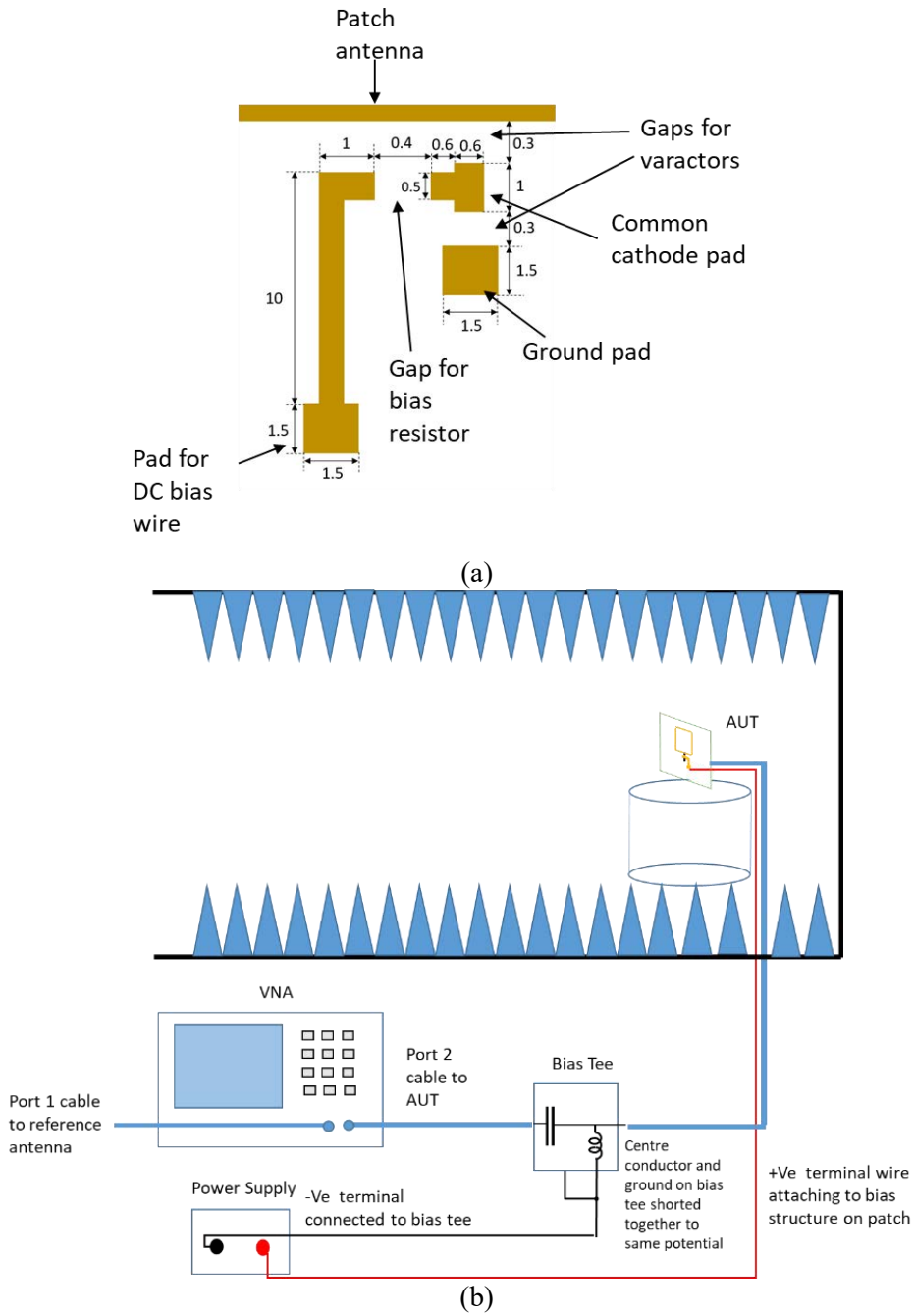

Figure 9.3 Common cathode biasing a) Layout of bias structure, all dimensions are in mm b) Bias setup for chamber testing

The bias structure shown in Figure 9.3a shows a central pad for the connection of the two cathode tabs. The anode tab of the top varactor is soldered directly onto the patch and the anode of the bottom diode is soldered onto a grounding pad which connects to the ground plane using a via. A DC ground is applied to the ground plane and the patch antenna using a bias tee shorted

together as shown in Figure 9.3b. The positive bias voltage is applied to the cathodes using a wire soldered to the pad at the end of the arm. There is a space for a bias resistor to connect the bias line to the common cathode point. The bias resistor value is required to be significantly higher than the reactance of the varactors and should satisfy the conditions in Equation 19 [7].

$$R_{bias} \gg \frac{1}{2\pi C \Delta f} \tag{19}$$

where:

C : Capacitance value of single varactor, pF

Δf : Frequency spacing between two-tones, Hz

The bias resistor value of 1MΩ was chosen as this satisfies the criteria.

A 90-degree line with an RF short fan stub was considered for applying the DC bias as this would remove the need for a bias resistor. However, as the patch antenna is frequency reconfigurable the electrical length of the line would change and stop it acting as an RF open as it was tuned in frequency.

9.2.2.1 Effect of Bias Structure on Radiation Patterns

The additional bias structure was simulated in CST to see the effects on the radiation characteristics. Figure 9.4a shows a close-up of the surface currents of a single bias structure. It is shown that the RF currents at 1.4GHz do not extend down the bias line towards the solder pads for the wire. Figure 9.4b shows the surface currents of a pair of bias structures at 1.4GHz. Again, there is no large currents extending down the bias structure.

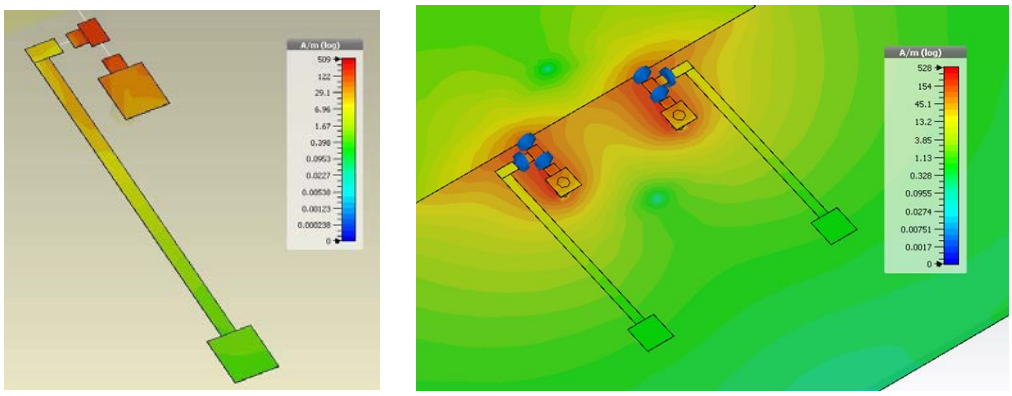

(a) (b)

Figure 9.4 Simulated surface currents at 1.4GHz a) Single bias structure b) Double bias structure

Figure 9.5 shows the radiation patterns for the patch with a single pair of common cathode varactors at 1.4GHz when the bias structure is and isn't included.

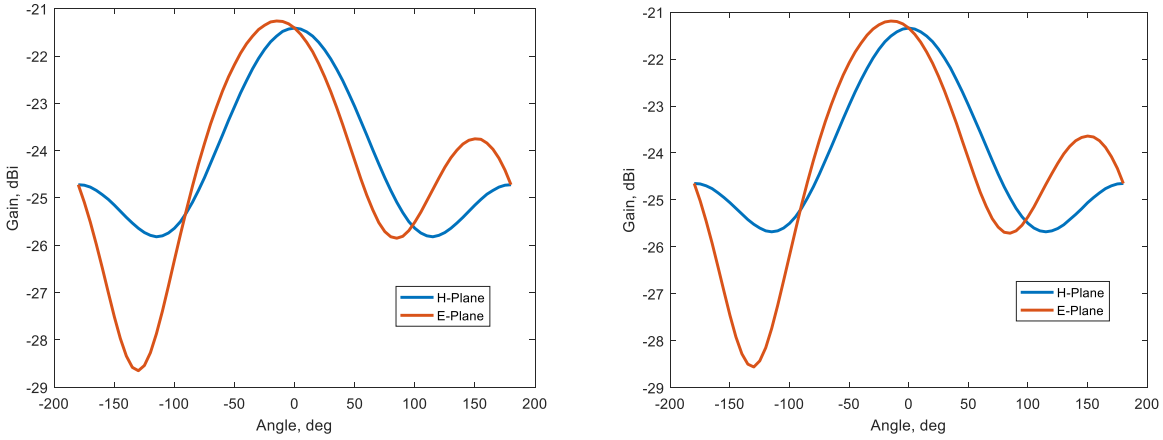

(a) (b)

Figure 9.5 Bias Line effect on radiation characteristics on antenna with single common cathode pair at 1.4GHz a) Bias structure included b) Bias structure not included

The extracted 3dB widths and main lobe directions of the patterns with and without the inclusion of the bias structure is given in Table 9.2.

Table 9.2 Extracted radiation characteristics from CST simulations of single common cathode patch at 1.4GHz with and without bias lines

Configuration	Main Lobe Direction (deg)		Angular Pattern Width (deg)	
	E-Plane	H-Plane	E-Plane	H-Plane
With Bias Lines	-14	0	131	146
Without Bias Lines	-14	0	130	144

Looking at the results shown in Table 9.2, the inclusion of the bias structure has a minimal effect on the radiation pattern. The simulations, however, do not include any models of the wires soldered onto the pads.

The fabricated antennas are shown in Figure 9.6a and 9.6b. The wires used to apply the DC bias are shown soldered onto the pads.

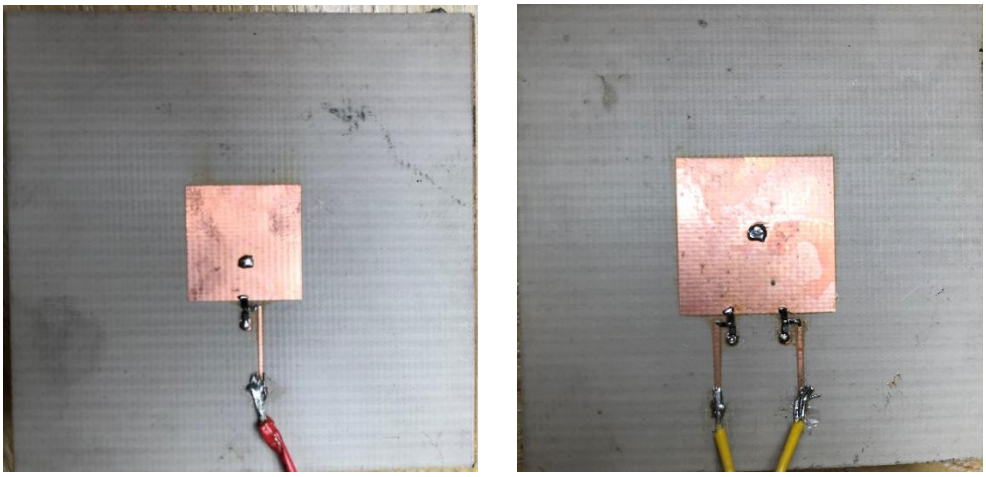

(a) (b)

Figure 9.6 Fabricated antennas a) Single common cathode varactor antenna b) Pair of common cathode varactor antenna

9.3 Results

9.3.1 Measured Reflection Coefficient

The measured reflection coefficient for the single common cathode pair and the double common cathode pair is shown in Figure 9.7a and 9.7b respectively.

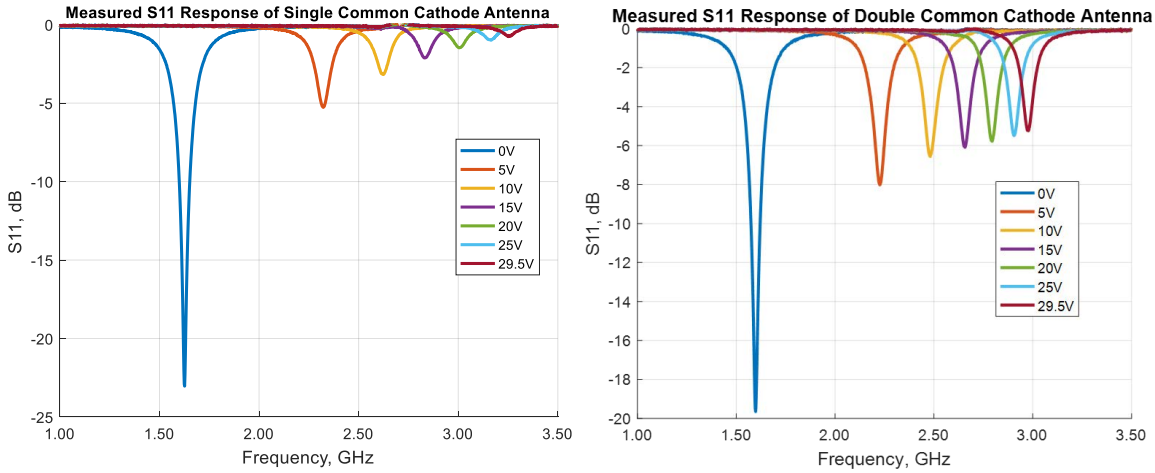

(a) (b)

Figure 9.7 Measured S_{11} response of antennas a) Single common cathode pair b) Pair of common cathode pair

As shown in previous sections as the frequency of operation increases the S_{11} response deteriorates.

9.3.2 Tunability

The measured and simulated tunabilities is given in Tables 9.3 and 9.4 respectively.

Table 9.3 Measured results for antennas with common cathode varactors. At 0V the nominal capacitance of the varactor is 9.24pF. At 29.5V the capacitance is 1.77pF

Antenna	Frequency at 0V (GHz)	Frequency at 29.5V (GHz)	Tunability (%)
Single Pair	1.63	3.25	66.40
Double Pair	1.60	2.98	60.26

Table 9.4 Simulated results for antennas with common cathode varactors. At 0V the nominal capacitance of the varactor is 9.24pF. At 29.5V the capacitance is 1.77pF

Antenna	Frequency at 0V (GHz)	Frequency at 29.5V (GHz)	Tunability (%)
Single	1.40	2.35	50.60
Double	1.33	2.16	47.56

9.3.2.1 Tolerance Investigation

Tables 9.3 and 9.4 show that the starting frequency of the fabricated antennas is around 200MHz lower than the design frequency. This is the largest amount by any investigation in this thesis. An investigation into the difference between simulated and measured resonant frequencies was undertaken in Chapter 5 section 5.3.2.1 where all parameters that can affect the resonant frequency are varied within reasonable tolerances. This investigation is repeated here with tolerances of: ±0.2mm for fabricated patch lengths, ±0.1 substrate dielectric constant and ±5% for varactor capacitance. Only the values that will increase the resonant frequency of the simulated antennas towards the measured frequency of the manufactured antennas are investigated. This will show if it is the tolerances of the fabricated antenna that is causing the shift up in frequency. The new values are listed in Table 9.5.

Table 9.5 New dimensions and properties of antenna with tolerances applied and new simulated resonant frequencies

Antenna	Dielectric Constant	Patch Length (mm)	Varactor Capacitance (pF)	Frequency (GHz)
Single Common Cathode	3.40	14.30	8.77	1.42
Double Common Cathode	3.40	19.80	8.77	1.37

Looking at the simulated results in Table 9.5 using the new values, the simulated antenna frequencies are not significantly closer to the measured results listed in Table 9.3. This indicates that it is not the fabrication tolerances that cause the difference between simulated and measured frequencies. It is therefore more likely that CST has increased difficulty when simulating the common cathode pairs compared to loading patches with single varactors as previously investigated.

9.3.3 Radiation Patterns

The measured radiation patterns for the two antennas at 5V intervals are given in Figure 9.8 and 9.9 respectively.

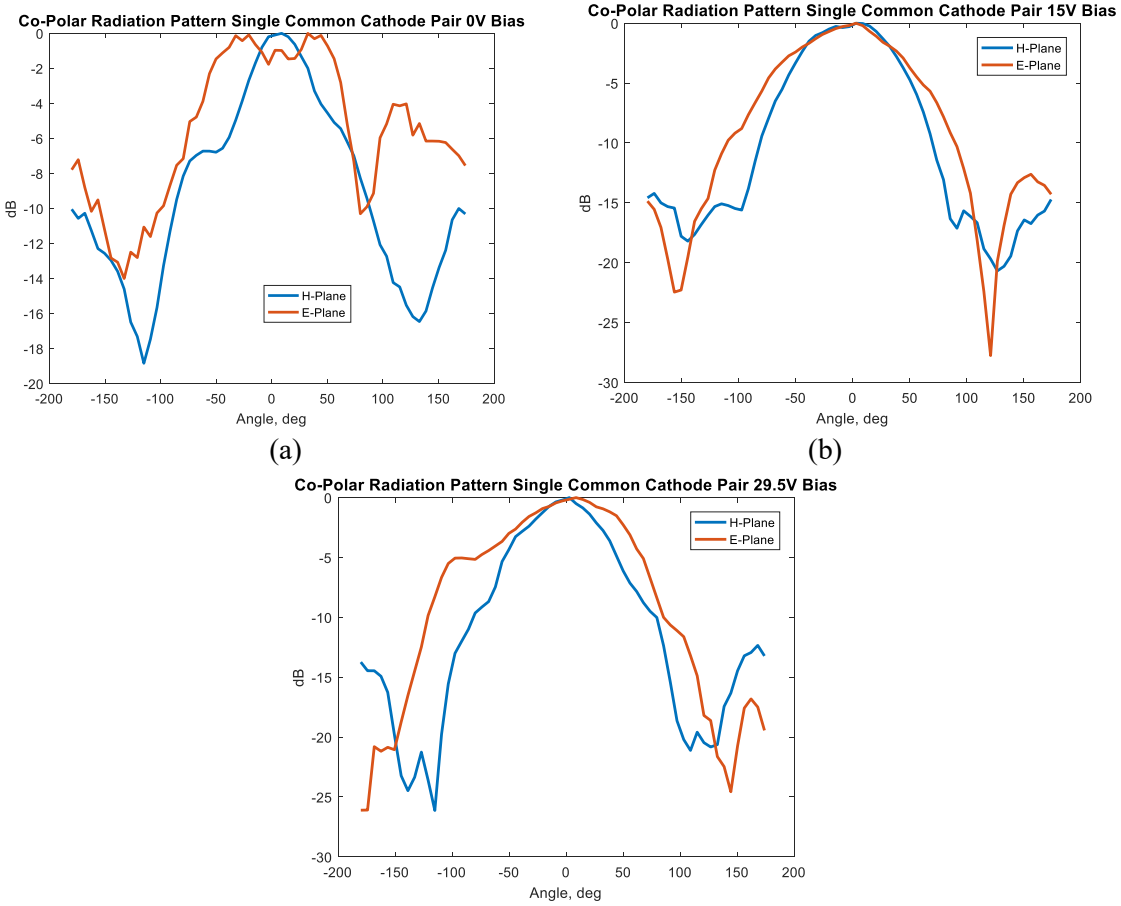

Figure 9.8 Measured radiation pattern single common cathode pair a) 1.63GHz with 0V bias b) 2.85GHz with 15V bias c) 3.25GHz with 29.5V

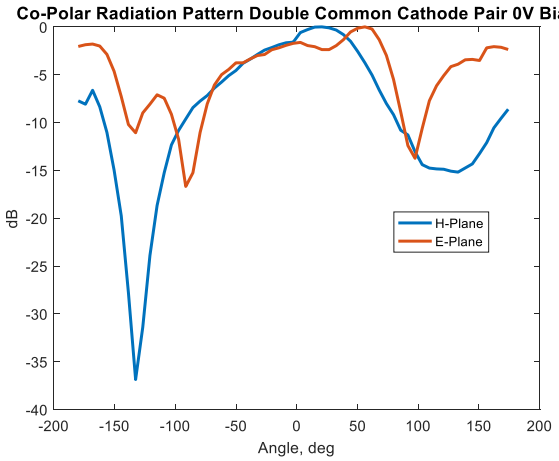

(a)

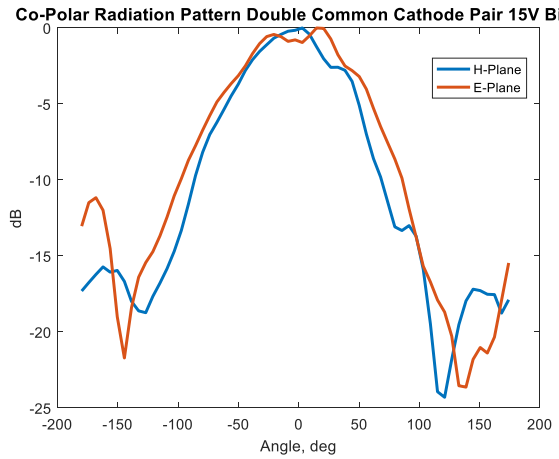

(b)

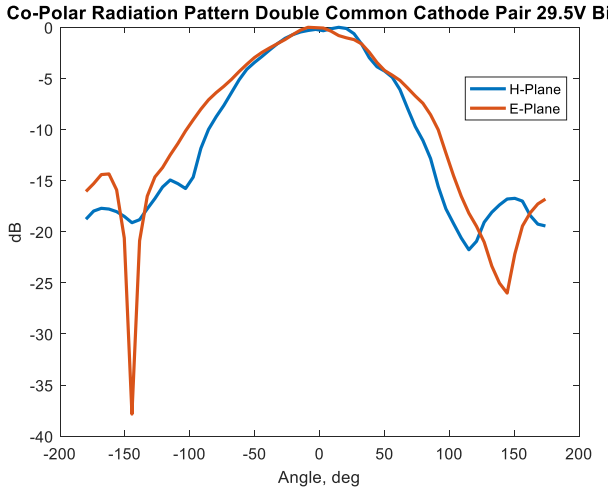

(c)

Figure 9.9 Measured radiation pattern pair common cathode pair a) 1.60GHz with 0V bias b) 2.66GHz with 15V bias c) 2.98GHz with 29.5V bias

9.3.4 Gain

For the antenna loaded with two common cathode pairs, as given in Table 9.6, the gain was measured across the bias voltage range in 5V intervals. Only a single gain point was measured for the single common cathode pair as given in Table 9.7.

Table 9.6 Measured gain values for antenna loaded with two common cathode pairs

Bias Voltage (V)	0.0	5.0	10.0	15.0	20.0	25.0	29.5
Frequency (GHz)	1.6	2.2	2.5	2.7	2.8	2.9	3.0
Gain (dBi)	-14.0	-7.1	-3.6	-3.4	-3.0	-2.4	-1.7

Table 9.7 Measured gain values for antenna loaded with single common cathode pair

Bias Voltage (V)	0.0
Frequency (GHz)	1.6
Gain (dBi)	-17.4

There is only one gain measurement for the single common cathode pair taken. This is because it was expected that the gain would increase as shown for the double common cathode pair in Table 9.6. Further investigations can be undertaken to verify this assumption.

9.3.5 IIP3 Measurements

The measured IIP3 points of the two different antennas are given in Table 9.8 and the measured tones are shown in Figure 9.10.

Table 9.8 Measured IIP3 points of antennas at 0V bias with common cathode varactors

Antenna	IIP3 (dBm)
Single Pair	+14.4
Double Pair	+16.9

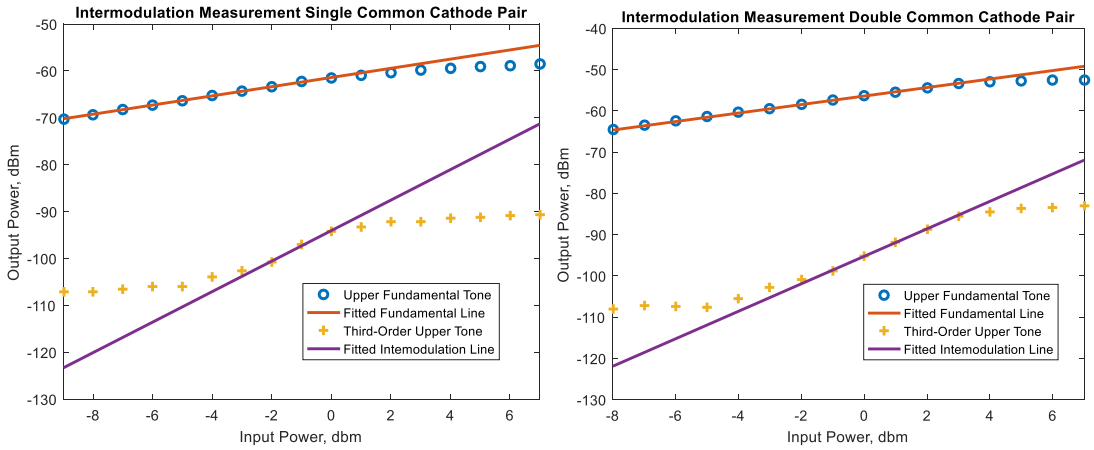

(a) (b)

Figure 9.10 Measured intermodulation products at 0V bias a) Single Common Cathode b) Pair Common Cathode

9.4 Discussion

The tunability of the two antennas investigated here perform differently to the investigation in Chapter 7. This was where the patch antenna loaded with two varactors had the greater tunability and area reduction when compared with a patch loaded with a single varactor. In this investigation the patch loaded with a single common cathode pair achieved the greater tunability and area reduction compared to the antenna loaded with two common cathode pairs, as shown in Table 9.9.

Table 9.9 Calculated area reduction of antennas with common cathode varactors

Antenna	Area Reduction (%)
Single Common Cathode	93.3
Double Common Cathode	87.2

The starting frequency of the antenna with a single common cathode pair is slightly greater than the antenna with two common cathode pairs. This higher starting frequency will give greater tunability as shown in Chapter 5. However, the frequency difference between the two antennas is not considered great enough to have a significantly increase the tunability.

Comparing the tunability of both antennas investigated here with the tunability of a single SMV1413 varactor loaded patch antenna as investigated in Chapter 8, a similar level of tunability is achieved. This comparable level of tunability is likely to have come from the increased frequency of operation of the antennas here compared to those in chapter 8.

Tables 9.6 and 9.7 show the measured gain of the antennas at 0V bias have poor gain values. The antenna loaded with a pair of common cathode varactors has the slightly superior gain value. This result is the same as in previous chapters where the antennas that had a smaller area reduction percentage, compared to an unloaded patch, exhibit superior gain characteristics. This same relationship was seen in the CST simulations with the extracted gain values given in Table

9.10. These simulated values are extracted at the 1.4GHz design frequency and are not scaled up to the same frequency as the ones measured.

Table 9.10 Simulated gain of common cathode antennas at 1.4GHz

Antenna	Gain (dBi)	Radiation Efficiency (dB)
Single Common Cathode	-21.3	-24.5
Pair Common Cathode	-15.7	-19.1

The measured radiation patterns for both the antennas show a dip in the E-plane cut as shown in Figures 9.8a and 9.9a. This dip is not seen in the simulations as shown by Figure 9.5a. The dip becomes less pronounced as the frequency of operation increases. This dip could have been caused by the wires apply the bias voltage to the varactors. However, this would also be apparent in the H-plane. As it is only in the E-plane this dip is most likely caused by the bias structure interacting with the patch. When the patch is tuned up in frequency the varactors exhibit a reduced loading effect and the bias structure becomes less influential and the dip in the E-plane disappears.

Looking at the data in Table 9.6, the gain of the antenna with two common cathode pairs increases as the frequency of operation increases. This increase in gain is a result of reduced varactor loading and the patch more closely resembling the correct size for the frequency of operation. There will also be an increase in quality factor of the varactors as the reverse bias voltage increases [8]. This will reduce power dissipation in the varactor and increase radiation efficiency as shown in Chapter 8.

Table 9.8 shows that the use of the common cathode varactors topology has improved linearity of the antennas. The measured IIP3 points of both antennas are greater than any other

configuration previously investigated in this thesis. The antenna loaded with a pair of common cathode varactors has the superior linearity. This is the same as was shown in Chapter 7 where loading a patch with two varactors improved the linearity over a single varactor.

The RF voltages across the varactors was extracted using the same procedure listed in Chapter 4 and are shown in Tables 9.11 and 9.12.

Table 9.11 Extracted RF voltage amplitude using CST for Single Common Cathode Antenna

Component	Extracted Peak Voltage (V)
Varactor 1	0.30
Varactor 2	0.02
Resistor 1	0.39

Table 9.12 Extracted RF voltage amplitude using CST for pair of common cathode antenna

Component	Extracted Peak Voltage (V)
Varactor 1	0.24
Varactor 2	0.24
Varactor 3	0.01
Varactor 4	0.01
Resistor 1	0.04
Resistor 2	0.04

The RF voltages across the varactors in the antenna loaded with the pair of common cathode varactors are less than the patch loaded with a single pair of common cathode varactors. In this configuration the lower the peak RF voltage the greater the IIP3 points, this is the same as was seen in Chapter 7.

9.5 Conclusion

This chapter has looked at two different common cathode configurations of varactor diodes. They are used to tune a patch that is designed for improved linearity over antennas using the single varactor configurations.

The key points from the analysis are:

1. The common cathode configuration has improved linearity over any configuration of single varactors investigated in this thesis.

2. A pair of common cathode varactors has better linearity compared to a single pair of common cathode varactors.

3. The poor gain of the two antennas investigated comes from the large area reduction of the patches. To decrease the area reduction and improve the gain lower capacitance abrupt diodes such as the SMV1405 could be used, this would come at a cost of reducing tunability.

4. The tunability of the patches is not reduced significantly compared to the single varactor configurations seen in Chapter 8.

5. As the reverse bias increases and the frequency of operation gets higher so does the gain of the antenna.

9.6 References

[1] R. G. Meyer and M. L. Stephens, “Distortion in Variable-Capacitance Diodes,” IEEE Journal of Solid-state Circuits, vol. SC-10, NO. 1, 1975

[2] M.Akaike, T.Ohira, K.Inagaki, and Q.Han,“Ananalys is of nonlinear terms in capacitance–voltage characteristic for anti-series-connected varactor–diode pair,” Int. J. RF Microw., vol. CAE-14, pp. 274–282, 2004.

[3] K. E. Mortensen, Variable Capacitance Diodes, Artech House, 1974.

[4] Arvind Keerti, Junyang Xiang, and Anh-Vu Pham, “High Power Linearized RF Phase Shifter Using Anti-Series Diodes”, IEEE Microwave and Wireless Components Letters., vol. 16, no. 4, pp. 200–203, Apr. 2006

[5] M. A. EI-Tanani, and G. M. Rebeiz, “A Two-Pole Two-Zero Tunable Filter with Improved Linearity,” IEEE Trans. Microw. Theory Tech., vol. 57, no. 4, pp. 830–839, Apr. 2009.

[6] K. Zeng, D. Psychogiou, W. N. Allen and D. Peroulis, “A continuously tunable 95-138 MHz bandpass resonator with 40 dBm IIP3,” 2015 IEEE International Conference on Microwaves, Communications, Antennas and Electronics Systems (COMCAS), Tel Aviv, Israel, November 2015.

[7] K. Buisman, L. C. N. D. Vreede, L. E. Larson, M. Spirito, A. Akhnoukh, Y. Lin, X.-D. Liu, and L. K. Nanver, “A Monolithic Low-Distortion Low-Loss Silicon-on-Glass Varactor-Tuned Filter With Optimized Biasing,” *IEEE Microwave and Wireless Components Letters*, vol. 17, no. 1, pp. 58–60, 2007.

[8] M. Norwood and E. Shatz, “Voltage variable capacitor tuning: A review,” Proceedings of the IEEE, vol. 56, no. 5, pp. 788–798, 1968.

10 Investigation of a Microstrip Patch Antenna with Common Cathode Varactors and Parasitic Patches

10.1 Introduction

This chapter looks at the design and fabrication of an antenna that uses two parasitic patches with U-slots cut outs to improve the gain of an antenna loaded with a pair of common cathode varactors. The antenna with the pair of common cathode varactors was chosen as it had the best linearity performance. The gain, tunability and linearity of the fabricated antenna is measured and discussed.

10.2 Design

The results in Chapter 9 showed that by using a pair of common cathode varactors, a tunable patch antenna with improved linearity can be fabricated at the cost of reduced gain. The reduction in gain is attributed to the reduced area of the patch antenna. A method commonly used to increase the gain of a microstrip patch is to use stacked parasitic patches and is investigated here [1].

10.2.1 Stacked Single Patch

The first configuration investigated is shown in Figure 10.1. A parasitic patch is stacked above the patch loaded with a pair of common cathode pairs by a distance $l_{spacing}$. The antennas investigated in this chapter use the same varactor diodes and substrate as those listed in Chapter 9. The patch antenna loaded with the pair of common cathode varactors has the same layout and dimensions as those shown in Figure 9.2b and Table 9.1. It will be referred to as the driven patch for the rest of this chapter.

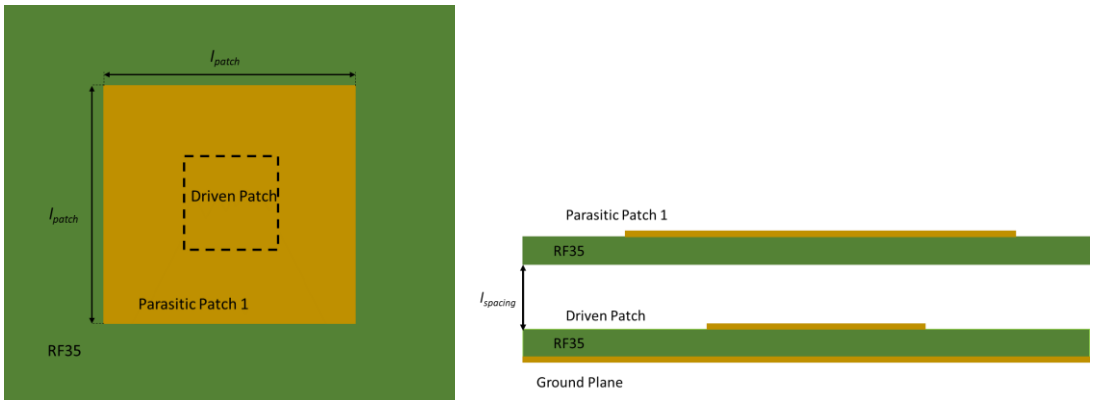

(a) (b)

Figure 10.1 Single Parasitic Patch a) Top down view of Parasitic Patch 1 b) Cross-Section of Stacked Patches

The parasitic patch needs to increase the gain across the whole frequency range of the driven patch. Specifically, it must do this at the lower frequencies where it was shown in Table 9.6 that the gain will be at its lowest value.

A parametric sweep of a parasitic patch with length, l_{patch}, between 30mm to 100mm was performed in CST. The spacing, $l_{spacing}$, between the patches was kept constant at values of 1mm, 3mm or 5mm. The gain was extracted at the start frequency of 1.40GHz using a capacitance value of 9.24pF and the end frequency of 2.4GHz with capacitance 1.77pF. Figure 10.2 shows the extracted gain values from the simulations.

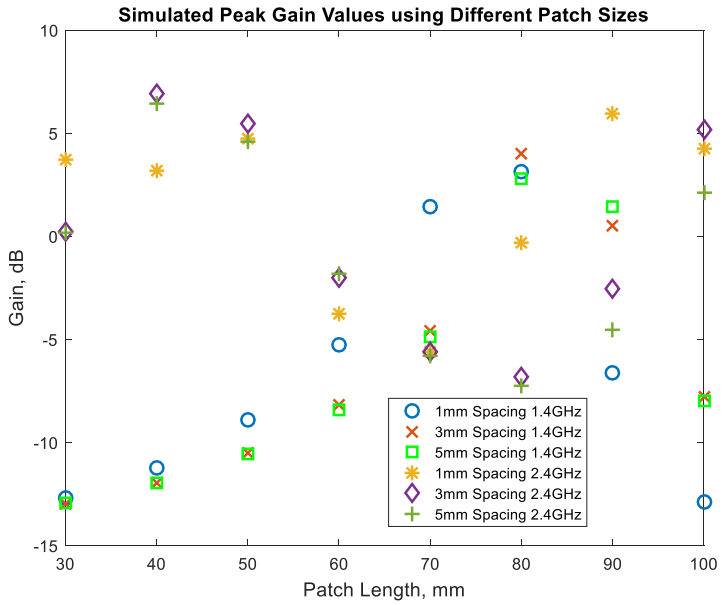

Figure 10.2 Extracted peak gain value at 1.4GHz and 2.4GHz from parasitic patch length sweep

Figure 10.2 shows that a single parasitic patch will have specific values of l_{patch} that are suited ideally to increasing the gain of the antenna at certain frequencies. Therefore, a single parasitic patch is not suited to increasing the gain across the entire frequency range. This is illustrated in Figure 10.3 where simulated radiation patterns at 1.40GHz and 2.39GHz for a parasitic patch with l_{patch}=80mm and $l_{spacing}$=3mm are shown.

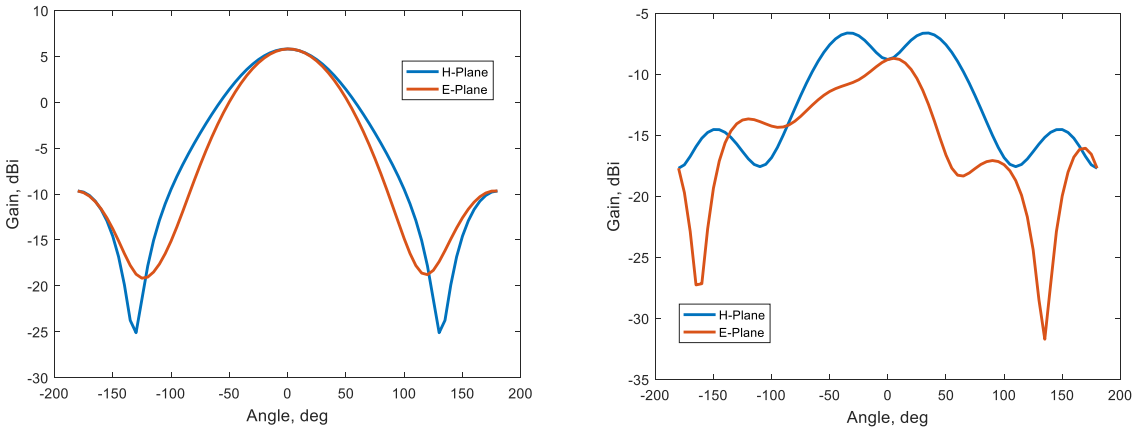

Figure 10.3 Simulated radiation pattern of driven patch with parasitic patch dimensions of l_{patch}=80mm, and $l_{spacing}$=3mm a) 1.40GHz b) 2.39GHz

Looking at Figure 10.3a, the radiation pattern at 1.40GHz is like that of a standard patch antenna. Figure 10.3b show the radiation pattern at 2.39GHz. Here a dip in the H-plane is clearly visible. This distortion to the radiation pattern comes from the large parasitic patch blocking the driven patch. The gain of the antenna with l_{patch} set to 80mm is shown to be poor at 2.39GHz. This shows that a single parasitic patch is not capable of increasing the gain across the entire frequency range.

10.2.2 Stacked Double Parasitic Patches

As each patch length was suited to a specific frequency the single patch configuration wasn't capable of increasing gain across the frequency band. Figure 10.4 shows a new antenna that uses a stacked double parasitic patch configuration. This design is intended to increase the gain at both the lowest and highest operating frequencies of the driven patch.

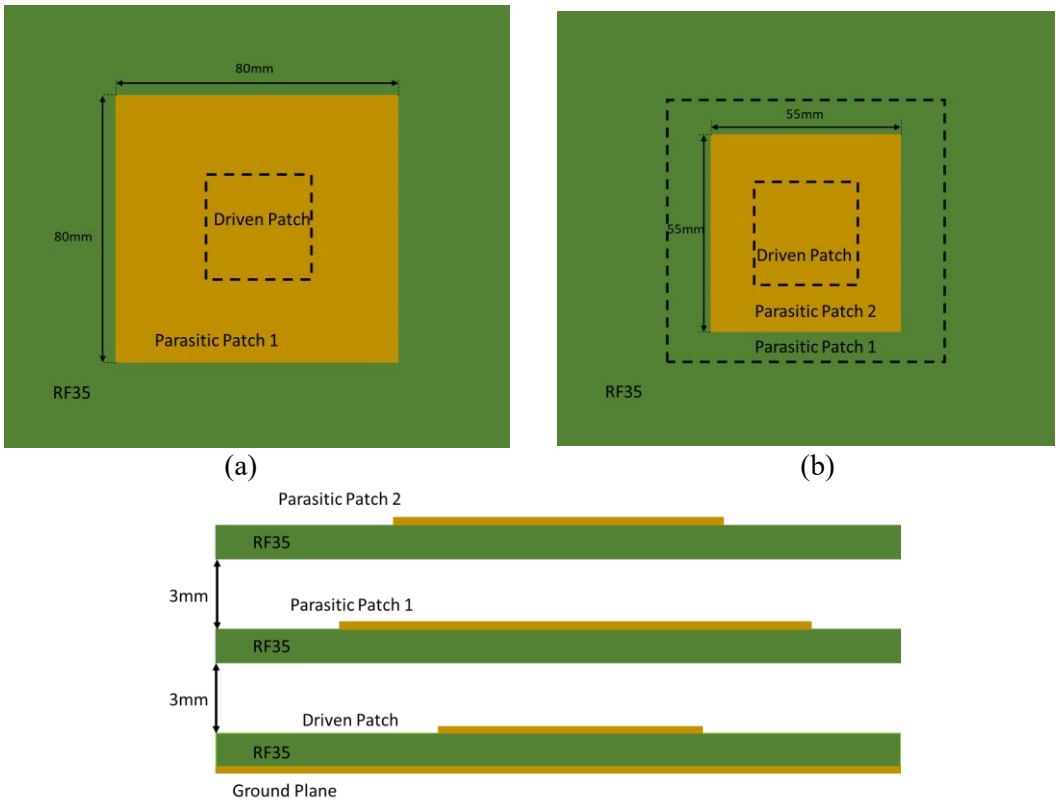

Figure 10.4 Double parasitic patch layout (a) Top down view lowest parasitic patch 1 (b) Top down view second parasitic patch 2 (c) Side profile of antenna

Parasitic patch 1 has edge lengths of 80mm which was shown to be effective at increasing the gain at 1.40GHz as seen in Figure 10.2. The top parasitic patch 2 has edge lengths of 55mm which work to increase the gain at 2.39GHz. Table 10.1 lists the extracted gain from the simulations at each frequency point investigated.

Table 10.1 Simulated gain values from two parasitic patch antenna. Capacitance values used to model the varactor at each frequency point are shown in brackets.

Frequency (GHz)	1.40 (9.24pF)	1.67 (4.85pF)	1.81 (3.77pF)	2.39 (1.77pF)
Gain (dBi)	+4.86	-3.55	-6.19	-6.28

Table 10.1 shows the gain of the antenna with two parasitic patches still decreases across the frequency band as seen in the single parasitic patch antenna. The decrease in gain against increasing frequency comes from having no coupling between the top parasitic patch and the driven patch. This is illustrated in Figure 10.5.

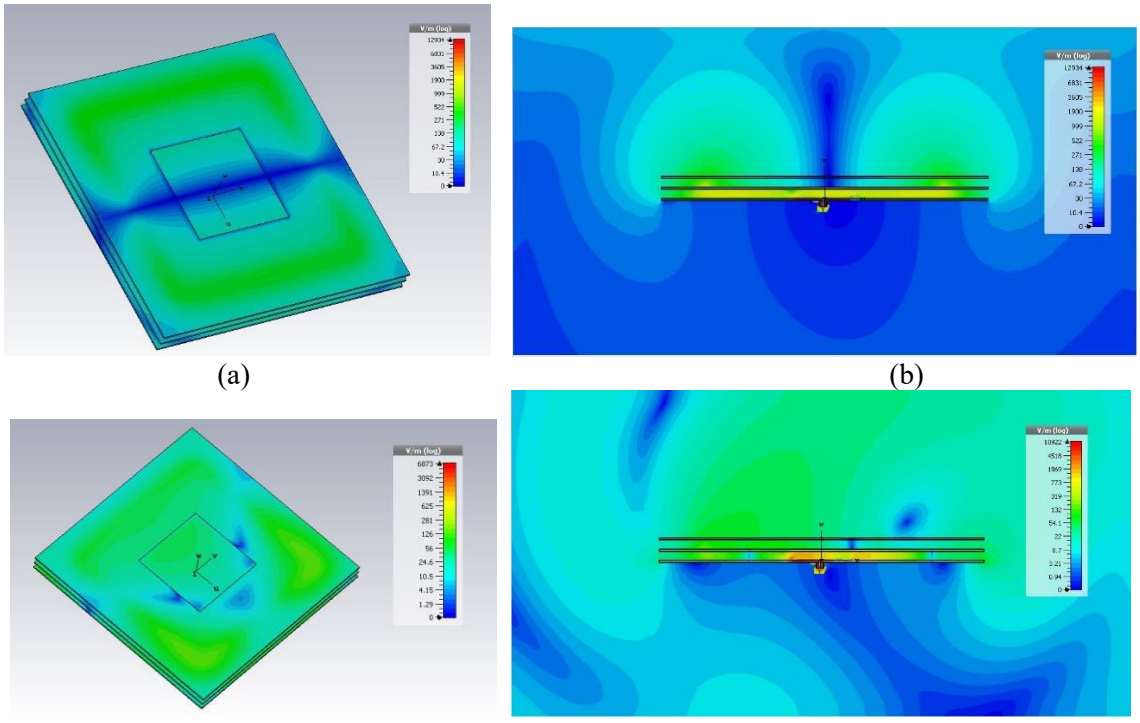

(a) (b) (c) (d)

Figure 10.5 Simulated E-Fields of patch with two parasitic patches (a) 1.40GHz (b) Side profile 1.40GHz (c) 2.39GHz (d) Side profile 2.39GHz

Figure 10.5a-b shows the simulated E-fields at 1.40GHz. The driven patch couples effectively with parasitic patch 1 which produces increased gain values at 1.40GHz. Figure 10.5c-d show the simulated E-Fields at 2.39GHz, which is the frequency where the top parasitic patch should be effective at increasing gain. However, as shown, there is weak coupling between parasitic patch 2 and the driven patch. This is indicated by stronger fields between the driven patch and parasitic patch 1 and the weaker fields between parasitic patch 1 and parasitic patch 2. The weak coupling is caused by parasitic patch 1 acting as a barrier.

Radiation cuts of the two parasitic patch antenna are shown in Figure 10.6. These are similar to those of the antenna with a single parasitic patch shown in Figure 10.3. This confirms that the larger parasitic patch 1 stops any coupling of the driven patch with parasitic patch 2 that is intended to increase gain at higher frequencies.

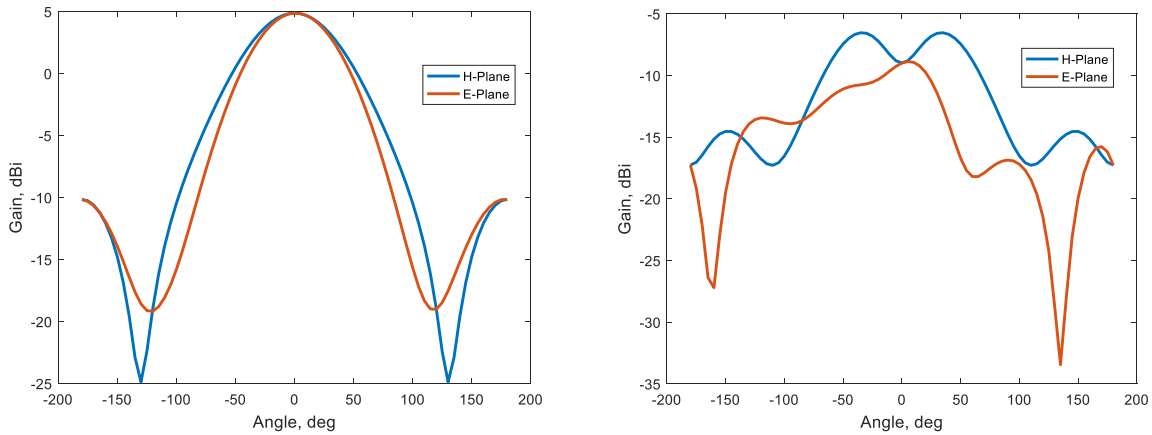

(a) (b)

Figure 10.6 Simulated radiation cuts of two parasitic patch antenna a) 1.40GHz b) 2.39GHz

A new design needs to be found that reduces the blocking nature of the parasitic patch 1 and that is also suited to increasing the gain at lower frequencies.

10.2.3 Expanding Quadrant Multiple Parasitic Patches

To address the issue of improving gain across the entire frequency range a new approach was taken. This configuration is based on having multiple patches in a quadrant configuration on stacked substrates [2]. This design is intended to increase the gain of the patch antenna at the lower operating frequencies, where the gain of the driven antenna is at its poorest, by coupling with the parasitic patches. Then, as the operating frequency of the driven patch increases, it no longer couples with the parasitic patches and operates independently at the frequencies where its gain is highest. The dimensions of the quadrant parasitic patch are given in Figure 10.7.

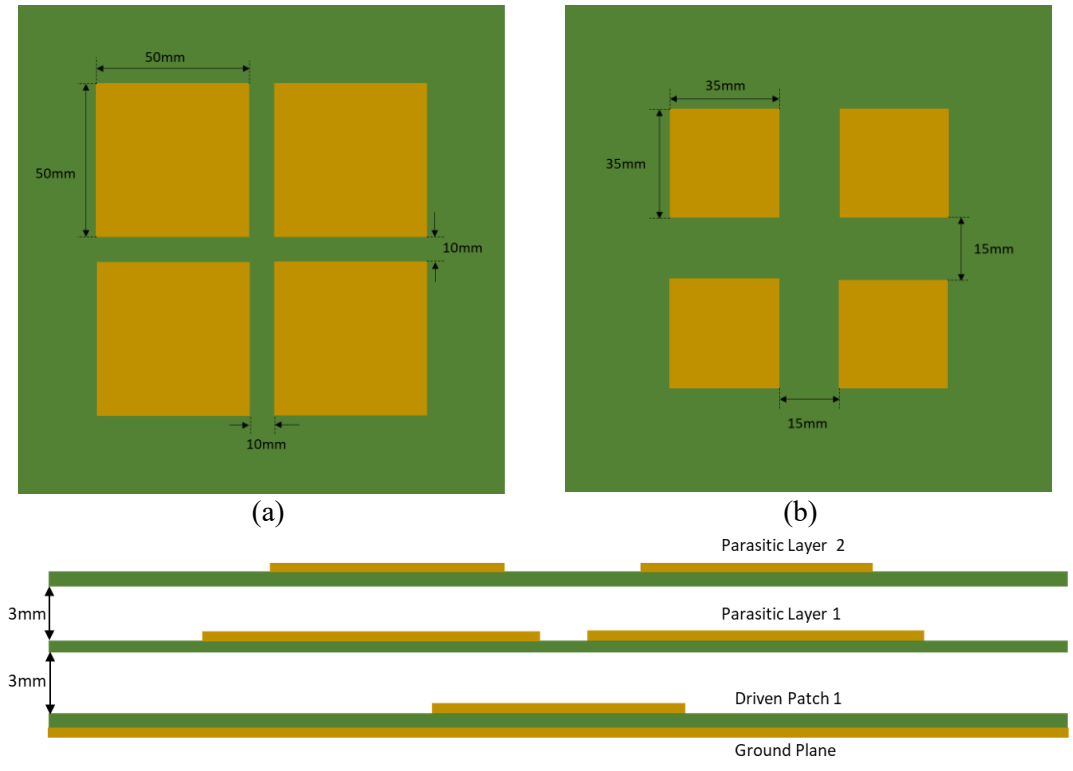

Figure 10.7 Stacked quadrant parasitic antenna a) Parasitic layer 1 b) Parasitic layer 2 c) Cross-section

It was found that the best performance of this configuration comes when the patches on the parasitic layer 1 are larger than the patches on the parasitic layer 2. This design operates at a slightly lower frequency of 1.20GHz and only tunes up to 2.20GHz.

The simulated radiation patterns of the quadrant antenna are shown in Figure 10.8. The radiation patterns at frequency points 1.20GHz, 1.52GHz and 1.65GHz are similar to a simple microstrip patch antenna. At 2.20GHz, however the E-plane cut shows a larger dip slightly off boresight. This is likely caused by the parasitic patches. However, this antenna configuration is an improvement on the single parasitic patch and dual parasitic patch where the dip occurred along boresight.

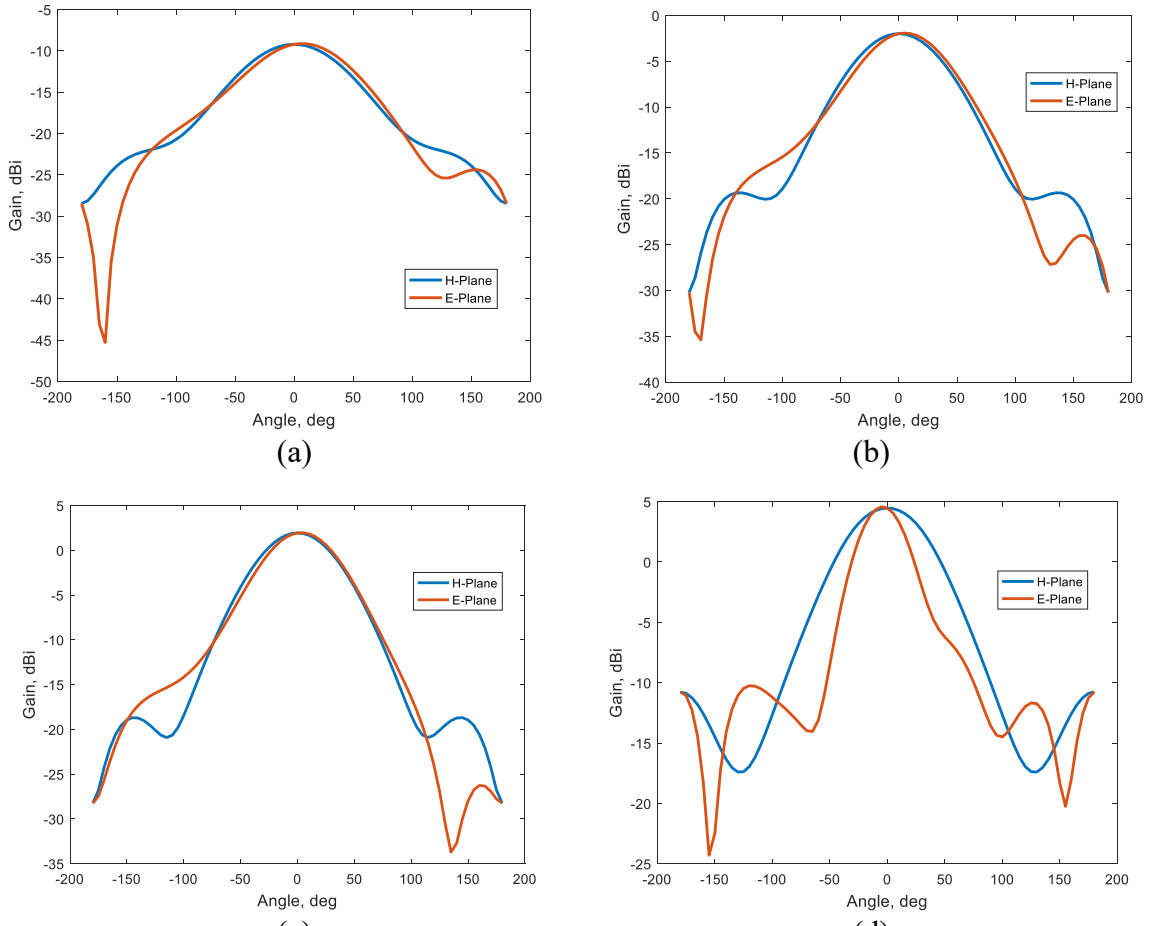

Figure 10.8 Simulated radiation pattern cuts for antenna with quadrant parasitic patch configuration a)1.20GHz b) 1.52GHz c) 1.65GHz d) 2.20GHz

The gain values were extracted from the radiation cuts and are shown in Table 10.2. Comparing the gain values to that of the dual parasitic patch design given in Table 10.1, it has improved gain at frequencies higher than 1.65GHz. The improved gain values at higher frequencies come at the

expense of gain at the lower operating frequencies as indicated by the gain at 1.20GHz in Table 10.2.

Table 10.2 Extracted Gain Simulations of quadrant parasitic patch configuration. Capacitance values used to model the varactor at each frequency point are shown in brackets.

Frequency (GHz)	1.20 (9.24pF)	1.52 (4.85pF)	1.65 (3.77pF)	2.2 (1.77pF)
Gain (dBi)	-9.14	-1.93	+1.96	+4.57

The quadrant antenna does improve the gain of the antenna across the entire frequency range compared to a patch loaded with a pair of common cathode varactors as investigated in Chapter 9.

This design has shown some improvements to that of the single or dual parasitic patch designs, but it is not sufficient to improve the gain performance across the frequency range.

10.2.4 U-slot Antennas

A commonly used method to improve the bandwidth of microstrip antennas is to remove a U-slot shape from the patch, this generates two closely spaced resonances [3,4]. Figure 10.9 shows a patch antenna with a U-slot removed, based on the dimensions given in [4]. The patch is on a foam substrate with dielectric constant of 1.05 and height of 5mm.

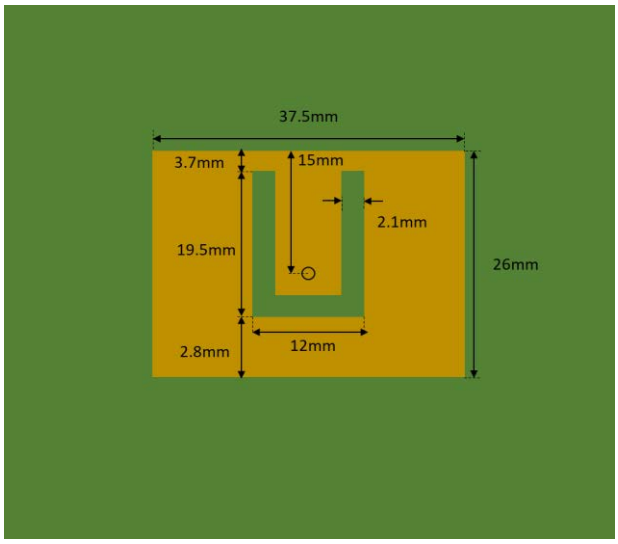

Figure 10.9 Microstrip patch antenna with U-Slot cut out (Adapted from [4])

The simulated reflection coefficient response for the patch shown in Figure 10.9 is given in Figure 10.10. Two separate resonances, one at 4GHz and the second at 5GHz, are shown.

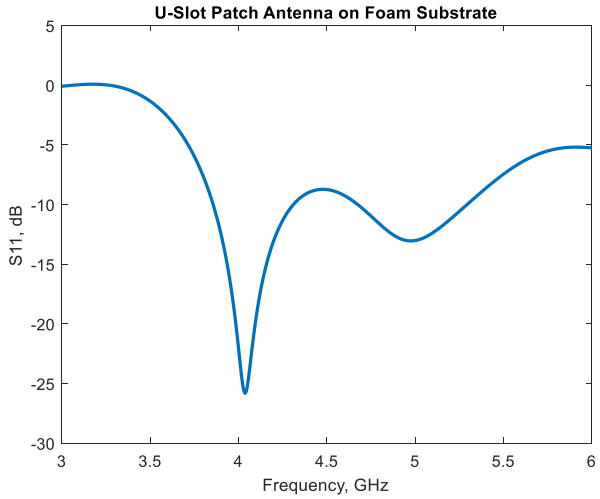

Figure 10.10 Reflection coefficient for patch antenna with U-slot cut out

The radiation patterns for the two distinct resonances at 4GHz and 5GHz are given in Figure 10.11. There is no significant difference between the two resonance radiation patterns.

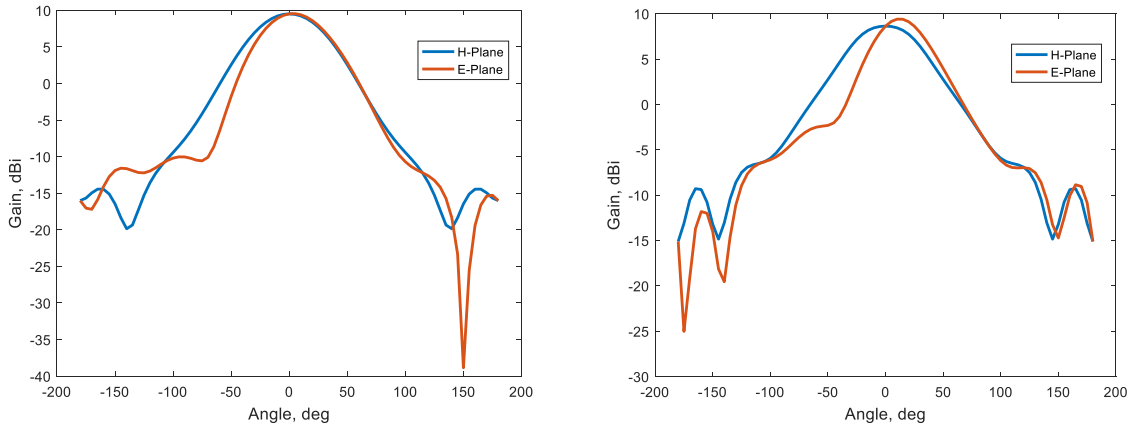

(a) (b)

Figure 10.11 Simulated radiation patterns of patch antenna with U-slot a) 4GHz b) 5GHz

The U-slot patch antenna shown in Figure 10.9 can be compared to a simple square patch designed on the same substrate as shown in Figure 10.12. They both operate at the same frequency of 4GHz.

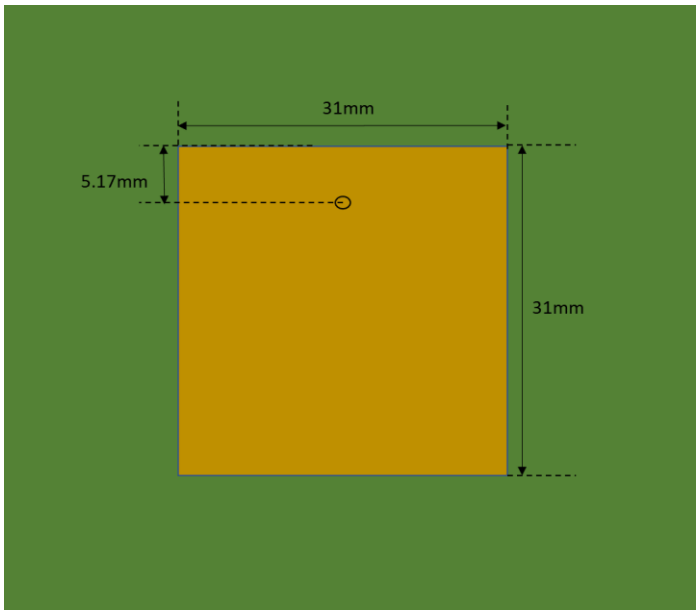

Figure 10.12 Dimension of square patch antenna on foam substrate

The simulated reflection coefficient of the square patch on foam substrate is shown in Figure 10.13.

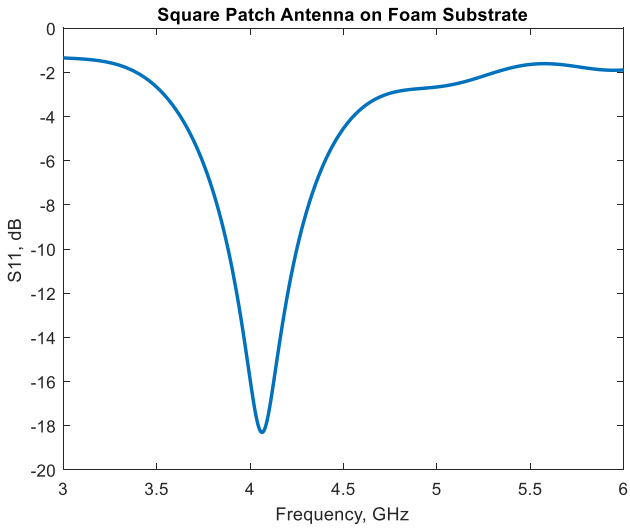

Figure 10.13 Simulated reflection coefficient response for simple square patch

Comparing the simulated reflection coefficient results of the patch with a U-slot and a square patch, it is apparent that the patch utilizing a U-slot has improved the operating bandwidth with the addition of the second resonance.

The radiation patterns for the square patch at 4GHz are given in Figure 10.14, The E-Plane cut is more asymmetrical than the same E-plane cut at 4GHz for the patch with a U-slot cut out. This is because the simple square patch has not been optimized fully as it is used only for comparison purposes.

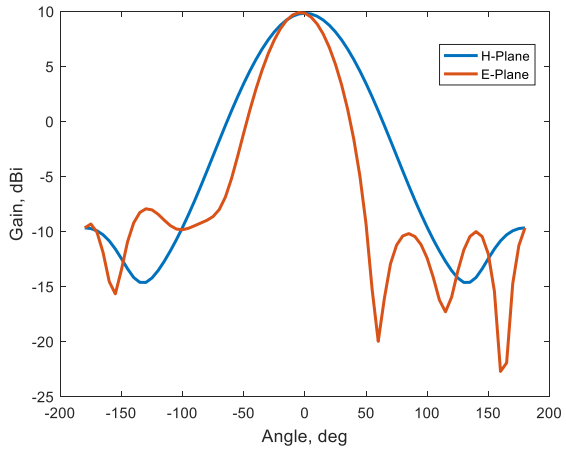

Figure 10.14 Simulated radiation patterns of square foam patch without U-slot at 4GHz

This technique of removing a U-slot shape from patch antennas is combined here with the stacked patch design previously investigated in section 10.2.2. The addition of the slots is intended to increase the operating frequency of the stacked patches whilst allowing coupling between the top parasitic patch 2 and the driven patch. As with the design in section 10.2.2 the lower parasitic patch is designed to increase gain at lower operating frequencies whilst the top patch increases gain at higher frequencies.

10.2.4.1 Single U-Slot Parasitic Patch

A single U-slot parasitic patch was first optimized to increase gain at the lower frequencies. The dimensions for this patch are shown in Figure 10.15.

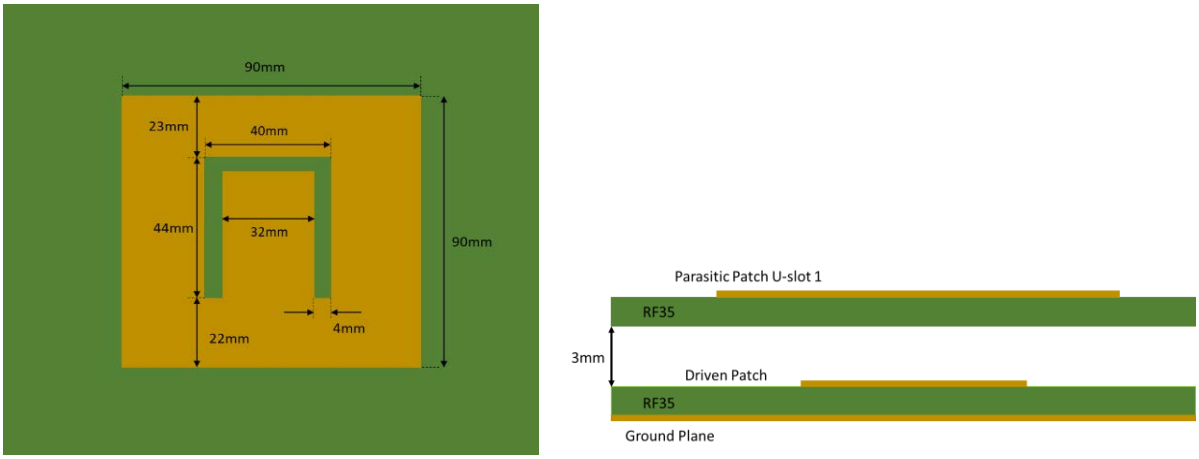

(a) (b)

Figure 10.15 Dimensions for single parasitic U-slot patch a) Top down view b) Side profile

The radiation cuts for a single parasitic U-slot patch at 1.35GHz are shown in Figure 10.16.

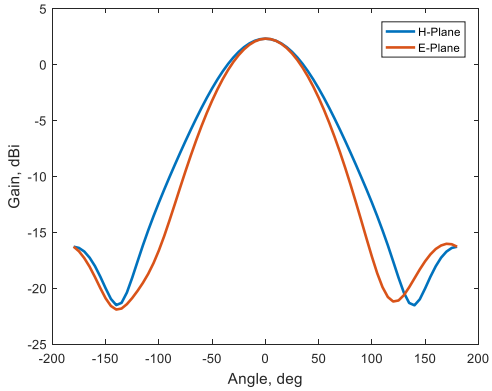

Figure 10.16 Simulated radiation patterns of single U-Slot parasitic patch at 1.35GHz

The addition of the U-slot parasitic patch has increased the gain at 1.35GHz to similar levels as shown in Figure 10.2 for a parasitic patch with no U-slot cut out. This indicates that the addition of U-slot does not degrade performance significantly.

10.2.4.2 Addition of a 40mm Parasitic Patch Above U-Slot Parasitic Patch 1

A smaller patch was then added to the model to investigate whether there is greater coupling between the driven patch and the top parasitic patch 2, and if this improves the gain at 2.4GHz. A 40mm patch with 3mm spacing was added as this gave the greatest gain value at 2.4GHz as shown in Figure 10.2. The new stacked configuration is shown in Figure 10.17.

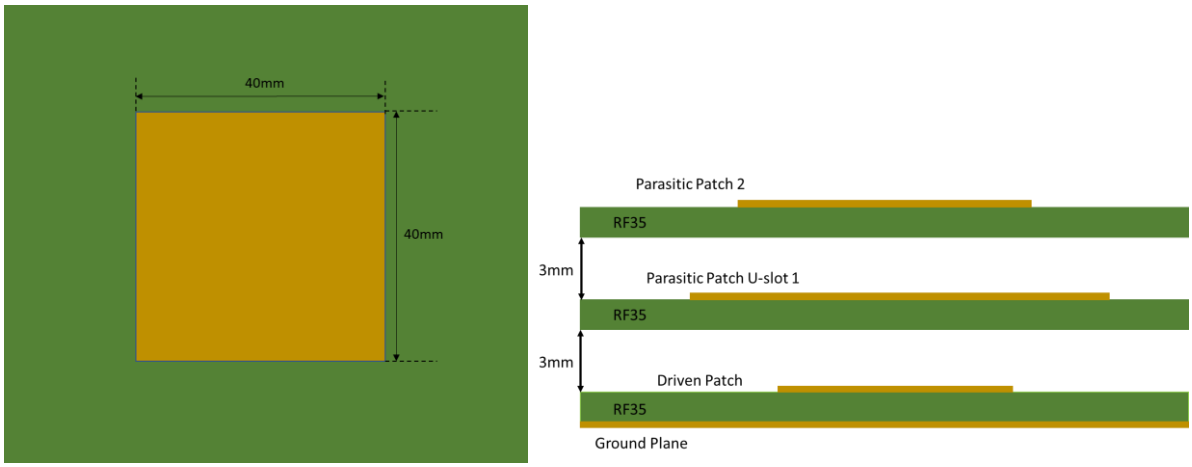

(a) (b)

Figure 10.17 Stacked antenna with parasitic patch 1 with U-slot and 40mm parasitic patch 2 a) Parasitic Patch 2 dimensions b) Side profile of stacked patches

Figure 10.18 shows the radiation patterns for the antenna in Figure 10.17. At 1.35GHz the patterns are very similar to the ones shown in Figure 10.16 for the antenna without the 40mm parasitic patch. This indicates that the addition of the smaller parasitic patch 2 does not affect the functioning of the parasitic patch U-Slot 1 at lower frequencies.

Figure 10.18 with the U-slots in parasitic patch 1 is compared with Figure 10.6 and no U-slots in Parasitic patch 1. It is shown that the dip in the H-plane at 2.39GHz has been reduced with the

addition of the U-slots. The gain at 2.39GHz is also improved with the addition of the 40mm parasitic patch 2 which was not seen previously in section 10.2.2.

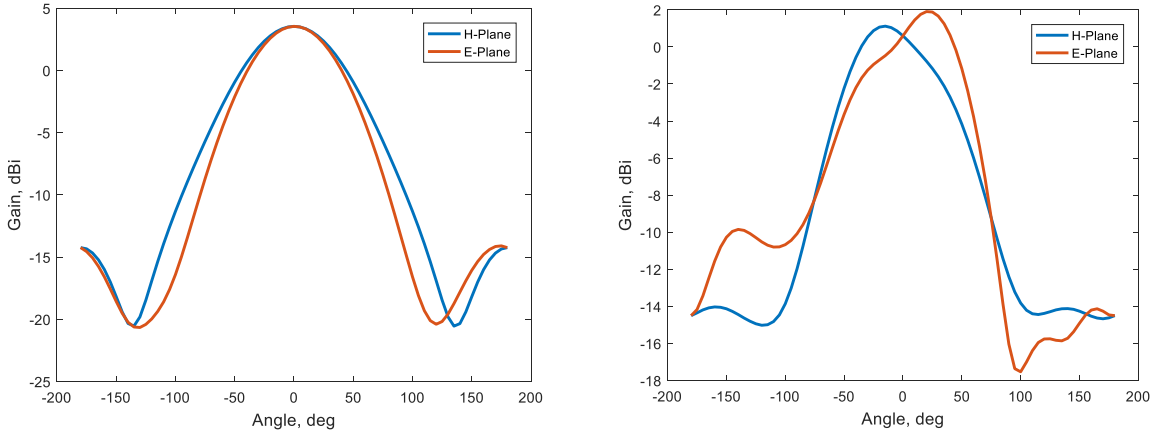

(a) (b)

Figure 10.18 Simulated radiation patterns for parasitic patch 1 U-slot and a stacked 40mm parasitic patch 2 a) 1.35GHz b) 2.39GHz

The E-Fields at 2.39GHz were simulated and are shown in Figure 10.19. Looking at the cross-section of the antenna shown in Figure 10.19b, it is apparent that there is improved coupling between the driven antenna and the parasitic patch 2. This is indicated by increased E-fields between parasitic patch U-slot 1 and parasitic patch 2. This improved coupling is facilitated by the addition of the U-slot cut out in the bottom parasitic patch.

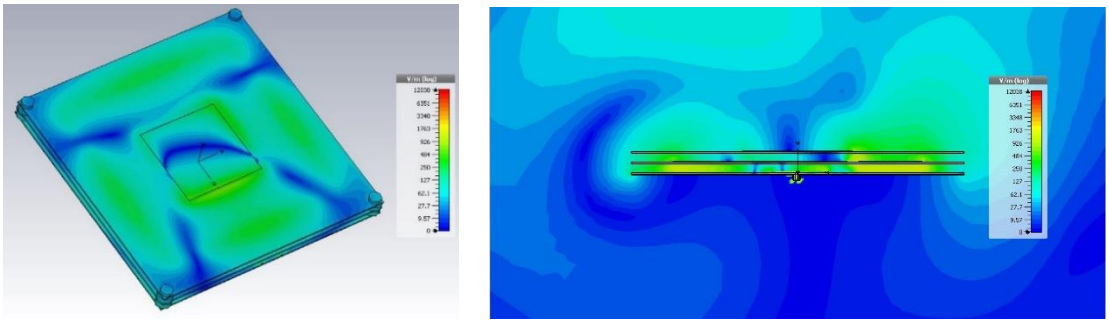

(a) (b)

Figure 10.19 Simulated E-fields of antenna with parasitic patch 1 with U-slot and 40mm parasitic patch 2 at 2.39GHz a) 3D b) Side Profile

The next stage is to improve the gain across the whole operating frequency range.

10.2.4.3 Multilayer U-Slot Parasitic Patches

A U-slot is now added to the top patch to increase the frequencies at which it will operate. The dimensions of the different parasitic patches were optimised in CST. The optimiser is required as there are a significant number of dimensions that need configured across multiple frequency points. The goals assigned to the optimizer were a reflection coefficient of -10dB and a gain value of +1dBi along boresight at the frequency points listed in Table 10.3. The values for the capacitance used in the simulation come from the datasheet which gives confidence in the values used in the simulation.

As the dimensions of parasitic patches are altered it will affect the resonant frequency. Therefore, the frequency values in Table 10.3 are only rough guides for the optimizer.

Table 10.3 Bias voltages, varactor capacitance values and frequency points chosen to optimise antenna

Bias Voltage (V)	Capacitance (pF)	Frequency (GHz)
0.00	9.24	1.35
2.50	4.85	1.71
5.00	3.77	1.83
30.00	1.77	2.39

From an initial simulation of the antenna it was found that the best results came when the U-slots in the parasitic patches faced in opposite directions. The spacing between the patches was kept at a constant 3mm through the optimization. This value was shown to be feasible in Figure 10.2 and is a common size for nylon spacers, which are readily available.

The optimised design for the parasitic U-slot patches are shown in Figure 10.20. The driven patch has the same layout and dimensions as given in Figure 9.2b and Table 9.1.

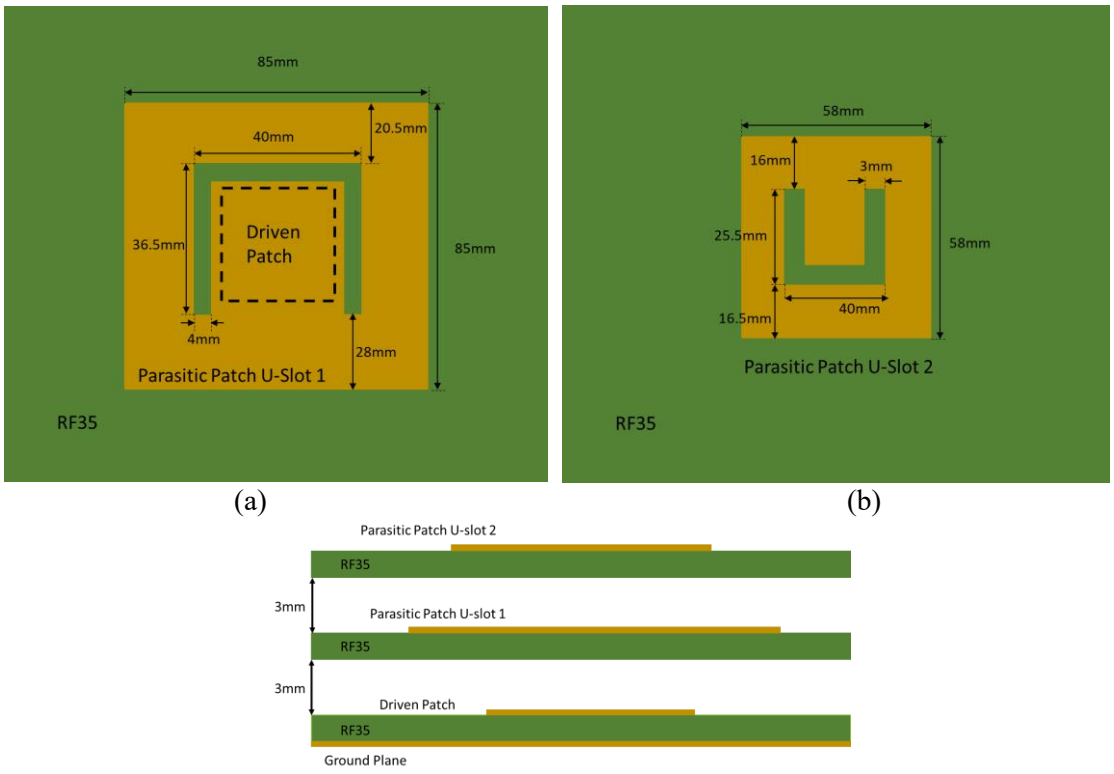

Figure 10.20 Dimensions for multilayer U-slot parasitic patch antenna a) Parasitic U-slot Patch 1 b) Parasitic U-slot Patch 2 c) Cross-Section of Stacked Spacing

The radiation patterns for the optimized antenna are shown in Figure 10.21 at the frequency points in Table 10.3. The H-plane patterns shown in Figure 10.21 are reasonably symmetric until the highest frequency point of 2.39GHz when there is a slight angle along boresight.

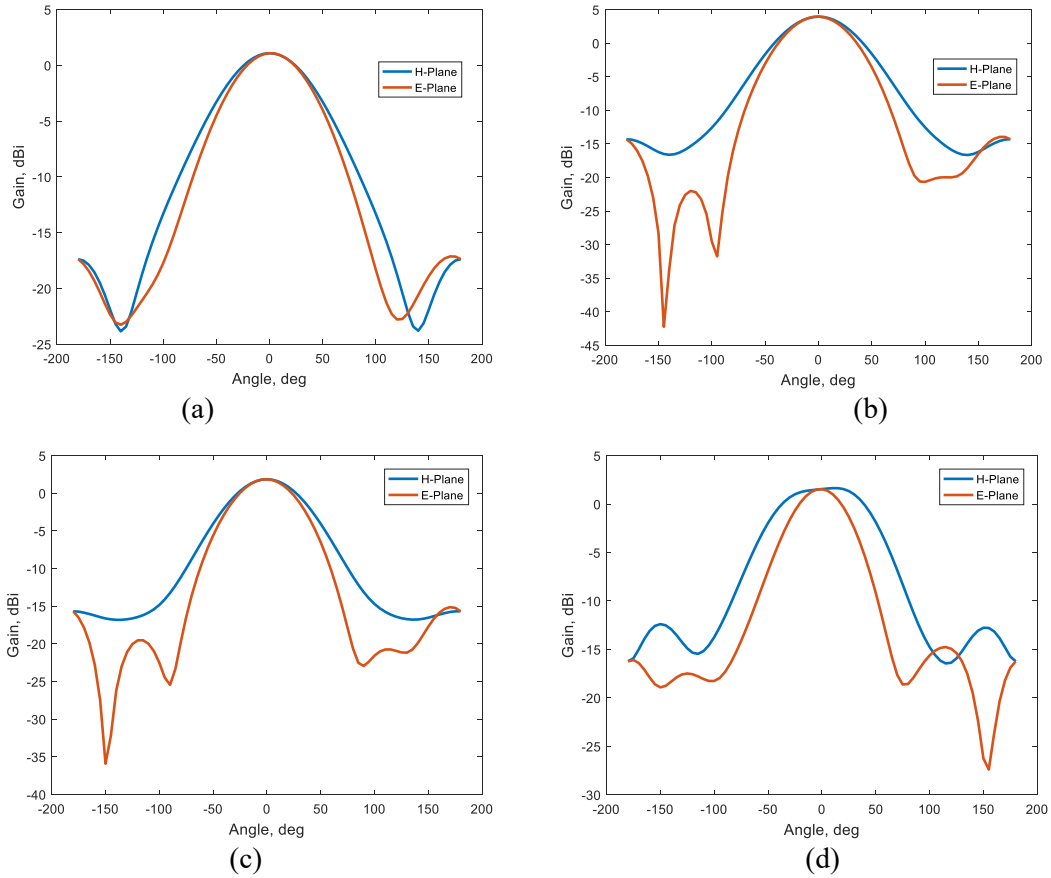

Figure 10.21 Simulated radiation patterns for multilayer U-slot parasitic patch antenna a) 1.35GHz b) 1.71GHz c) 1.83GHz d) 2.39GHz

The peak extracted gain from the radiation patterns is listed in Table 10.4. All these extracted values meet the optimiser goal of +1dBi.

Table 10.4 Extracted gain from simulated radiation patterns for multilayer U-slot parasitic patch antenna. Capacitance values used to model the varactor at each frequency point are shown in brackets.

Frequency (GHz)	1.35 (9.24pF)	1.71 (4.85pF)	1.83 (3.77pF)	2.39 (1.77pF)
Gain (dBi)	+1.08	+3.95	+1.86	+1.74

There were other dimensions of the patches shown in Figure 10.20 that would give much greater gain values at specific frequencies shown in Table 10.4. However, these came at the expense of reducing gain at other frequency points. The dimensions in Figure 10.20 were chosen as they gave the most consistent gain across the frequency points chosen.

Figure 10.22 shows the simulated reflection coefficient. At 1.35GHz the reflection coefficient does not go below the -10dB specified in the optmiser. The dual band nature is exhibited when a varactor capacitance value of 9.24pF and 4.85pF is used. This dual resonance is expected due to the U-slot response as shown in Figure 10.10. Attempts to remove the dual resonances and improve the reflection coefficient were made but these came at the expense of the gain values. It was therefore decided to keep the configuration that had the dual resonances.

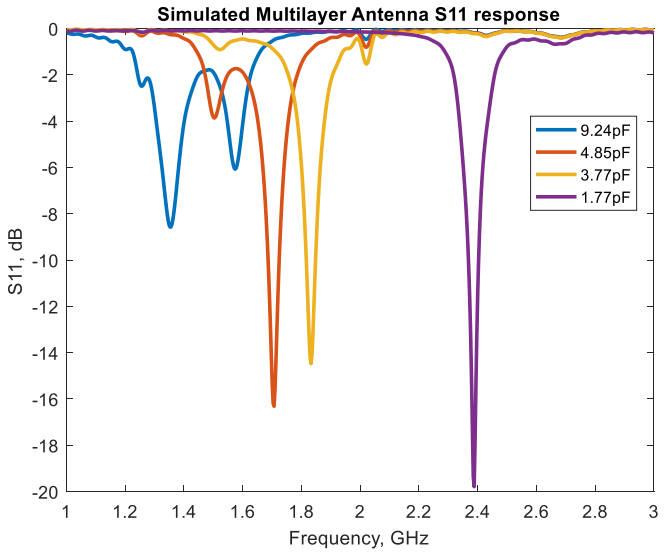

Figure 10.22 Reflection coefficient of optimized antenna at different capacitance values

The fabricated antenna is shown in Figure 10.23. The patches are separated using nylon screws and spacers. The substrate area was increased so the screws and spacers were sufficiently far enough from the antenna to not affect the radiation pattern of the antenna.

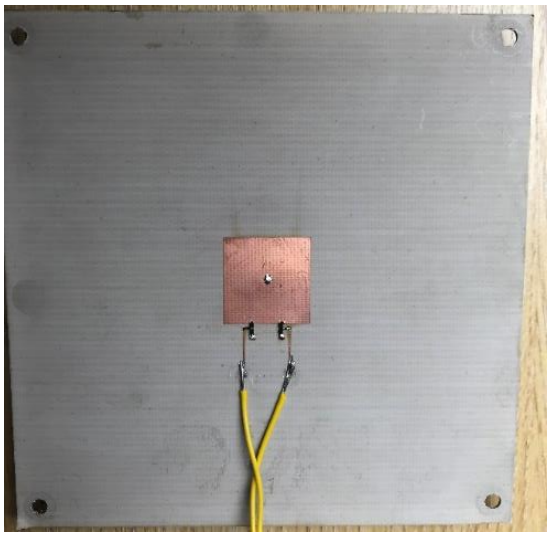

(a)

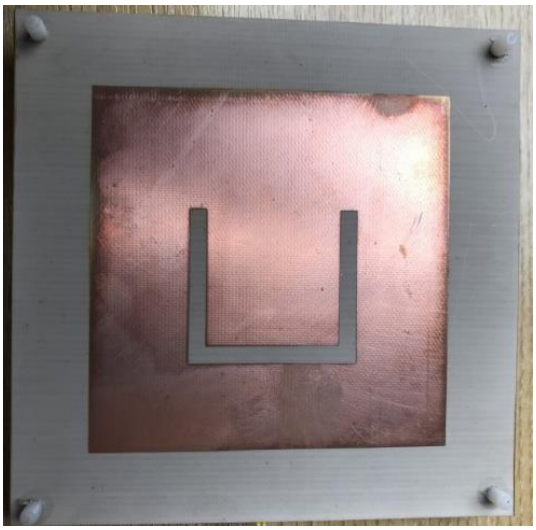

(b)

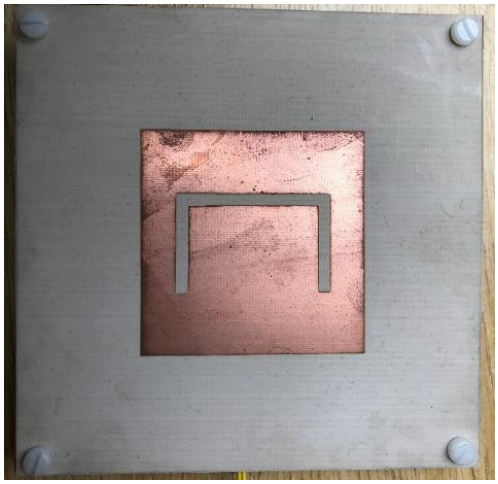

(c)

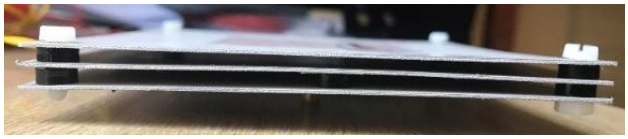

(d)

Figure 10.23 Fabricated multilayer U-slot parasitic patch antenna a) Driven Patch b) Parasitic U-slot Patch 1 c) Parasitic U-slot Patch 2 d) Side Profile

10.3 Results

10.3.1 Measured Reflection Coefficient

The measured S_{11} response for multilayer U-slot parasitic patch antenna is shown in Figure 10.24.

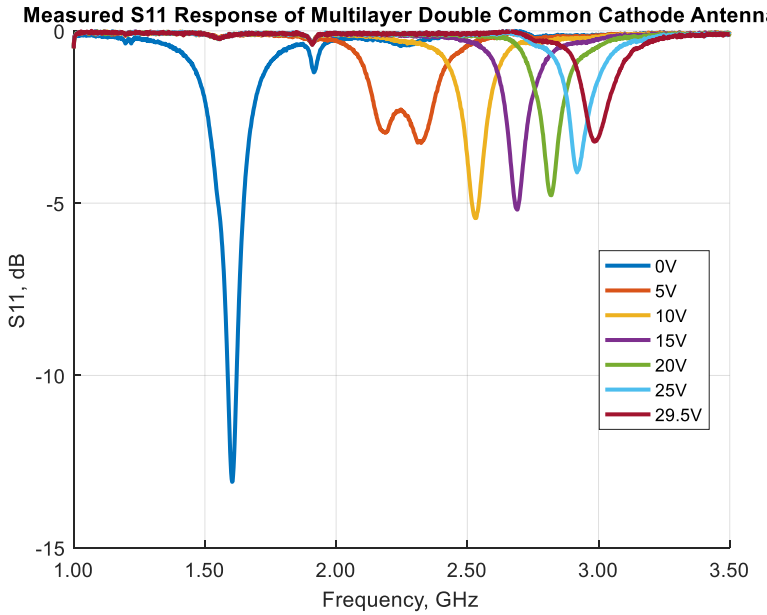

Figure 10.24 Measured S_{11} response of antennas multilayer U-slot parasitic patch antenna

It is seen in previous sections that as the bias voltage increases and the frequency of operation increases the S_{11} response deteriorates. This deterioration in the measured S_{11} response is opposite to the trend seen in the simulated S_{11} response shown in Figure 10.22.

10.3.2 Tunability

The measured and simulated tunability is given in Tables 10.5 and 10.6 respectively.

Table 10.5 Measured tunability of multilayer U-slot parasitic patch antenna. At 0V the nominal capacitance of the varactor is 9.24pF. At 29.5V the capacitance is 1.77pF

Antenna	Frequency at 0V (GHz)	Frequency at 29.5V (GHz)	Tunability (%)
Multilayer	1.55	3.00	63.70

Table 10.6 Simulated tunability of multilayer U-slot parasitic patch antenna. At 0V the nominal capacitance of the varactor is 9.24pF. At 29.5V the capacitance is 1.77pF

Antenna	Frequency at 0V (GHz)	Frequency at 29.5V (GHz)	Tunability (%)
Multilayer	1.36	2.39	54.9

10.3.3 Radiation pattern

The measured radiation patterns for the multilayer U-slot parasitic patch antenna are shown in Figure 10.25.

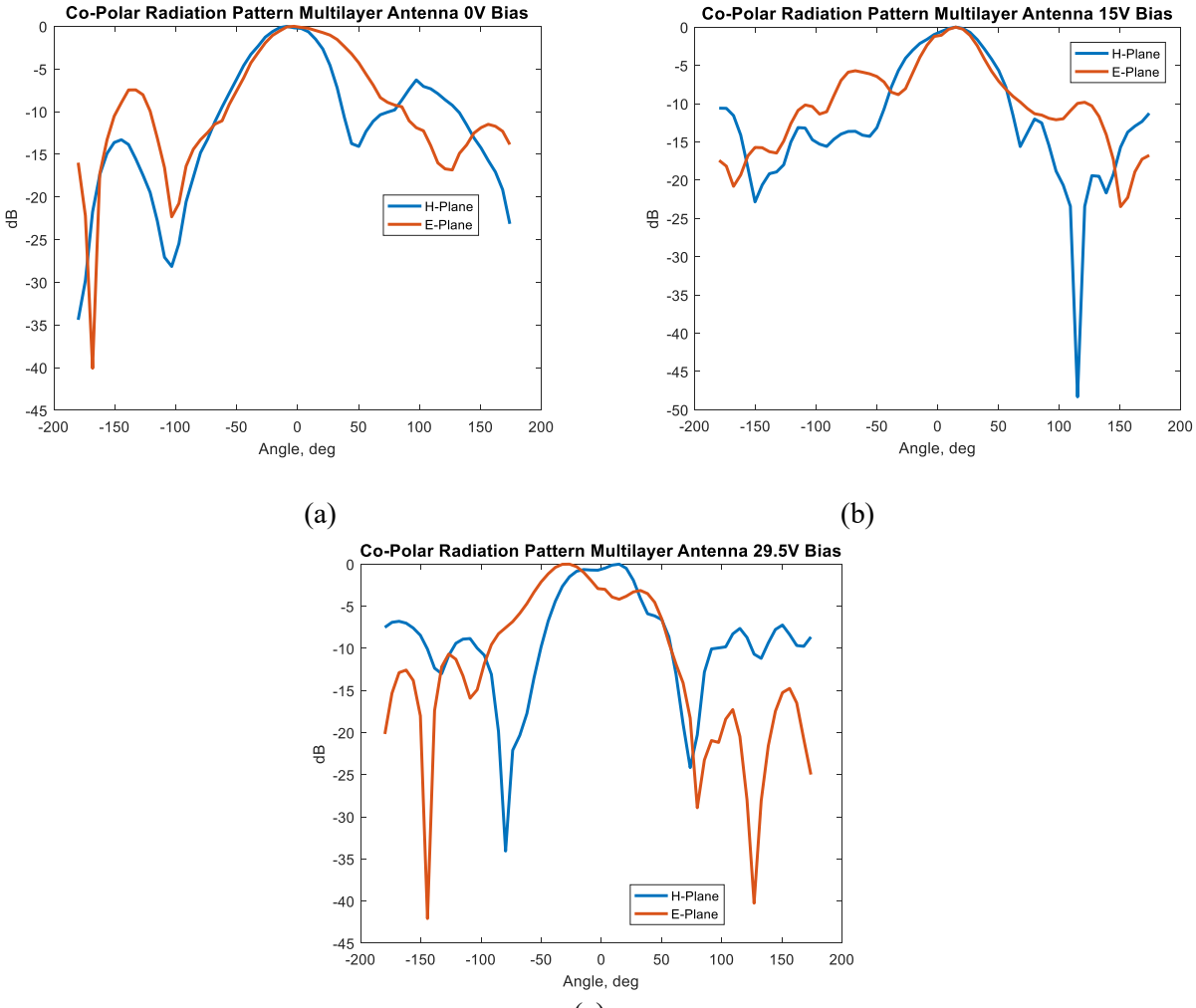

Figure 10.25 Measured radiation pattern of multilayer U-slot parasitic patch antenna a)1.55GHz with 0V bias b) 2.69GHz with 15V bias c) 3.00GHz with 29.5V bias

10.3.4 Gain

The measured gain values across the bias voltage range at 5V intervals are given in Table 10.7. Values for the simulated gain of the antenna at bias voltages with corresponding capacitance values from the datasheet are shown in Table 10.8.

Table 10.7 Measured gain values for multilayer U-slot parasitic patch antenna

Bias Voltage (V)	0.0	5.0	10.0	15.0	20.0	25.0	29.5
Frequency (GHz)	1.55	2.21	2.47	2.69	2.80	2.91	3.00
Gain (dBi)	-8.5	+5.8	-0.7	-2.8	-2.8	-4.5	-1.2

Table 10.8 Simulated gain values for multilayer U-slot parasitic antenna. Capacitance values used to model the varactor at each frequency point are shown in brackets.

Bias Voltage (V)	0.0 (9.24pF)	5.0 (3.77pF)	10.0 (2.85pF)	20.0 (2.13pF)	29.5 (1.77pF)
Frequency (GHz)	1.35	1.83	2.00	2.23	2.39
Gain (dBi)	+1.1	+1.9	-1.3	+0.1	+1.7

10.3.5 IIP3 Measurements

The measured IIP3 point of the antenna is given in Table 10.9 and Figure 10.26 shows the measured data.

Table 10.9 Measured IIP3 point of multilayer U-slot parasitic antenna at 0V bias

Antenna	IIP3 (dBm)
Multilayer Antenna	+16.9

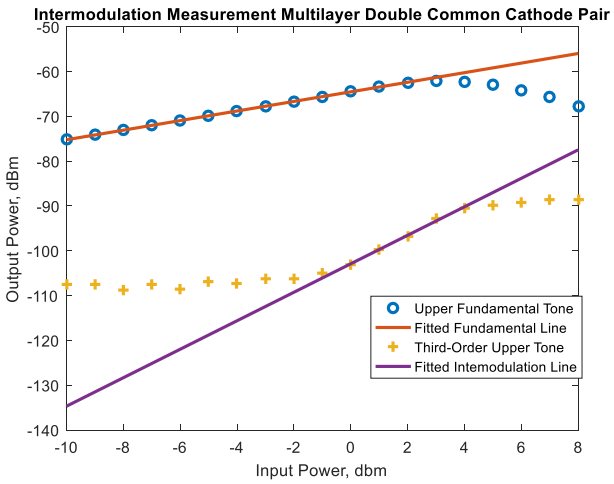

Figure 10.26 Measured intermodulation products of multilayer U-slot parasitic patch antenna at 0V bias

10.4 Discussion

The measured tunability of the antenna is greater than the tunability of the simulated antenna as shown by Tables 10.5 and 10.6. This is similar to the results seen in Chapter 9. This increase in tunability is attributed to measured frequency at 0V bias being greater than that of the simulated antenna. The lower simulated frequency at 0V bias is attributed to CST having issues with the common cathode configuration of the varactors, as suggested in Chapter 9. Comparing the measured tunability of the antenna loaded with a pair of common cathode varactors given in Table 9.3, and the antenna with parasitic patches in Table 10.5, an increase of 3.44% is seen by adding parasitic patches.

The addition of the parasitic patches with a spacing of 3mm above the driven patch did not reduce the design frequency significantly compared to the double common cathode seen in Chapter 9. It was expected that they would provide some form of capacitive loading.

The measured radiation patterns shown in Figure 10.25 show the main beam along boresight at bias voltages of 0V and 15V. However, the patterns do show a narrower main beam, and higher sidelobes than designed. Asymmetry is exhibited in both the E-plane and H-plane patterns at all

bias voltages. The radiation pattern with 29.5V bias volyage shows there is a dip in the main beam which suggests there is still blocking from the U-slot parasitic patch 1.

It is difficult to compare the simulated radiation patterns with the measured radiation patterns as they operate at different frequencies. However, the fabricated antenna radiation patterns are shown to behave differently to the simulated patterns shown in Figure 10.21.

Like the radiation patterns, it is difficult to extract any meaningful comparison between the measured gain values in Table 10.7 and the simulated gain values in Table 10.8 due to the frequency difference at each bias voltage. A more meaningful comparison is to look at the measured gain values of the double common cathode antenna investigated in Table 9.6 where the frequencies are closer to the antenna measured here. The gain of the multilayer U-slot parasitic patch is an improvement at all bias voltages except 25V where it shows a decreases of 2.1dB. The most notable improvement comes at 5V bias where the gain has increased by a value of 12.9dB.

The difference in the gain and radiation patterns between the simulations and measurements comes from the frequency difference and difficulties with the fabrication of the antenna. The most major issue with the fabrication of the antenna was the substrate holding the parasitic U-slot patches bowing in at the middle. This issue is highlighted in Figure 10.27 where the bowing of parasitic patches 1 and 2 are seen.

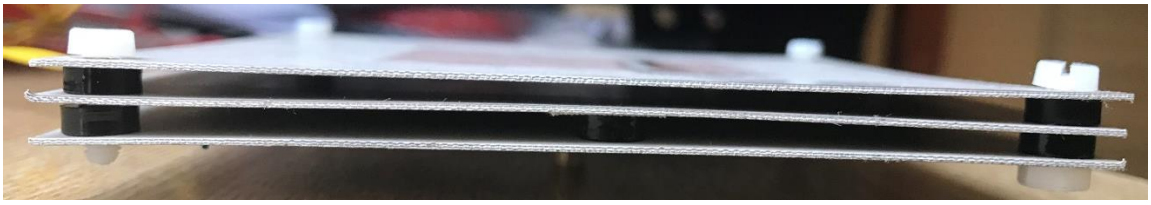

Figure 10.27 Bowing of antenna substrates

The bowing is caused by the large size of the substrates required for the frequencies investigated here. This is made worse by the thickness of the substrate only being 0.76mm and only one side of the substrate being metallized as there is no ground plane. Extra nylon spacers where taped at the midway point between the screws at the corners to help keep the spacing more consistent. The spacers are shown in Figure 10.27 between the driven patch and parasitic patch 1. These extra spacers will not help with any bowing in the centre of the patches.

The measured linearity of the antenna is the same as that of the double common cathode patch antenna investigated in Chapter 9. This result is to be expected as the only additions to the antenna are passive structures in the form of U-slot parasitic patches. These will not affect the linearity at the power levels investigated here.

This antenna design requires refinement to improve the performance. Most importantly the substrate used to support the parasitic patches could be changed to a ceramic such as alumina. This would provide more rigidity and have better electrical properties, most notably an improved loss tangent [5]. Using Alumina would require the parasitic patches to be redesigned due to the increased dielectric constant of 9.8. However, the dimensions should not be changed dramatically as the parasitic patches do not have a reference ground plane.

Different shape parasitic patches could be used to increase the gain: E-shaped or additional U-slots could be added. Adding more U-slots may have the added benefit of reducing the size of the parasitic patches as well as improving coupling between the driven patch and the higher frequency patches. Additional patches could be added to facilitate the gain at higher frequencies at the expense of increasing the height.

10.5 Conclusion

This chapter has looked at improving the gain characteristic of a tunable antenna using the double common cathode configuration of varactors by adding two parasitic patches with U-slot cut outs. The major findings where:

1. Multiple patches of different sizes are required to increase the gain of a tunable patch antenna across its frequency range.
2. The addition of U-slots in parasitic patches allow increased coupling between the driven patch and stacked parasitic patches.
3. An improvement in gain is seen at multiple frequency points compared to two pair common cathode antenna at a cost of a larger antenna size.
4. The tunability of the antenna is slightly improved by the addition of parasitic patches compared to two pair common cathode antenna.
5. The linearity of the antenna is not affected by the addition of the parasitic patches.
6. The fabrication of the antenna is important, specifically in reducing any bowing of the substrates.

10.6 References

[1] S. Egashira and E. Nishiyama, “Stacked microstrip antenna with wide bandwidth and high gain,” IEEE Transactions on Antennas and Propagation, vol. 44, no. 11, pp. 1533–1534, 1996.

[2] T. Seki, N. Honma, K. Nishikawa, and K. Tsunekawa, “A 60-GHz multilayer parasitic microstrip array antenna on LTCC substrate for system-on-package,” IEEE Microwave and Wireless Components Letters, vol. 15, no. 5, pp. 339–341, 2005.

[3] S. Weigand, G. Huff, K. Pan, and J. Bernhard, “Analysis and design of broad-band single-layer rectangular u-slot microstrip patch antennas,” IEEE Transactions on Antennas and Propagation, vol. 51, no. 3, pp. 457–468, 2003.

[4] R. Bhalla and L. Shafai, “Resonance behavior of single U-slot and dual U-slot antenna,” IEEE Antennas and Propagation Society International Symposium. 2001 Digest. Held in conjunction with: USNC/URSI National Radio Science Meeting (Cat. No.01CH37229), pp. 700–703, 2001.

[5] F. Keister, “An Evaluation of Materials and Processes for Integrated Microwave Circuits,” IEEE Journal of Solid-State Circuits, vol. 3, no. 2, pp. 131–137, 1968.

11 Conclusion

This thesis set out to investigate the effects of tunability, gain and linearity in reconfigurable antennas and how they inter-relate. The linearity of an antenna is an important parameter as intermodulation products can appear in the channels of adjacent users. This is an often-overlooked property when engineers design reconfigurable antennas. A gap was identified in the literature were there were no fundamental investigations looking into the parameters of an antenna that effect the tunability, gain and linearity and this thesis addresses this issue. A frequency reconfigurable microstrip patch using a varactor diode was identified as a popular antenna in the literature. Some preliminary investigations into linearity of frequency agile antennas had been undertaken and could be taken further.

This study addressed five main research questions:

- How does the frequency and substrate affect the tunability, gain and linearity of a varactor tuned patch antenna?
- How does the location of the varactors on the radiating and non-radiating edge aeffect tunability, gain and linearity?
- How does the number of varactors affect the tunability, gain and linearity of a varactor tuned patch antenna?
- How do different varactor types affect the tunability, gain and linearity?
- Is there a configuration of varactors that improves all three of these parameters?

By investigating these research questions, the body of knowledge has been taken forward from the previous point of performing intermodulation tests as an after-thought on an already designed antenna.

There were common results between the individual investigations that gave reinforcement to the findings. When a larger total capacitance was added to a patch, whether this was from a greater number of varactors being added in Chapter 7 or a single varactor with a larger capacitance in Chapter 8, it causes reduction in gain due to miniaturization of the physical patch area but increases the tunability.

Increasing the number of varactors on a patch antenna improved the linearity performance as shown in Chapter 7. The results in Chapter 6, show that using four varactors may provide better results in tuning and linearity if a designer places them in the correct position on the patch.

These investigations led to the development of a novel antenna based on the findings of the research questions. This new antenna uses parasitic patches with U-slot cut outs and the common cathode configuration of varactors to provide an antenna that has improved linearity and gain over the frequency range while not compromising the tunability.

This work has shown that the antenna geometry, fabrication materials and placement of a tunable component need to be considered when designing reconfigurable microstrip patch antennas as they all have a different effect on tunability, gain and linearity.

11.1 Future Research

This body of work looked at the microstrip patch antenna which is one of the simplest forms of antenna. However, investigations into reconfigurable antennas and their linearity properties can be expanded upon in many ways. Some potential areas to further investigate are:

- Use patches with different lengths and shapes i.e. rectangle, circular, H-shaped.
- Look at antenna types that are suited to a specific application such as a planar Inverted-F antenna for mobile handsets. Does the choice of substrate improve linearity and tunability as found in Chapter 4?

- Patches that are reconfigurable in polarization and pattern.
- Combining PIN diodes and varactors and how they interact.

11.2 Limitation of Study

There are areas of this study that have been limited in their application and are identified here.

11.2.1 Modelling and Antenna Design

An accurate model of the varactor for both forward and reverse bias should be modelled in a circuit simulator with a harmonic balance. This would have allowed for extraction of the intermodulation product voltages; these can then be modelled in CST to predict the radiated power levels of intermodulation products. This would have given more insight into the behaviour of antennas and helped to correlate the voltages across the varactors and the measured IIP3 points.

11.2.2 Testing Methodology

The antenna chamber, as discussed in Chapter 4, had moveable podiums for the antenna measurements which allows for multifunctionality. However, it did not guarantee accurate alignment of the antennas. Every effort was made to align the podiums and antennas with the equipment available. The antenna misalignment may have impacted upon the gain measurements. Some ways to improve the measurements could be to use lasers to accurately align the antennas in the chamber. Another solution would be to have fixed podiums in the chamber and mechanical mounts. This would come at a cost of reduced adaptability.

12 Appendix A Review of Two Tone Spacing

Table A.1 shows a summary of the frequency tones and spacings used for two-tone testing from the literature.

Table A.1 Assessment of two-tone frequency spacing from literature

Component type	Centre Frequency	Lower Tone	Upper Tone	Difference in frequency	Difference as a percentage of centre frequency	References
Microstrip Antenna	1.175GHZ	1.1725GHz	1.1775GHz	5MHz	0.4%	[1]
Microstrip Antenna	1.35GHz	1.3475GHz	1.3525GHz	5MHz	0.37%	[1]
Microstrip resonator loaded with FE varactor	4GHz	3.999GHz	4.001GHz	2MHz	0.05%	[2]
Component in microstrip line	2GHz	1.9995GHz	2.0005GHz	1MHz	0.05%	[3]
Varactor tuned helical antennas	498MHz	494MHz	502MHz	8MHz	1.6%	[4]
Pin diode tuned antennas	2.452GHz	2.451GHz	2.453GHz	2MHz	0.815%	[5]
Tunable bandpass filter	1.05GHz-1.35GHz			100KHz	0.0095%-0.0074%	[6]
Tunable bandpass filter	Single varactor: 1.39-1.81GHz Back pair: 1.52-1.95GHz			1MHz	Single:0.07%-0.055% Back pair: 0.066% - 0.051%	[7]

12.1 References

[1] S. Yong, “Design and Analysis of Pattern Null Reconfigurable Antennas,” Ph.D dissertation, Dept. Electr. Comput. Eng., Univ. Illinois at Urbana-Champaign, Urbana, IL, 2012.

[2] A. Kozyrev, A. Ivanov, T. Samoilova, O. Soldatenkov, K. Astafiev, and L. C. Sengupta, “Nonlinear response and power handling capability of ferroelectric BaxSr1−xTiO3 film capacitors and tunable microwave devices,” *Journal of Applied Physics*, vol. 88, no. 9, pp. 5334–5342, 2000.

[3] E. K. Kowalczuk, R. D. Seager, and C. J. Panagamuwa, “Power handling of a photoconductive microwave switch,” *2016 Loughborough Antennas & Propagation Conference (LAPC)*, 2016.

[4] M. Sonkki, M. Berg, J. Pihlaja, S. Karhu, H. Jantunin, and E. Salonen, “Varactor tunable helical antenna,” *2nd European Conference on Antennas and Propagation (EuCAP 2007)*, 2007.

[5] R. Goncalves, N. B. Carvalho, and P. Pinho, “Intermodulation in active reconfigurable antennas,” 2014 International Workshop on Integrated Nonlinear Microwave and Millimetre-wave Circuits (INMMiC), 2014.

[6] C. Ge, X.-W. Zhu, X. Jiang, and X.-J. Xu, “Analysis of Weakly Nonlinear Effect for Varactor-Tuned Bandpass Filter,” *IEEE Transactions on Microwave Theory and Techniques*, vol. 63, no. 11, pp. 3641–3650, 2015.

[7] M. El-Tanani and G. Rebeiz, “A Two-Pole Two-Zero Tunable Filter With Improved Linearity,” *IEEE Transactions on Microwave Theory and Techniques*, vol. 57, no. 4, pp. 830–839, 2009.